JOURNAL OF FOOD PROCESS ENGINEERING

D.R. HELDMAN
and
R.P. SINGH
COEDITORS

FOOD & NUTRITION PRESS, INC.

OLUME 18, NUMBER 1 MARCH 1995

JOURNAL OF FOOD PROCESS ENGINEERING

All articles for publication and inquiries regarding publication should be sent to DR. D.R. HELDMAN, COEDITOR, *Journal of Food Process Engineering*, Food Science/Engineering Unit, University of Missouri-Columbia, 235 Agricultural/Engineering Bldg., Columbia, MO 65211 USA; or DR. R.P. SINGH, COEDITOR, *Journal of Food Process Engineering*, University of California, Davis, Department of Agricultural Engineering, Davis, CA 95616 USA.

All subscriptions and inquiries regarding subscriptions should be sent to Food & Nutrition Press, Inc., 2 Corporate Drive, P.O. Box 374, Trumbull, CT 06611 USA.

One volume of four issues will be published annually. The price for Volume 18 is $142.00, which includes postage to U.S., Canada, and Mexico. Subscriptions to other countries are $162.00 per year via surface mail, and $173.00 per year via airmail.

Subscriptions for individuals for their own personal use are $112.00 for Volume 18, which includes postage to U.S., Canada and Mexico. Personal subscriptions to other countries are $132.00 per year via surface mail, and $143.00 per year via airmail. Subscriptions for individuals should be sent directly to the publisher and marked for personal use.

The *Journal of Food Process Engineering* (ISSN:0145-8876) is published quarterly (March, June, September and December) by Food & Nutrition Press, Inc.—Office of Publication is 2 Corporate Drive, P.O. Box 374, Trumbull, Connecticut 06611 USA.

Second class postage paid at Bridgeport, CT 06602.

POSTMASTER: Send address changes to Food & Nutrition Press, Inc., 2 Corporate Drive, P.O. Box 374, Trumbull, Connecticut O6611 USA.

JOURNAL OF FOOD PROCESS ENGINEERING

JOURNAL OF FOOD PROCESS ENGINEERING

Journal of FOOD PROCESS ENGINEERING

VOLUME 18 NUMBER 1

Coeditors: D.R. HELDMAN
R.P. SINGH

FOOD & NUTRITION PRESS, INC.
TRUMBULL, CONNECTICUT 06611 USA

ISSN 0145-8876

Printed in the United States of America

CONTENTS

PREDICTION OF BEEF CARCASS CHILLING TIME AND MASS LOSS

P. MALLIKARJUNAN[1] and G.S. MITTAL[2]

School of Engineering, University of Guelph
Guelph, Ontario, Canada N1G 2W1

Accepted for Publication March 1, 1994

ABSTRACT

Predictive equations to compute the chilling time, mass loss at the end of chilling, temperature history at the geometric center of round and mass loss history during beef carcass chilling were developed using validated computer models and response surface analysis. Central composite rotatable design was used to obtain quadratic response surfaces for various chilling parameters. Temperatures at the geometric center of round muscle were predicted within 95% confidence interval. Mass loss histories were also predicted within 95% confidence interval after 5 h postmortem. Temperature predictions were within ±2C and mass loss predictions were within ±1.0%.

INTRODUCTION

Nomograms for predicting temperatures at the geometric center of a round muscle for different initial carcass masses, air velocities and ambient temperatures were developed by Bailey and Cox (1976). These nomograms were based on the results obtained from experiments conducted over many years. These nomograms covered limited ranges of air velocities, ambient temperatures and initial carcass masses. The nomograms for ambient temperatures below 0C were not available, and also the effects of carcass fat cover thickness and relative humidity were lacking.

Drumm *et al.* (1992) have used the nomograms of Bailey and Cox (1976) for predicting the round muscle temperature, and found a good agreement with the experimental values. They compared the temperatures after 10 h and 24 h postmortem only. The other important criterion during chilling is the mass loss

[1] Present address: Center for Food Safety Quality Enhancement, University of Georgia, Griffin, GA 30223-1797.

[2] Please send correspondence to: Dr. G.S. Mittal, School of Engineering, University of Guelph, Guelph, ON, Canada N1G 2W1.

Journal of Food Process Engineering **18** (1995) 1–15.

during chilling. Nomograms to predict the mass loss during chilling were not reported in the literature.

The objective of this study was to develop models for predicting chilling time, mass loss at the end of chilling, temperature history at the geometric center of the round and mass loss history during beef carcass (sides) chilling. The study used validated heat and mass transfer models for computing the temperature and mass loss histories during chilling.

METHODS AND MATERIALS

The variables selected for this study are: carcass fat cover thickness, initial carcass mass (i.e., mass of one side), air velocity, ambient temperature and relative humidity. A central composite rotatable design for the five variables was selected (32 factorial + 10 star + 1 center = 43 combinations). The lower and upper levels of the process/carcass parameters are summarized in Table 1. Simulations were performed on all the combinations using the heat and mass transfer models (Mallikarjunan and Mittal 1994). The governing equations for heat and mass transfer in 2-dimensional cartesian coordinates are (the list of symbols are given at the end):

$$\frac{\partial}{\partial t}(\rho C_p T) = \frac{\partial}{\partial x}(k_x \frac{\partial T}{\partial x}) + \frac{\partial}{\partial y}(k_y \frac{\partial T}{\partial y}) + \bar{q} \tag{1}$$

$$\frac{\partial}{\partial t}(m) = \frac{\partial}{\partial x}(D_m \frac{\partial m}{\partial x}) + \frac{\partial}{\partial y}(D_m \frac{\partial m}{\partial y}) \tag{2}$$

Initial and boundary conditions:

$$T = T_o \text{ and } m = m_o \text{ for } t = 0 \tag{3}$$

$$(k_x \frac{\partial T}{\partial x} n_x + k_y \frac{\partial T}{\partial y} n_y) = h_t(T_s - T_a) - S_f \rho_d L_v \frac{\partial m}{\partial t} \tag{4}$$

$$-D_m \rho_d (\frac{\partial m}{\partial x} n_x + \frac{\partial m}{\partial y} n_y) = h_m(P_s - P_a) \tag{5}$$

TABLE 1.
PROCESS/CARCASS PARAMETERS AND THEIR LEVELS

Parameters	Low				High
	-2	-1	0	1	2
Carcass fat cover thickness, mm	3	5	7	9	11
Initial carcass mass, kg	120	135	150	165	180
Air velocity, m/s	0.5	1.125	1.75	2.375	3
Ambient temperature, C	-10	-7	-4	-1	2
Relative humidity, %	85	88.75	92.5	96.25	100

The Eq. 1 and 2 with initial and boundary conditions (Eq. 3, 4 and 5) were solved using the finite element method. The physical properties such as: thermal conductivity, specific heat and density were calculated using the models of Choi and Okos (1986) based on the composition and temperature. Surface heat transfer coefficient was calculated using the relationship between Nu, Re and Pr number for a flow across a vertical plate (Kreith and Black 1980). Surface mass transfer coefficient was calculated using $h_t/(h_m L_v) = 64.7$ Pa/K (Daudin and Swain 1990). The moisture diffusivity values were estimated based on the data provided by Mittal and Blaisdell (1984) for meat emulsions. The model was validated against extensive experimental data. The details are given elsewhere (Mallikarjunan and Mittal 1994).

The simulated results were used to develop quadratic response surfaces with significant quadratic interactions at 95% significance level. GLM procedure of the Statistical Analysis System (SAS 1989) was used.

Experimental data, obtained to validate the heat and mass transfer models, were used to verify the accuracy of the prediction equations. The steers were slaughtered at the abattoir of the University of Guelph under conventional commercial practices. One side of the carcass was used for the experiments. The carcasses were chilled at 0C ambient temperature for first 24 h chilling. Later, to decrease the temperature at the geometric center of the round to 5C or lower, the following two chilling schemes were used: (1) 0C ambient temperature, and (2) −5C ambient temperature. The relative humidity, air velocity, temperature at various carcass locations and total carcass mass were measured and were recorded using a multi-channel data logger. The details are given elsewhere (Mallikarjunan and Mittal 1994).

RESULTS AND DISCUSSION

For predicting the temperature at the geometric center of the round muscle, regression analysis was performed on the logarithmic values of the temperature ratios (Y) against time.

$$Y = \frac{T - T_A}{T_o - T_a} \tag{6}$$

where T = temperature at any time t, T_a = ambient temperature, T_o = initial temperature, and,

$$\begin{aligned} \log(Y) &= C_T + S_1 \cdot t \quad \text{for } t \leq 24h \\ \log(Y) &= C_T + (S_1 - S_2) \cdot 24 + S_2 \cdot t \quad \text{for } t > 24h \end{aligned} \tag{7}$$

where the values for the coefficients C_T, S_1 and S_2 were obtained in terms of the carcass/process parameters (Table 2) as follows:

$$\begin{aligned} C_T = {} & C_0 + C_1F + C_2M_I + C_3V_a + C_4T_a + C_5FT_a + C_6M_IT_a \\ & + C_7V_aT_a + C_8F^2 + C_9M_I^2 + C_{10}V_a^2 + C_{11}T_a^2 \end{aligned} \tag{8}$$

$$\begin{aligned} S_1 = {} & C_o + C_1F + C_2M_I + C_3V_a + C_4T_a + C_5FT_a \\ & + C_6M_IT_a + C_7V_aT_a + C_8V_a^2 + C_9T_a^2 \end{aligned} \tag{9}$$

$$S_2 = C_0 + C_1M_I + C_2T_a + C_3M_IT_a \tag{10}$$

For predicting the mass loss history during chilling, regression analysis was performed for the logarithmic values of mass loss and time.

$$\log(M_L) = C_M + S_M \cdot \log(t) \tag{11}$$

where the values for the coefficients C_M and S_M were obtained in terms of the carcass/process parameters (Table 3).

TABLE 2.
COEFFICIENTS FOR PREDICTIVE MODEL FOR THE TEMPERATURE HISTORY AT THE GEOMETRIC CENTER OF THE ROUND MUSCLE

Parameters	DF	MSS	Estimate	SEE
A. Intercept (C_T) for predicting the temperature history				
Intercept	1		1.714	0.156
F	1	1.6	-0.0955	0.0052
M_I	1	0.4	-0.0183	0.002
V_a	1	1.6	-0.250	0.013
T_a	1	1.1	0.0718	0.0046
$F*T_a$	1	0.1	0.000947	0.0002
M_I*T_a	1	1.2	-0.000432	0.000027
V_a*T_a	1	0.1	0.00317	0.00064
F*F	1	1.6	0.00685	0.00036
M_I*M_I	1	0.6	0.0000706	0.0000065
V_a*V_a	1	1.7	0.0717	0.0037
T_a*T_a	1	0.3	0.00118	0.00016
Error	31	0.005		
B. Slope (S_1) for predicting the temperature history during the first 24 h chilling				
Intercept	1		-0.140	0.0035
F	1	5.0	-0.00100	0.00014
M_I	1	98.7	0.000594	0.000019
V_a	1	2.2	-0.00855	0.00187
T_a	1	8.3	-0.00610	0.000687
$F*T_a$	1	1.8	-0.000125	0.00003
M_I*T_a	1	8.1	0.0000528	0.000004
V_a*T_a	1	2.5	-0.000467	0.0000965
V_a*V_a	1	1.0	0.00159	0.00052
T_a*T_a	1	9.0	0.000208	0.0000224
Error	33	0.1		
C. Slope (S_2) for predicting temperature history after 24 h chilling				
Intercept	1		-0.133	0.0119
M_I	1	8.3	0.000546	0.000079
T_a	1	7.1	-0.0158	0.0025
M_I*T_a	1	4.2	0.0000806	0.0000165
Error	39	0.18		

$Pr > |T| \leq 0.05$ for all

TABLE 3.
COEFFICIENTS FOR PREDICTIVE MODEL FOR THE MASS LOSS HISTORY DURING CHILLING

Parameter	DF	MSS	Estimate	SEE
A. Intercept (C_M) for predicting the mass loss history				
Intercept	1		10.094	2.043
F	1	2.8	0.0133	0.00137
V_a	1	0.24	-0.348	0.121
T_a	1	0.8	-0.00470	0.0009
RH	1	1.8	-0.342	0.044
RH*M_I	1	22.4	-0.0000538	0.000002
V_a*RH	1	0.2	0.00342	0.0013
RH*RH	1	2.1	0.0020	0.00024
Error	35	0.03		
B. Slope (S_M) for predicting the mass loss history				
Intercept	1		-5.673	1.056
F	1	1.8	-0.00332	0.000663
M_I	1	0.8	-0.00825	0.00244
V_a	1	6.0	0.541	0.0586
T_a	1	2.1	0.0675	0.0123
RH	1	3.9	0.161	0.0217
M_I*RH	1	0.84	0.0000912	0.000026
V_a*T_a	1	0.53	0.00218	0.00079
V_a*RH	1	4.6	-0.00514	0.00063
T_a*RH	1	1.6	-0.000627	0.00013
RH*RH	1	5.7	-0.00104	0.000115
Error	32	0.07		

$Pr > |T| \leq 0.05$ for all

$$C_M = C_O + C_1F + C_2V_a + C_3T_a + C_4RH + C_5M_IRH + C_6V_aRH + C_7RH^2 \quad (12)$$

$$S_M = C_O + C_1F + C_2M_I + C_3V_a + C_4T_a + C_5RH + C_6M_IRH + C_7V_aT_a + C_8V_aRH + C_9T_aRH + C_{10}RH^2 \quad (13)$$

The Eq. 7 and 11 can be used to find the temperature histories at the geometric center of round and mass histories during chilling. The same equations, after required modifications, can be used to obtain the chilling time required to chill the beef carcass for a desired round temperature and the mass at the end of chilling.

As a specific case, the chilling time required to chill the geometric center of round to 5C was obtained from the simulation results. The mass loss at the end of chilling when the geometric center of the round reached 5C was also obtained. From the response surfaces, for predicting the chilling time required to chill the geometric center of the round to 5C, the following equation was developed:

$$\Theta_c = C_0+C_1F+C_2M_I+C_3V_a+C_4T_a + C_5M_IT_a + C_6V_aT_a + C_7T_a^2 \quad (14)$$

For predicting the mass loss at the end of chilling when the geometric center of the round reached 5C, the following equation was developed:

$$M_L' = C_0 + C_1M_I + C_2V_a + C_3T_a + C_4M_IRH + C_5M_IT_a + C_6VaRH + C_7V_aT_a + C_8T_aRH + C_9T_a^2 \quad (15)$$

The values for the coefficients of the above equations are given in Tables 4 and 5, for chilling time and mass loss at the end of chilling, respectively.

For all the parameters (temperature and moisture histories, chilling time required to reach 5C at the geometric center of the round, and mass loss at the end of chilling), plots were obtained for observed against predicted values with confidence intervals at 95% level (Fig. 1–4).

In predicting the temperature history at the geometric center of the round muscle, the predicted values were higher than the observed data for first 3–5 h (Fig. 1). The variations between the observed and predicted data ranged from -5 to -10C during this period. Similarly, at the end of chilling, the predictions were below the observed data by 1–2C for -7C ambient temperature treatments. Overall, the observed data were predicted within the confidence intervals at 95% level ($\pm$2C). Thus, the equations can be used to obtain the temperature history within $\pm$ 2C after 5 h postmortem. Bailey and Cox (1976) reported a linear response for the Log(Y) with time throughout the chilling period. In the present study, a change in slope was observed after 24 h postmortem

TABLE 4.
COEFFICIENTS FOR PREDICTIVE MODEL FOR CHILLING TIME

Source	DF	MSS	Estimate	SEE
Intercept	1		-21.568	2.351
F	1	24.9	-0.394	0.062
M_I	1	517.4	0.430	0.015
V_a	1	10.8	-1.491	0.354
T_a	1	5.1	1.435	0.497
M_I*T_a	1	8.9	0.0117	0.003
V_a*T_a	1	2.5	-0.148	0.074
T_a*T_a	1	116.2	0.231	0.017
Error	35	0.6		

$Pr > |T| \leq 0.05$ for all

TABLE 5.
COEFFICIENTS FOR PREDICTIVE MODEL FOR MASS LOSS AT THE END OF CHILLING

Source	DF	MSS	Estimate	SEE
Intercept	1		1.314	0.257
M_I	1	0.6	0.0693	0.0079
V_a	1	0.7	5.759	0.584
T_a	1	0.9	1.484	0.137
M_I*RH	1	0.5	-0.000678	0.000084
M_I*T_a	1	0.04	0.000743	0.00034
V_a*RH	1	0.6	-0.0560	0.0063
V_a*T_a	1	0.2	0.0402	0.0082
T_a*RH	1	0.9	-0.0150	0.0014
T_a*T_a	1	0.5	0.0158	0.002
Error	33	0.008		

$Pr > |T| \leq 0.05$ for all

for all the chilling combinations. The nomograms (Bailey and Cox 1976) also produced higher error during the first 5 h of postmortem. The nomograms of Bailey and Cox (1976) provide higher error in temperature predictions with decrease in ambient temperature below 0C, and also predicted higher chilling time.

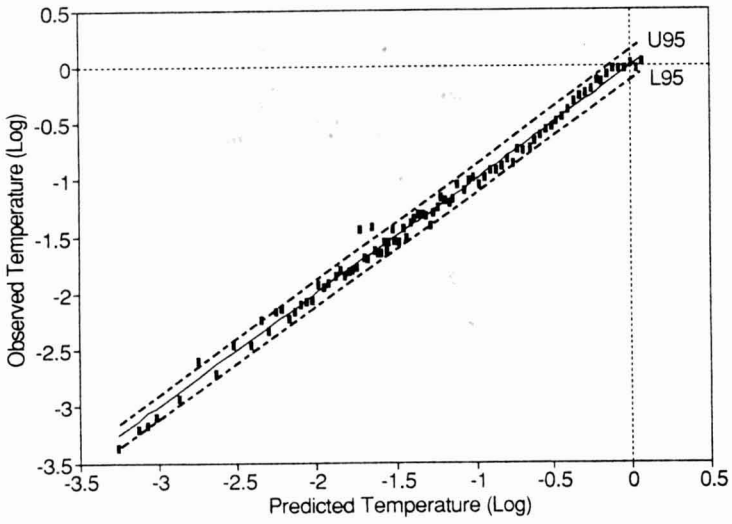

FIG. 1. OBSERVED VERSUS PREDICTED TEMPERATURES AT THE GEOMETRIC CENTER OF THE ROUND MUSCLE

■: Observed data; dashed lines represent upper and lower confidence intervals at 95% level.

In predicting the mass loss history, the predicted values were higher during the initial chilling period (up to 5 h postmortem) due to magnified error resulted using the logarithmic data for linear regression (Fig. 2). The variations were as high as 20%. After 5 h postmortem, the predictions were in good agreement with the observed data within 95% confidence interval ($\pm$1%). Thus, the equations developed for obtaining the cumulative mass loss during chilling can be used with confidence as the chilling process normally goes beyond 24 h postmortem.

For chilling time (Fig. 3), the predictions were in good agreement with the observed data, and the observations were within the confidence intervals at 95% level. Similarly, the predicted values for the mass loss at the end of chilling were also in close agreement with the observed data (Fig. 4).

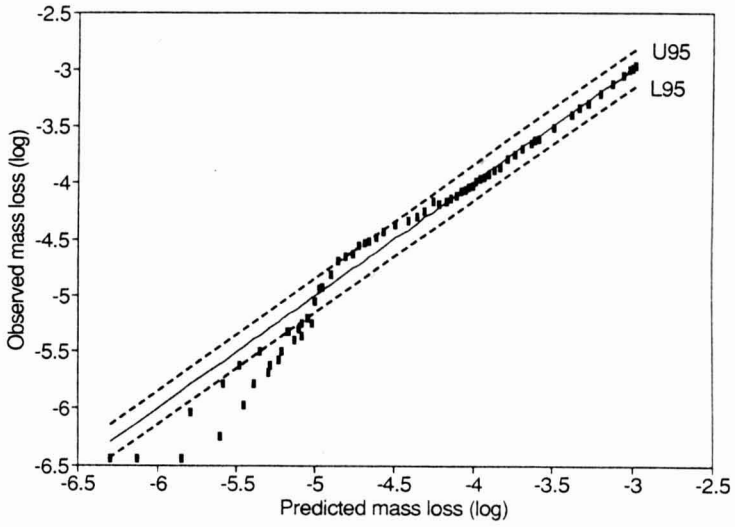

FIG. 2. OBSERVED VERSUS PREDICTED MASS LOSSES DURING CHILLING
■: Observed data; dashed lines represent upper and lower confidence intervals at 95% level.

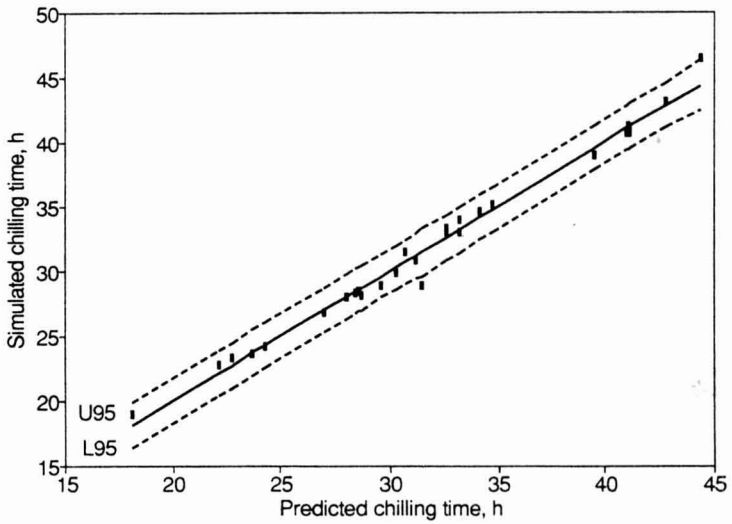

FIG. 3. OBSERVED VERSUS PREDICTED CHILLING TIMES
■: Observed data; dashed lines represent upper and lower confidence intervals at 95% level.

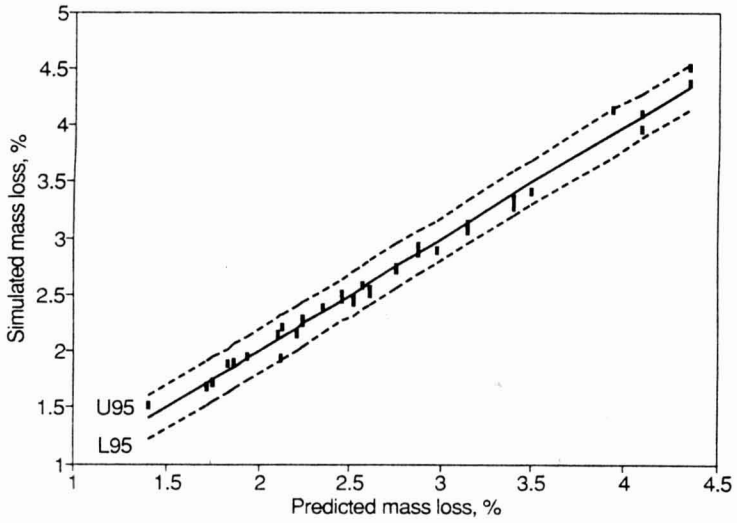

FIG. 4. OBSERVED VERSUS PREDICTED MASS LOSSES AT THE END OF CHILLING
■: Observed data; dashed lines represent upper and lower confidence intervals at 95% level.

Using the procedure described in Appendix, the chilling time required to reach 5C at the geometric center of the round and mass loss at the end of chilling were calculated. The chilling times were also calculated using the nomograms provided by Bailey and Cox (1976). Extrapolations were performed for temperatures below 0C as described by Drumm *et al.* (1992). The results are presented in Table 6. Using Bailey and Cox (1976) method, the chilling time predictions were good for ambient temperatures at 0C. The error increased with the decrease in ambient temperature below 0C. The predictions from the present method were in good agreement with the experimental data and predicted the chilling time within ± 2 h. Mass loss predictions were in good agreement with the experimental data of Mallikarjunan and Mittal (1994) and predicted the mass loss within $\pm 1.0\%$.

CONCLUSIONS

Predictive equations were developed to obtain the chilling time, mass loss at the end of chilling, temperature history at the geometric center of the round muscle and mass loss history during chilling. In predicting the temperature at the geometric center of round, the predictions were within the 95% confidence interval. In predicting the mass loss histories also, the predictions were within the 95% confidence interval after 5 h postmortem. Temperature predictions were within ± 2C and mass loss predictions were within $\pm 1.0\%$.

TABLE 6.
COMPARISON OF OBSERVED CHILLING TIME AND MASS LOSS WITH MODEL PREDICTIONS

T_a after 24 h, °C	F, mm	M_I, kg	Chilling time, h			Experimental mass loss, %	Predicted mass loss, %
			Experimental	Bailey & Cox	Present method		
0	3	128	38	38	40	3.58	4.03
-5	8	142	36	29	35	3.44	3.41
0	4	160	49	48	47	3.58	4.03
-2	7	122	36	30	35	3.25	3.51
-2.5	10	174	40	34	42	3.17	3.21
0	9	143	46	42	45	3.55	4.16

The air velocity is 0.5 m/s, relative humidity is 90%, and the ambient temperature for first 24 h of chilling is 0 C for all the experiments.

NOMENCLATURE

ρ	Density, kg/m^3
ρ_d	Density of dry matter, kg/m^3
Θ_c	Chilling time, h
C_0 to C_{11}	Regression coefficients
C_M	Intercept for predicting mass loss history
C_p	Specific heat, J/(kg.K)
C_T	Intercept for predicting temperature history
D_m	Moisture diffusivity, m^2/s
DF	Degrees of freedom
F	Fat cover thickness, mm
h_m	Surface mass transfer coefficient, kg of water/(Pa.m^2.s)
h_t	Surface heat transfer coefficient, W/(m^2.K)
k_x, k_y	Thermal conductivities in x and y directions, W/(m.K)
L_v	Latent heat of vaporization, J/kg
m	Moisture content, dry basis
m_o	Initial moisture content, dry basis
M_I	Initial carcass mass, kg
M_L	Cumulative mass loss, fraction
M_L'	Mass loss at the end of chilling, fraction
MSS	Mean sum of squares
n_x, n_y	Direction cosines
Nu	Nusselt number

P_a	Partial vapor pressure of air, Pa
Pr	Prandtl number
P_s	Partial vapor pressure at the carcass surface, Pa
$\bar{q}$	Heat generation due to ATPase reaction, W/m^3
Re	Reynolds number
RH	Relative humidity, %
S_1	Slope for predicating temperature during first 24 h chilling
S_2	Slope for predicting temperature after 24 h chilling
S_f	Shape factor, m
S_M	Slope for predicting mass loss history
SEE	Standard error of estimate
t	Time, s
T	Carcass temperature, C or K
T_a	Ambient temperature, C or K
T_o	Initial temperature, C or K
T_s	Surface temperature, C or K
V_a	Air velocity, m/s
x,y	Cartesian coordinates, m
Y	Temperature ratio, dimensionless

APPENDIX

Procedure for Calculating Temperature at the Geometric Center of Round for a Multi-Zone (Different Ambient Conditions) Chilling Scheme

(1) Calculate the coefficients C_T, S_1 and S_2 for the given fat cover thickness, initial carcass mass, air velocity, ambient temperature for the first zone, using Eq. 8, 9 and 10 and values from Table 2.
(2) Calculate the temperature ratio (Y) from the coefficients using Eq. 7.
(3) Calculate the temperature at the end of that zone.
(4) Calculate a new Y using the meat temperature of the current zone conditions and air temperature of second zone.
(5) Calculate the coefficients C_T, S_1 and S_2 for the given fat cover thickness, initial carcass mass, air velocity, ambient temperature for the next zone.
(6) Calculate the equivalent number of hours required in the next zone conditions to achieve the temperature after the current zone.
(7) Add this equivalent hours to the next zone hours and use this to calculate the temperature at the end of next zone. Repeat this for all the zones.
(8) To obtain the chilling time required to reach 5C at the geometric center of the round, the time duration for the final zone can be changed and the procedures 1 to 7 can be repeated.

Worked Example

Fat cover thickness = 8 mm, initial carcass mass = 142 kg, two chilling zones; for the first zone, ambient temperature is 0C for first 24 h and air velocity is 0.5 m/s. For the second zone, ambient temperature is −5C for 12 h with an air velocity of 0.5 m/s.

For the first zone: $C_T = 0.2528$, $S_1 = -0.00642$
Thus, $\log(Y) = 0.2528 - 0.00642*24 = -1.288$
or, $Y = 0.2757$, thus, temperature at the end of first zone = 10.6C
The coefficient for second zone: $C_T = 0.0075$, $S_1 = -0.0636$, $S_2 = -0.0324$
Equivalent time = 17.3 h
Time for calculations in zone 2 = 12 + 17.3 = 29.3 h
Thus, $\log(Y) = 0.0075 + (-0.0636 + 0.0324)*24 - 0.0324*29.3 = -1.622$
$Y = 0.1974$
Temperature at the end of second zone = 3.6C

Similar Procedure Can Be Obtained for Predicting the Mass Loss for the Same Example with a Relative Humidity of 90% During Both the Chilling Zones

First zone:
The coefficients: $C_M = -4.918$, $S_M = 0.643$
$\text{Log}(M_L) = -3.569$
Mass loss at the end of first zone = 0.0282 or 2.82%

Second zone:
The coefficients: $C_M = -4.895$, $S_M = 0.586$
Equivalent time = 31.4
Time for calculation in second zone = 31.4 + 12 = 43.4
$\text{Log}(M_L) = -3.38$
Mass loss at the end of chilling = 0.0341 or 3.41%

REFERENCES

BAILEY, C. and COX, R.P. 1976. *The Chilling of Beef Carcasses*, The Institute of Refrigeration, London, U.K.

CHOI, Y. and OKOS, M.R. 1986. Effect of temperature and composition on the thermal properties of foods. In *Food Engineering and Process Applications*, Vol. 1, (M. Le Maguer and P. Jelen, eds.) pp. 93–101, Elsevier Applied Science Publishers, London.

DAUDIN, J.D. and SWAIN, M.V.L. 1990. Heat and mass transfer in chilling and storage of meat. J. Food Eng. *12*, 95–115.

DRUMM, B., McKENNA, B.M. and JOSEPH, R.L. 1992. Line chilling of beef. 1. Predicting the temperature. J. Food Eng. *15*, 285–312.

KREITH, F. and BLACK, W.Z. 1980. *Basic Heat Transfer*. Harper & Row Publishers, pp. 237–271, New York.

MALLIKARJUNAN, P. and MITTAL, G.S. 1994. Heat and mass transfer during beef carcass chilling — modelling and simulation. J. Food Eng. *23*, 277–292.

MITTAL, G.S. and BLAISDELL, J.L. 1984. Heat and mass transfer properties of meat emulsion. J. Food Sci. Technol. *17*, 94–98.

SAS 1989. SAS/STAT® User's Guide, Ver. 6.04, Vol. 2, SAS Institute, Cary, NC.

THERMAL PROCESS SIMULATION OF CANNED FOODS UNDER MECHANICAL AGITATION[1]

J.G. BICHIER[2], A.A. TEIXEIRA[3], M.O. BALABAN[4] and T.L. HEYLIGER[2]

[2]*FMC Corporation*
Food Processing Systems Division
2300 Industrial Avenue, Box A
Madera, CA 93639

[3]*Agricultural Engineering Department*
P.O. Box 110570
[4]*Food Science and Human Nutrition Department*
P.O. Box 110370
University of Florida
Gainesville, FL 32611-0370

Accepted for Publication March 1, 1994

ABSTRACT

This paper describes how the distributed parameter conduction-heating numerical model was modified and tested to accurately predict the can center temperature for canned foods which exhibit combined heat transfer of pure conduction with added forced convection caused by mechanical agitation. This innovation will open the door to more widespread use of such mathematical models as part of the control system logic for making accurate adjustments to process conditions in response to unexpected retort temperature deviations on-line during thermal processing of canned foods in agitating retorts.

INTRODUCTION

Among the most important applications of heat transfer models in food processing is the design and evaluation of thermal processes used in the commercial sterilization of canned foods. Thermal processing consists of heating food containers in pressurized steam retorts at a constant retort temperature for prescribed lengths of time. These process times are calculated on the basis of achieving sufficient bacterial inactivation in each container to comply with public health standards and to insure that the probability of spoilage will be less than some minimum. Associated with each thermal process are

[1]Florida Agricultural Experiment Station Journal Series No.R-02944

Journal of Food Process Engineering **18** (1995) 17–40.

always some degradation of heat-sensitive vitamins and other quality factors that are undesirable. Because of these quality and safety factors, great care is taken in the calculation of these process times and in the control of time and temperature during processing to avoid either underprocessing or over-processing. The heat transfer considerations that govern the temperature profiles achieved within the container of food are critical factors in the determination of time and temperature requirements for sterilization.

These heat transfer considerations are also important in the development of mathematical models capable of predicting internal product temperature in response to unexpected changes in boundary conditions. If sufficiently accurate, such models could be used to predict the product temperature history at any specified location within the can for any set of processing conditions and container size. Thus, they would preclude the need to carry out repeated heat penetration tests in the laboratory or pilot plant for alternative process designs. A second advantage is that the retort temperature need not be held constant, but could vary in any prescribed manner throughout the process, and the model would predict the correct product temperature history at the can center or slowest heating location. This capability would be invaluable for simulating the process conditions experienced in continuous sterilizer systems, in which cans pass from one chamber to another experiencing a changing retort temperature at the can wall. Another important application of these models is in the rapid evaluation of an unscheduled process deviation, such as when an unexpected drop in retort temperature occurs during the process. The model could quickly predict the product center temperature history in response to such a deviation, and calculate the delivered sterilizing value for comparison with the target value specified for the product, as reported by Teixeira (1989). Datta *et al.* (1986) went one step further in proposing the use of such a heat transfer model in conjunction with a computer-based on-line control system in which the retort temperature would be continuously monitored and read as the boundary temperature at specified time intervals through thermocouples placed within the retort. The predicted can center temperature would then be continuously updated at each time step by a numerical solution of the heat conduction equation for a finite cylinder, and used to calculate the corresponding cumulative lethality (sterilization value) at each time step as well. The control logic would allow heating to proceed until the designated sterilization value was attained at the end of heating, regardless of unexpected deviations that might occur during the process.

A disappointing limitation of these control system concepts has been that the numerical heat transfer model upon which they rely is capable of predicting the product center temperature accurately only when the product heats by pure conduction. Unfortunately, most canned foods exhibit some degree of natural or forced convection during heating, particularly when handled through

rotary-type retorts, which impart mechanical agitation during the thermal process. In such cases the pure conduction-heating model is poor predictor of internal product temperature as shown by Teixeira *et al.* (1992). The explanation stems from the fact that the conduction-heating model only makes use of the slope of a heat penetration curve in order to derive a value for the thermal diffusivity. This allows the model to reproduce the correct slope when model-predicted temperatures are plotted on a semi-log heat penetration curve, but the model has no provision for taking into account the intercept, which is needed to correctly position the curve when forced convection takes place under mechanical agitation.

As a result of heating experiments with canned bentonite suspensions in an agitated water bath, Teixeira *et al.* (1992) showed that the semilog heat penetration curve produced by heating under agitation revealed a significant change in intercept as well as slope from the curve produced when heated still (near pure conduction). Further, when model-predicted temperatures were compared with experimentally measured temperatures, there was good agreement with the still cook, but significant error with the agitated cook that could be corrected by reporting the calculated temperatures after a constant time-shift. The time-shift, in turn, could be computed from the difference in the intercepts between the semilog heating curves for pure conduction and agitated cook having the same slope.

The work reported in this paper was an attempt to confirm the preliminary findings of Teixeira *et al.* (1992) by reviewing the basis of the time-shift concept in terms of heat transfer theory, and testing the modified numerical conduction-heating model on actual foods (canned tomato sauce) processed in an industrial pilot plant retort capable of simulating the commercial scale continuous rotary-cook retorts widely used in the U.S. food canning industry. Most importantly, the testing protocol was designed to challenge the model performance in response to unexpected retort process deviations by comparing predicted temperatures with measured temperatures under both constant and varying retort temperature with both still and agitated cooks.

METHODOLOGY

Modification of the Conduction Heating Model

The heat transfer model used throughout this work was first developed by Teixeira *et al.* (1969, 1975) for simulating the thermal processing of conduction-heated canned foods. The model is a numerical solution of the two-dimensional heat conduction equation for a finite cylinder, which describes the temperature distribution over time and space as follows:

$$\frac{\partial T}{\partial t} = \alpha\left[\frac{\partial^2 T}{\partial r^2} + \frac{1}{r}\frac{\partial T}{\partial r} + \frac{\partial^2 T}{\partial h^2}\right] \tag{1}$$

where T = temperature at any internal product location at any time
t = time
r = radial position in cylinder
h = vertical position in cylinder
α = thermal diffusivity;

with boundary condition:

$$T_{boundary} = T_R\ (t) \tag{2}$$

where T_R = retort temperature.

This boundary condition assumes an infinite heat transfer coefficient at the can surface, and is valid for most processes during their heating phases because of drop-wise steam condensation at the container surface. Although this is usually not true during the cooling phase when surface heat transfer coefficients are much lower, the resulting error in predicted temperatures and lethality is both insignificant and safe, since the model will predict slightly less lethality than is actually achieved during cooling (Teixeira *et al.* 1984).

Equation (1) is expressed in the form of finite differences for numerical solution by digital computer below:

$$\begin{aligned} T_{(ij)}(t+\Delta t) = T_{(ij)}^{(t)} &+ \frac{\alpha\Delta t}{\Delta r^2}\left[T_{(i-1,\,j)} - 2T_{(ij)} + T_{(i+1,\,j)}\right]^{(t)} \\ &+ \frac{\alpha\Delta t}{2r\Delta r}\left[T_{i-1,j)} - T_{(i+1,\,j)}\right]^{(t)} \\ &+ \frac{\alpha\Delta t}{\Delta h^2}\left[T_{(i,j-1)} - 2T_{(i,\,j)} + T_{(i,\,j+1)}\right]^{(t)} \end{aligned} \tag{3}$$

Where the finite differences are discrete increments of time and space defined as small fractions of process time and container height and radius (Δt, Δh, and Δr, respectively); i and j denote the sequence of radial and vertical increments away from the can wall and mid-plane.

The cylindrical container is imagined to be subdivided into volume elements which appear as layers of concentric rings having rectangular cross sections as illustrated in Fig. 1 for the upper half of the container. Temperature nodes are assigned at the corners of each volume element on vertical plane as shown in

Fig. 2 where i and j are used to denote the sequence of radial and vertical volume elements, respectively.

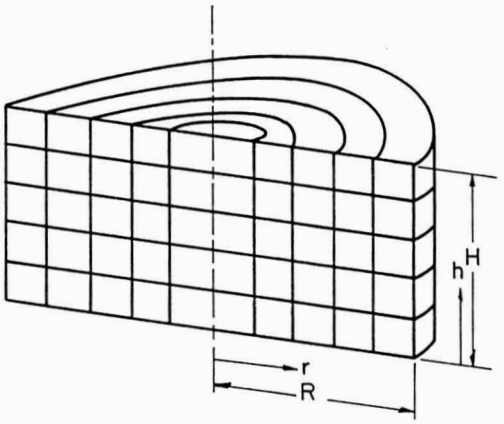

FIG. 1. SUBDIVISION OF CYLINDRICAL CONTAINER FOR APPLICATION OF FINITE DIFFERENCES

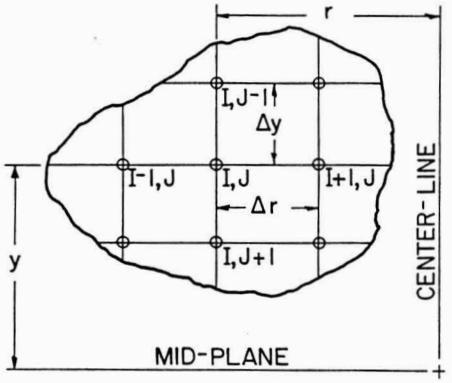

FIG. 2. LABELING OF GRID NODES IN MATRIX OF VOLUME ELEMENTS ON VERTICAL PLANE FOR COMPUTER ITERATION BY FINITE DIFFERENCES

By assigning appropriate boundary and initial conditions to all the temperature nodes (interior nodes set at initial product temperature, and surface nodes set at retort temperature), the new temperature reached at each node can be calculated after a short time interval that would be consistent with the thermal diffusivity of the product. This new temperature distribution is then taken to replace the initial one, and the procedure repeated to calculate the temperature distribution after another time interval. In this way, the temperature at any point in the container at any instant in time is obtained. At the end of process time, when steam is shut off and cooling water is admitted to the retort, the cooling process is simulated by changing the boundary conditions from retort temperature T_R to cooling temperature T_C at the surface nodes and continuing with the computer iterations described above.

Because of condensing steam on the can wall, the boundary condition assumes an infinite heat transfer coefficient at the can surface. The thermal diffusivity (α) is derived from the slope of a semilog plot of heat penetration test data (usually reported as the heating rate factor f_h) using Ball and Olson (1957) equations for finite cylindrical objects:

$$\alpha = \frac{.398}{\left[\frac{1}{R^2} + \frac{.427}{H^2}\right] f_h} \tag{4}$$

where f_h is the inverse slope of the straight line portion of the semilog heat penetration curve (time per log cycle).
R is the radius of the can
H is the half-height of the can.

In this way, the value obtained is more of an "apparent" thermal diffusivity that may also take into account the thermal capacitance of the can itself and small impedances to heat transfer at the boundary in addition to internal product resistance. Thus, if a heat penetration test is conducted under agitation, the resulting steeper slope of the semilog heat penetration curve will produce an apparent thermal diffusivity of higher value than that obtained under a still cook. This enables the model to predict the correct *rate* of internal temperature response to boundary conditions, but cannot account for the initial earlier response that is consistently observed with agitated cooks.

Considerable light can be shed on this issue by reviewing early food science literature on thermal processing of canned foods. Ball (1923, 1928) first attempted to derive a model for can center temperature based on the observation that the can center temperature approached the retort temperature logarithmically. When experimental time-temperature data were plotted on inverse

semilog paper to produce the heat penetration curves in Fig. 3, it was found that the data points were arranged in a curved line that become straighter as the heating time progressed. Both conduction and convection heating products were found to follow this elementary pattern as shown by the family of curves in Fig. 3.

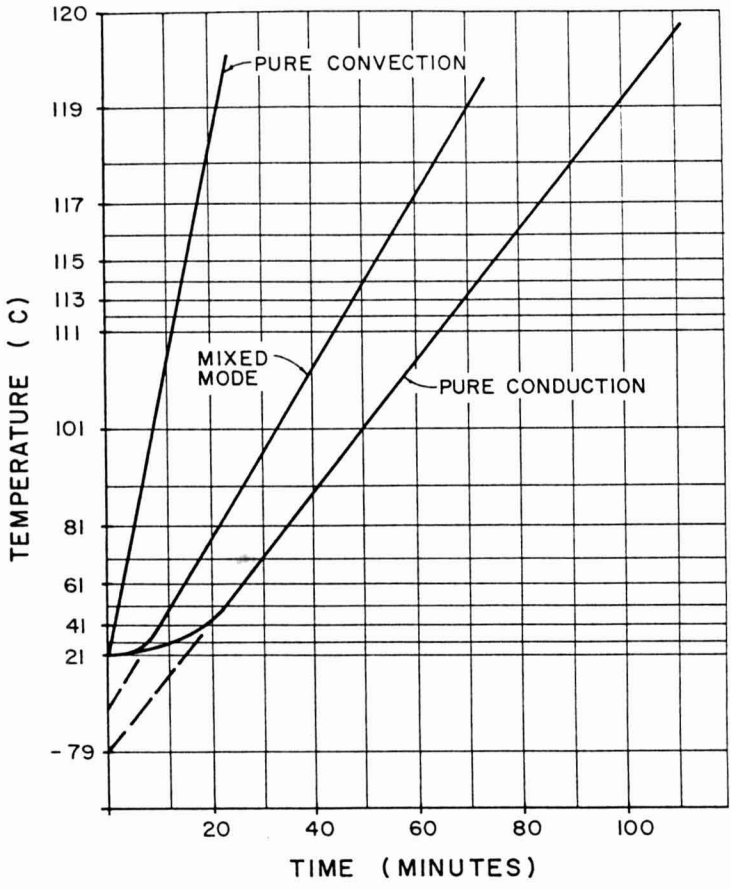

FIG. 3. HEAT PENETRATION CURVES FOR PRODUCTS WITH DIFFERENT HEATING CHARACTERISTICS

Ball's Formula is based on the equation of the straight line portion of the curves shown in Fig. 3, and can be given as:

$$\log[(T_R - T) / (T_R - T_o)] = - (1/f_h)\ t + \log j \qquad (5)$$

where T = product center temperature
T_R = retort temperature
T_o = product initial temperature
t = time
f_h = inverse slope of straight line (time per log cycle)
j = lag factor indicating intercept of straight line

The j-value can be calculated from the plot as follows:

$$j = (T_R - T_p) / (T_R - T_o) \qquad (6)$$

where T_p is the pseudoinitial temperature where the straight line portion of the curve intercepts the ordinate. Taking note that the curves in Fig. 3 are plotted on an inverted semilog graph with the top line labeled one degree below retort temperature, the j-values for each of the three curves shown can be calculated as follows for:

pure conduction: $j = 121 - (-79)/121 - 21 = 200/100 = 2.0$
forced convection: $j = 121 - 21/121 - 21 = 100/100 = 1.0$
mixed mode: $j = 121 - (-29)/121 - 21 = 150/100 = 1.5$

This range of j-values for foods in cylindrical cans is familiar to most food scientists. They recognize a j-value of 2 as pure conduction and a j-value of 1 as perfect mixing, and that most food products exhibit j-values in between 1 and 2.

If the numerical conduction model were used to simulate the original heat penetration test from which the thermal diffusivity had been obtained for a product with an intermediate j-value (mixed mode), and both predicted and experimental can center temperatures were plotted on a semilog graph, the results would appear as shown in Fig. 4. The significant observation to be made here is that the straight-line portions of both heat penetration curves lie parallel to each other, and that the temperature history predicted by the model is in error only by a constant time delay $\Delta t = (t_2 - t_1)$ that can be calculated from the j-value. Therefore, for the practical purpose of being able to use existing numerical heat conduction models for on-line process control, it may suffice to simply adjust the elapsed process time by this time delay factor in the computer program.

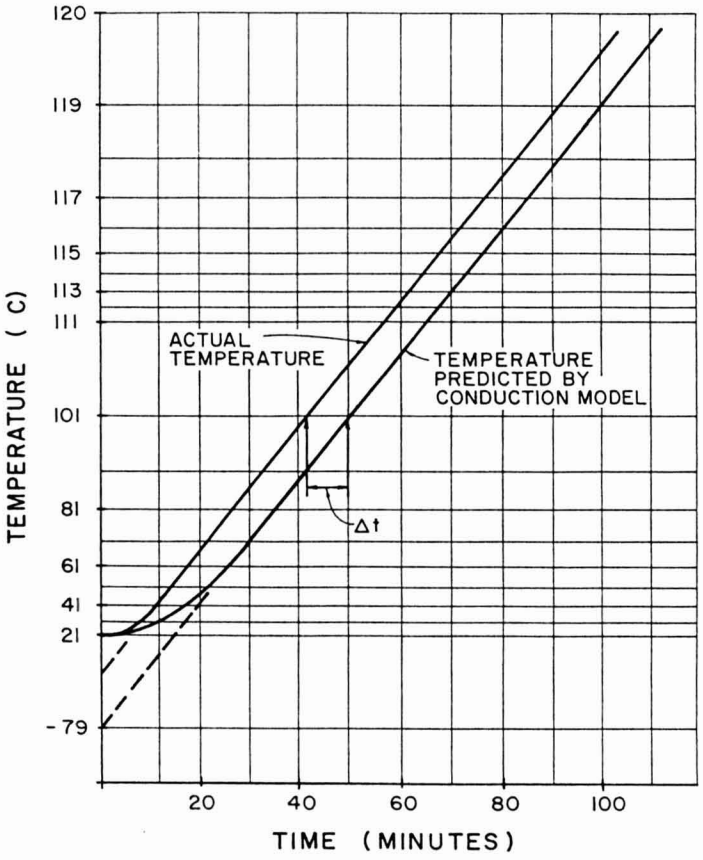

FIG. 4. HEAT PENETRATION CURVES FOR A FOOD PRODUCT EXHIBITING ADDED FORCED CONVECTION HEAT TRANSFER UNDER AGITATION (ACTUAL TEMPERATURE), AND THE CORRESPONDING PREDICTED TEMPERATURE WHEN THE SAME HEATING FACTOR (f_h) WAS USED IN TEIXEIRA'S PURE CONDUCTION MODEL

This time shift can be determined by rearranging the equation of the heat penetration curve (Eq. 5) to find time at initial temperature (T_o):

$$\text{Log}(T_{ret} - T_o) = \text{Slope} * t + \text{Log}(T_{ret} - T_{pi}) \quad (7)$$

$$t = f*Log\left(\frac{T_{ret}-T_{pi}}{T_{ret}-T_o}\right) = f*Log(j). \quad (8)$$

Therefore,

$$(t_2-t_1) = f\ Log(j_2) - f\ Log(j_1) = Log\ (j_2/j_1). \quad (9)$$

Since $j_2 = 2.0397$ for finite cylinders under pure conduction (Ball and Olson 1957), then

$$(t_2-t_1) = f\ Log(2.0397/j_1) \quad (10)$$

The time shift derived above was programmed into Teixeira's algorithm to obtain the modified heat-conduction model. Since the time shift remains constant throughout heating, the value of the time shift is calculated at the beginning of the program before the iterative routine that predicts the center temperature T(t) from Eq. (3). After the predicted temperature is calculated by the conduction model, the simulation time at which T(t) is reached is displayed as elapsed time minus time shift in the output file as shown on the flow diagram in Fig. 5. The same procedure is used during cooling, but with a separate cooling time shift calculated from the cooling lag factor.

Additionally, once the temperature history at the cold spot can be accurately predicted by the numerical computer model, the degree of sterilization or bacterial lethality (F_o) can be calculated from this temperature history using the General Method by numerical integration of the following expression over time using the trapezoidal rule:

$$F_o = \int_o^t 10^{\left[\frac{T-Tref}{Z}\right]} dt \quad (11)$$

where: F_o is process lethality in minutes at Tref,
T is temperature at any point in time,
Tref is the process reference temperature (usually 121C),
Z is a factor which relates the temperature dependency of the first order rate constant, and is expressed as the temperature difference required for a ten-fold change in first order rate constant.

Design of Experiments for Testing Model Performance

The experimental portion of this work was designed around the comparison of measured temperatures from industrial pilot plant tests with the predicted

temperatures from the modified heat transfer model. The first test was used to determine heating and cooling factors (f and j values), and to evaluate the model performance for normal processes (constant retort temperatures). The data from subsequent tests were used to evaluate model performance under process deviations (varying retort temperatures), which are described in more detail in the next section.

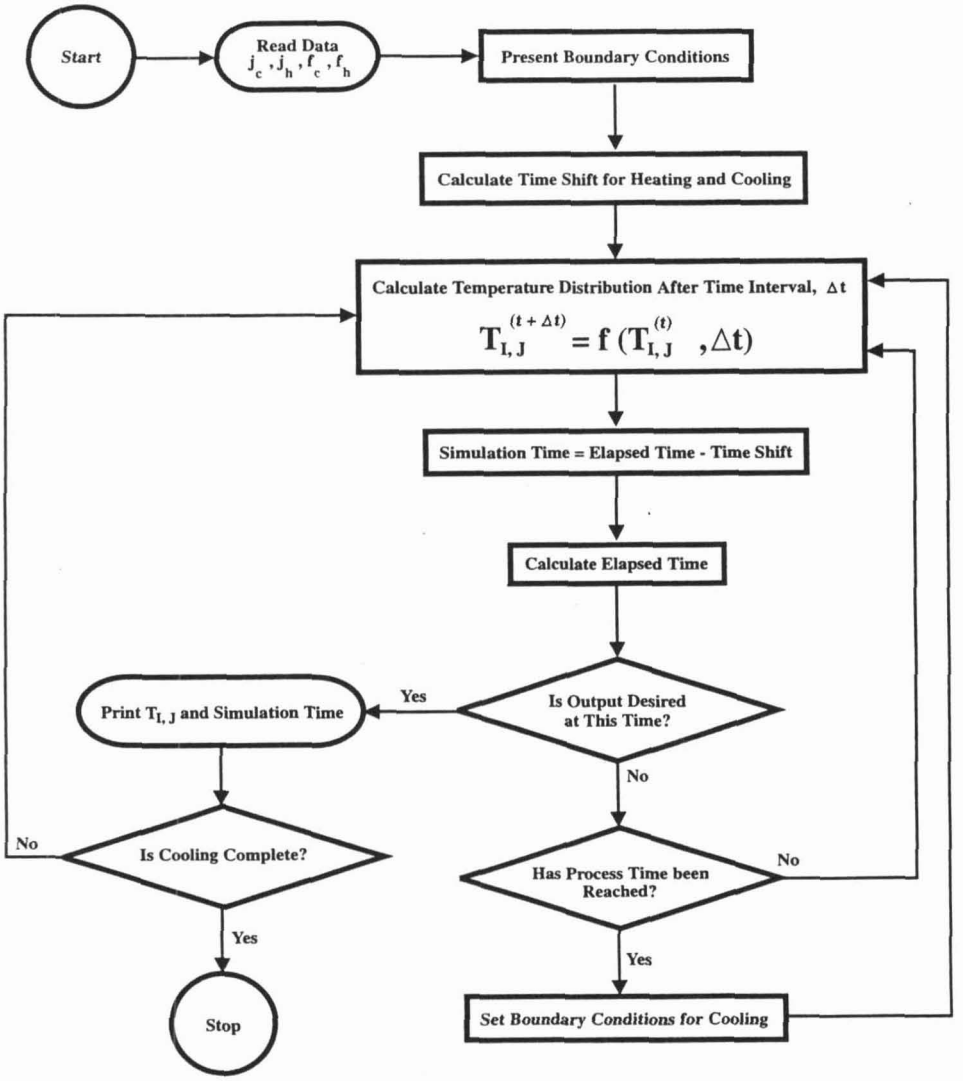

FIG. 5. FLOW DIAGRAM SHOWING HOW TIME SHIFT WAS INCORPORATED INTO THE COMPUTER PROGRAM OF TEIXEIRA *ET AL.* (1969)

A total of 33 runs were made in an FMC Steritort (an instrumented laboratory retort capable of simulating a continuous rotary cooker) at the FMC Food Processing Systems Division Laboratory in Madera, CA using tomato sauce (5.9% solids content). At this concentration the tomato sauce would exhibit near conduction heat transfer under still cook conditions, while exhibiting added forced convection heat transfer under agitation. At least three replicated runs of the following conditions were carried out in the Steritort:

(1) still cook, no temperature deviations (constant retort temperature)
(2) agitated cook, no temperature deviations (constant retort temperature)
(3) still cook, with temperature deviations (varying retort temperature)
(4) agitated cook, with temperature deviations (varying retort temperature).

In the preparation of samples for these experiments, bulk concentrate tomato puree at 13.6% solids content was diluted to 5.9% (Kern Industry, City of Industry, CA 91749, 6 lbs 10 oz cans). The prepared batch was enough to fill 27 300 × 407 cans (3 in. diameter by 4 7/16 in. high) leaving 1/4 in. head space. Nine cans were processed in the Steritort at one time in each of three replicate heat penetration tests. Heat penetration data were collected with CNS copper-constantan thermocouples using C-9 locking receptacles and S-28 rotary contactors (Ecklund-Harrison Technologies, Inc., Ft. Myers, FL). Thermocouples were placed to read the temperature at the geometric center of the can, and were calibrated against a mercury-in-glass thermometer during the preheat of the Steritort at 121.1C. The signals from thermocouples were collected using a Kaye Digistrip II process monitor (Kaye Instruments, Inc., Bedford, MA). Temperature-time data from the Kaye were transmitted a PC-computer for spreadsheet manipulations.

The runs under constant retort temperature were used to generate semilog heat penetration curves, from which the heat penetration factors (f_h, f_c, j_h, j_c) could be obtained. These factors were defined in Eq. (4) and (5); they describe the slopes and intercepts of the straight line portion of the semilog heat penetration and cooling curves, and were determined by linear regression of the straight line portion of semilog curves of heat penetration tests. For accurate modelling of the cooling portion of the process, the cooling rate factor was simply assumed equal to the heating rate factor ($f_c = f_h$), while the cooling lag factor (j_c) was determined by an iterative search routine which minimized the error between predicted and measured can center temperatures during the transition of the boundary condition from hot steam to cool water at the can surface. This technique was recommended by Manson (1992) as an effective and practical means of dealing with the mathematical discontinuity which occurs during the sudden transition from heating to cooling, and the nonuniform temperature distribution within the product at that time.

During these heat penetration tests, it was also important that the retort be brought up to processing temperature as quickly as possible in order to achieve a close approximation to a step change in boundary condition at the beginning of heating, and likewise with the introduction of cooling water at the beginning of cooling. Only when obtained under such step-change boundary conditions do the heating factors truly represent the heating characteristics of the product-container system under agitation. When subsequently used in a mathematical heat transfer model, they allow accurate prediction of the internal temperature in response to the slower boundary condition changes that occur in large production-scale retorts.

RESULTS AND DISCUSSIONS

Heating and Cooling Factors

Raw data taken from one of the still-cook heat penetration tests are presented graphically for 4 separate cans in Fig. 6a. Similarly, raw data from one of the agitated cook heat penetration tests (5 separate cans) are presented in Fig. 6b. These data clearly reveal how the can center temperatures behaved

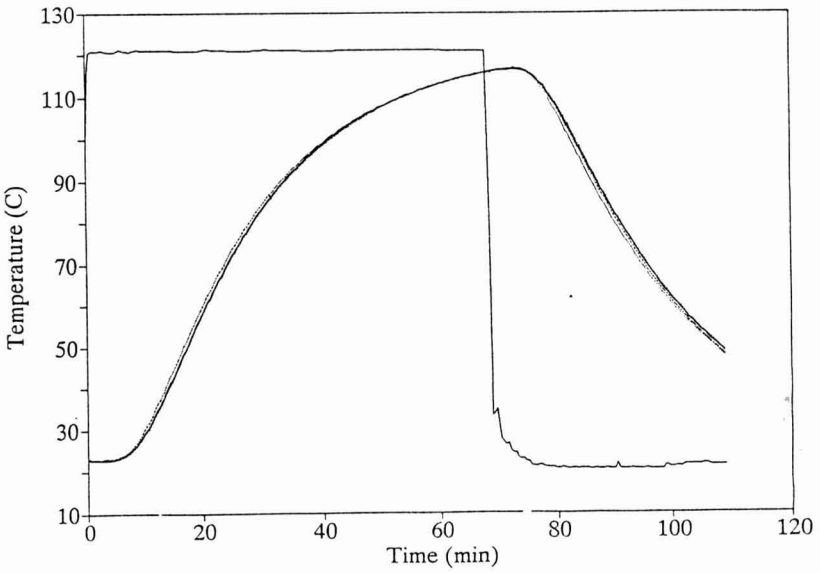

FIG. 6a. TEMPERATURE-TIME PROFILES OF RAW DATA TAKEN FROM 4 SEPARATE CANS (300 × 407) OF TOMATO SAUCE DURING HEAT PENETRATION TEST UNDER STILL COOK

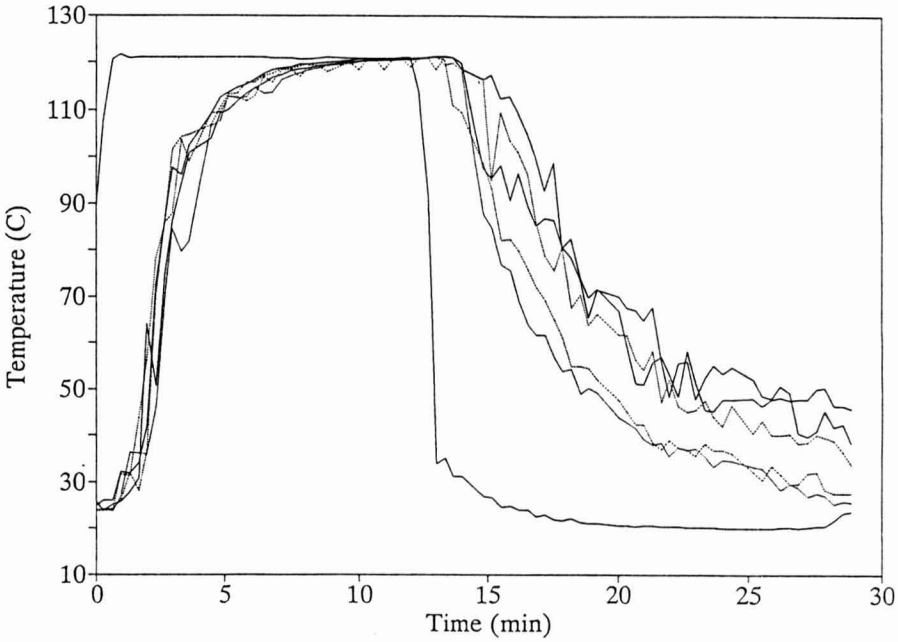

FIG. 6b. TEMPERATURE-TIME PROFILES OF RAW DATA FROM 5 SEPARATE CANS (300 × 407) OF TOMATO SAUCE DURING HEAT PENETRATION TEST UNDER AGITATED COOK

much more smoothly with less variability under still cook than under agitated cook process conditions. Such variation under rotary cooker type retort systems is not uncommon, since agitation is intermittent and depends upon rolling and sliding coefficient of friction between can and reel surface, which can vary from can to can and spline to spline. Also, the cans were filled manually, which allowed the possibility of variation in head space. The can-to-can variability in heating and cooling factors under agitated cook conditions was dealt with by determining the extent of variability and choosing the factors from the worst-case heat penetration data (slowest heating and fastest cooling), resulting in least sterilization value.

Heating factors (f_h and j_h) were obtained from linear regression of the straight-line portion of the semilog heat penetration curves for each of the test can data sets shown in Fig. 6a and 6b, and are tabulated in Tables 1a and 1b along with values calculated for apparent thermal diffusivity (α) for still cook

and agitated cooks, respectively. Goodness of straight-line fit with actual data points is given by the correlation coefficient (R^2), and can be seen to be much better under still cook-processing (0.9999) than under agitated cook processing (0.95–0.99), as would be expected because of the intermittent nature of the agitation mode. The sterilization value was calculated by numerical integration of the temperature-time history of each test can, using trapezoidal rule on Eq. (11), and the data set producing the least sterilization value (worst case) was chosen for subsequent use in the model. These data sets are shown in Table 1c, along with the cooling rate factors (f_c) which were taken equal to the heating rate factors (f_h) and the cooling lag factors (j_c) which were determined from the iterative search routine. It can be seen how the apparent thermal diffusivity (α) of the product increased ten-fold as a result of mechanical agitation.

TABLE 1a.
REPLICATE HEATING RATE FACTORS (f_h), LAG FACTORS (j_h) AND APPARENT THERMAL DIFFUSIVITIES (α) FOR RETORT UNDER STILL COOK FROM HEAT PENETRATION DATA SHOWN IN FIG. 6a

can	f_h (min)	j_h	R^2	α(in^2/min)
TC6	44.532	1.709	0.99996	0.0167
TC8	45.221	1.687	0.99995	0.0165
TC9	44.440	1.750	0.99996	0.0168
TC10	44.933	1.754	0.99997	0.0166

TABLE 1b.
REPLICATE HEATING RATE FACTORS (f_h), LAG FACTORS (j_h) AND APPARENT THERMAL DIFFUSIVITIES (α) FOR RETORT UNDER AGITATED COOK WITH A REEL SPEED OF 5 RPM FROM HEAT PENETRATION DATA SHOWN IN FIG. 6b

can	f_h (min)	j_h	R^2	α(in^2/min)
TC6	4.455	1.461	0.9475	0.168
TC7	4.129	2.025	0.9904	0.181
TC8	4.173	1.440	0.9646	0.179
TC9	3.965	2.034	0.9900	0.188
TC10	3.698	2.034	0.9900	0.202

TABLE 1c.
HEATING AND COOLING FACTORS FOR THE CAN PRODUCING THE LEAST STERILIZATION VALUE (F_o) IN A HEAT PENETRATION TEST[b]

Product/ Process	f_h (min)	j_h	f_c	j_c	α (in^2/min)
Tomato sauce/ Static cook	45.22 ±0.64[a]	1.69 ±0.06	45.22	1.65	0.0165
Tomato sauce/ Agitated cook	4.17 ±0.64	1.44 ±0.06	4.17	1.93	0.179

[a] ± Indicates the variation of factors within the same test.
[b] Values were taken from "worst case" data set for conservative use of the model, and are not values.

Model Performance Under Constant Retort Temperature

Figures 7a and 7b compare model-predicted center temperature with measured center temperature in response to a steady boundary condition (constant retort temperature) under still cook and agitated cook processes, respectively. As can be seen from Fig. 7a, agreement between predicted and measured temperature in the lethal range (above 100C) is extremely close and hardly distinguishable under still cook conditions. For the agitated cook process shown in Fig. 7b, slight disagreement can be found, but only because of the erratic nature of the actual measured temperature profile, as explained earlier. In most cases, predicted center temperatures agreed within one-half centigrade degree of measured temperature within the lethal range apart from the erratic nature of agitated product temperatures. Disagreement between model predictions and actual data near the beginning of heating and toward the end of cooling are to be expected because the linear regression and iterative search routine used to obtain heating factors was deliberately designed to achieve accuracy in the high lethal temperature range late in the heating phase and early in the cooling phase where bacterial lethality is rapidly accumulated (temperatures above 100C).

More importantly, the model estimation of cumulative lethality (F_o) was close to, but always slightly below the F_o attained by the actual data (Tables 2a, 2b); hence, the simulation model is safe and conservative. Among the data collected, the case with the greatest error, that is the case in which the difference between actual and predicted F_o was the largest, was approximately 5% for predictions under static conditions and 12% for predictions under agitated conditions.

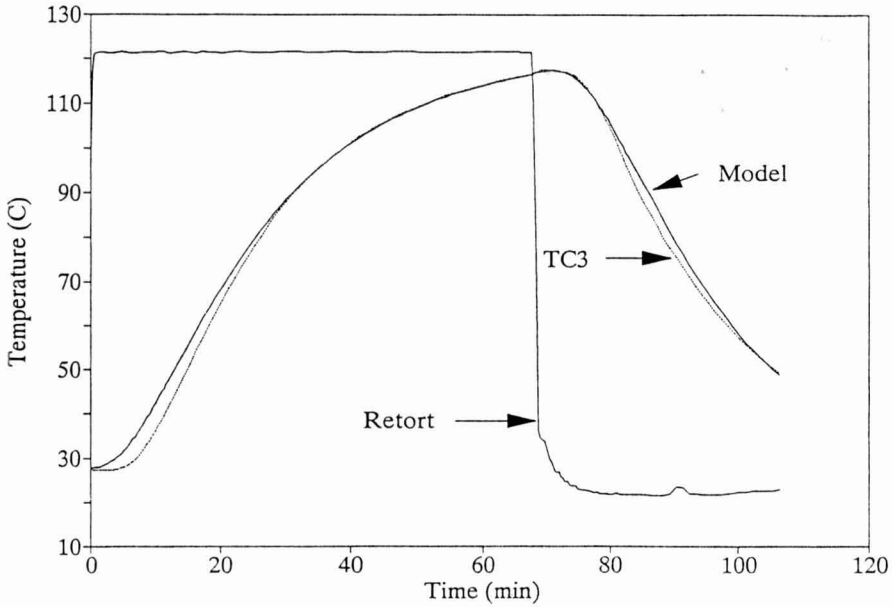

FIG. 7a. COMPARISON BETWEEN PREDICTED (MODEL) AND ACTUAL (TC3) TEMPERATURES FOR TOMATO SAUCE (5.9% SOLID CONTENT) PACKED IN 300 × 407 CANS UNDER STILL COOK

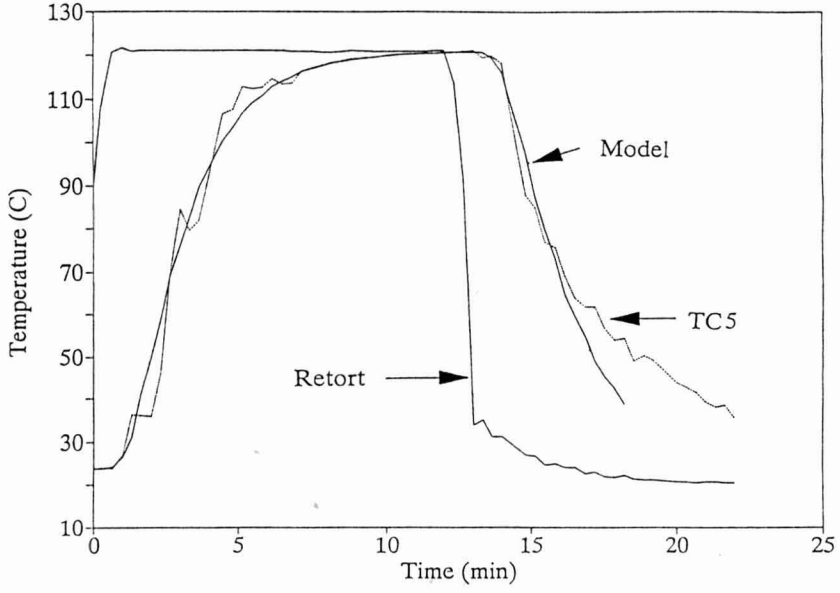

FIG. 7b. COMPARISON BETWEEN PREDICTED (MODEL) AND ACTUAL (TC5) TEMPERATURES FOR TOMATO SAUCE (5.9% SOLID CONTENT) PACKED IN 300 × 407 CANS UNDER AGITATED COOK WITH A 5 RPM REEL SPEED

TABLE 2a.
COMPARISON OF PROCESS LETHALITY CALCULATED FROM THE ACTUAL DATA WITH THE LETHALITY PREDICTED BY THE MODEL UNDER STILL COOK CONDITIONS

Data from Test #1	Actual F_o (min)	Predicted F_o (min)	Percentage Difference (%)
TC2	5.97	5.67	5.03
TC3	6.05	5.89	2.64
TC4	5.92	5.87	0.84
TC5	5.97	5.81	2.68
TC6	5.77	5.61	2.77
TC8	5.56	5.39	3.06
TC9	5.77	5.70	1.21
TC10	5.82	5.75	1.20
Avg.	5.85	5.71	2.43

TABLE 2b.
COMPARISON OF PROCESS LETHALITY CALCULATED FROM THE ACTUAL DATA WITH THE LETHALITY PREDICTED BY THE MODEL UNDER AGITATED COOK CONDITIONS

Data from Test #4	Actual F_o (min)	Predicted F_o (min)	Percentage Difference (%)
TC2	5.42	5.01	7.56
TC3	4.71	4.56	3.18
TC4	6.55	6.12	6.56
TC5	7.61	6.70	11.96
TC6	5.89	5.48	6.96
TC7	6.61	6.02	8.93
TC8	5.56	5.39	3.06
TC9	6.06	5.70	5.94
TC10	7.00	6.44	8.00
Avg.	6.16	5.71	6.91

Model Performance in Response to Retort Temperature Deviation (Unsteady Boundary Condition)

The most challenging test of the model was to examine its performance in response to an unsteady boundary condition in which the retort temperature was made to deviate in a random fashion as might occur during loss and regain of steam pressure several times during a cook. Results from such a test under both still cook and agitated cook are shown in Fig. 8a and 8b, respectively. During these tests, the retort temperature was deliberately lowered for a period of time and then recovered twice during the process. The first deviation occurred early in the process when the product center temperature was still below the retort temperature during the deviation. The second deviation occurred relatively late in the process when the product center temperature could end up higher than the retort (boundary) temperature during the deviation. The results show remarkably good agreement between predicted and measured responses to each deviation under both still and agitated cooks.

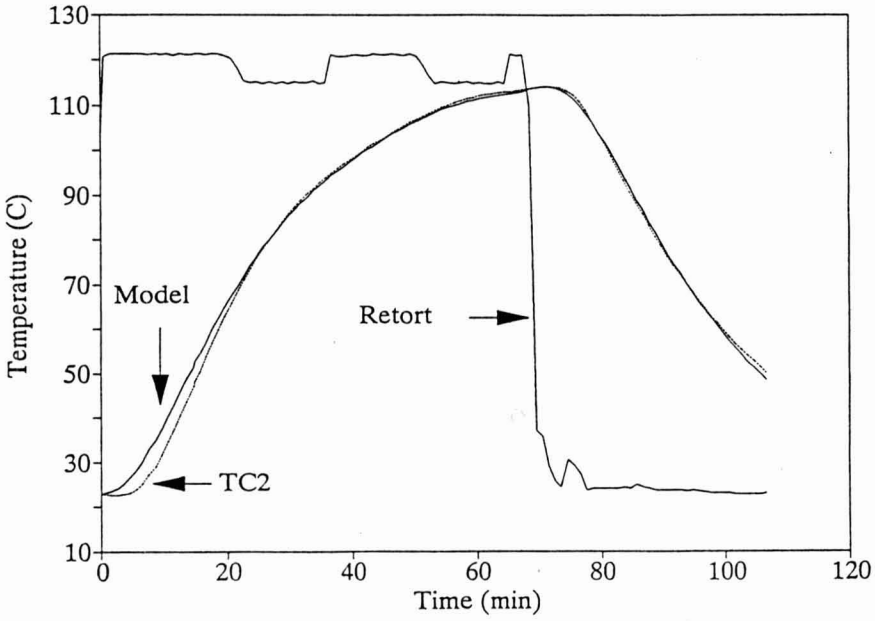

FIG. 8a. COMPARISON BETWEEN PREDICTED (MODEL) AND ACTUAL (TC2) TEMPERATURES FOR TOMATO SAUCE (5.9% SOLID CONTENT) PACKED IN 300 × 407 CANS UNDER STILL COOK WHEN −6C DOUBLE DEVIATIONS WERE SCHEDULED FOR 10 MIN EACH AT DIFFERENT TIMES DURING THE PROCESS

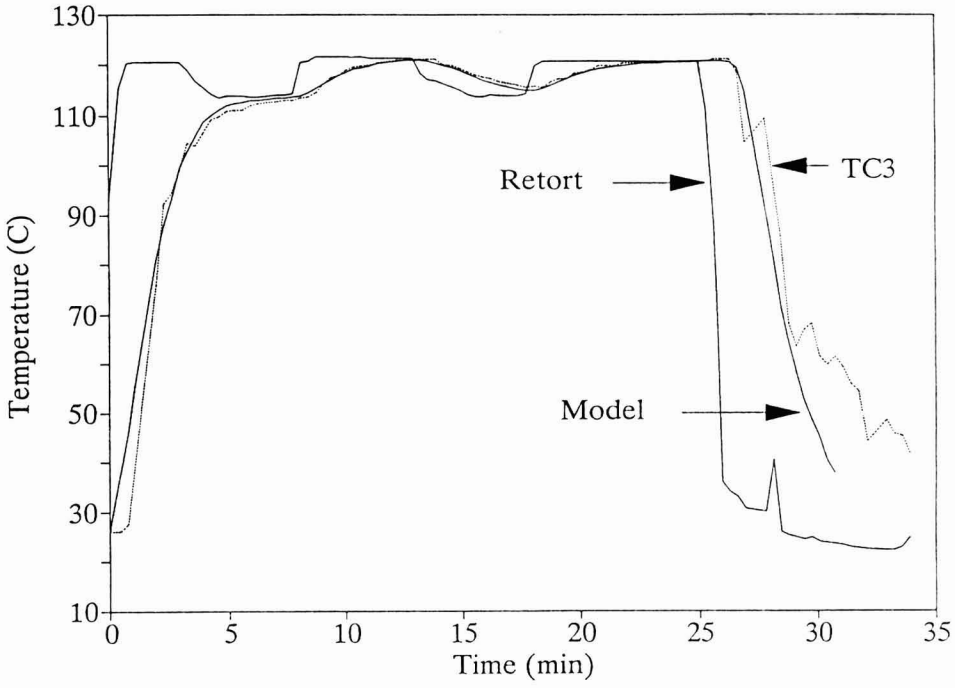

FIG. 8b. COMPARISON BETWEEN PREDICTED (MODEL) AND ACTUAL (TC3) TEMPERATURES FOR TOMATO SAUCE (5.9% SOLID CONTENT) PACKED IN 300 × 407 CANS UNDER AGITATED COOK WITH A 5 RPM REEL SPEED WHEN −6C DOUBLE DEVIATIONS WERE SCHEDULED FOR 10 MIN EACH AT DIFFERENT TIMES DURING THE PROCESS

Also, a predicted process lethality was calculated from the temperature-time history predicted by the model, and compared with the actual process lethality calculated from the measured temperature-time history on Table 3 for each of the test runs with process deviations reported here. Since the calculation of lethality is dependent upon the temperature history, comparing how closely the predicted lethality is to the actual lethality for the process is a method of evaluating the accuracy of the model. The lethality predicted for the still cook shown in Fig. 8a was 3.5 min, while the actual lethality was 3.7 min; thus agreeing within 5% of each other. Similarly, the percentage difference calculated for the double deviation under the agitated cook shown in Fig. 8b is 10% for a predicted lethality of 11.6 min and an actual lethality of 12.9 min.

TABLE 3.
STERILIZATION LETHALITY (F_o) CALCULATED FROM MODEL PREDICTED AND ACTUAL MEASURED TEMPERATURE HISTORIES AT PRODUCT CENTER FOR STILL COOK AND AGITATED COOK PROCESSES SHOWN IN FIG. 8a AND 8b

Process / F_o	Model	Actual	Error
Still Cook (Fig. 7a)	3.5	3.7	5%
Agitated Cook (Fig. 7b)	11.6	12.9	10%

Interesting observations can be made upon closer examination of the lethal temperature range under agitation. Figure 9 is a zoom-up of Fig. 8b in the neighborhood of the two deviations, which magnifies the difference between the model performance and actual measured temperature data under agitated cook. In the first deviation, the lowered retort temperature simply reduced the temperature gradient (driving force) across the product, resulting in slow-down of the heating rate. Thus, the internal center temperature continued rising although at a slower rate. In the second deviation, the retort temperature fell below the internal product center temperature, thus reversing the temperature gradient across the product and causing cooling of the product as seen by the responding decline in product center temperature.

Note, however, that in both cases the actual product temperature responded more slowly than the model. This slower response was likely caused by changes in the surface heat transfer coefficient. Under normal processing the condensation of steam on the outside surface of the can gives a very high heat transfer coefficient. This was the basis for assuming that the outside heat transfer coefficient (h_o) is infinite. Hence, in the conduction model the nodes for the can wall are assigned the retort temperature, and, thus, the model makes no provision for an outside heat transfer coefficient in its numerical solution of the transient heat conduction equation. Therefore, any change in h_o would be invisible to the model. When deviations in retort temperature occur, such as a temporary loss of steam, the outside heat transfer coefficient may significantly decrease due to the temporary absence of film condensation. Such a decrease reduces the rate of heat transferred to the can. Since the model assumes infinite h_o, it would predict faster can center temperature responses to the deviation than the corresponding actual data. Hence, two distinct cases of temperature prediction would result from changes in h_o:

(1) If the temperature of the can center is lower than the retort temperature during the deviation, the model will overpredict the center temperature, as shown in Fig. 9 (first deviation).
(2) If the temperature of the can is higher than the retort temperature, the model will underpredict the center temperature as shown in Fig. 9 (second deviation).

It is also important to note that these differences are not perceptible in the case of the still cook process because heat transfer within the product occurs predominantly by pure conduction, which considerably dampens the product center temperature response to changes at the boundary.

Since the response curve of the heat transfer model would be used to calculate the cumulative lethality or sterilizing value at the center of the product

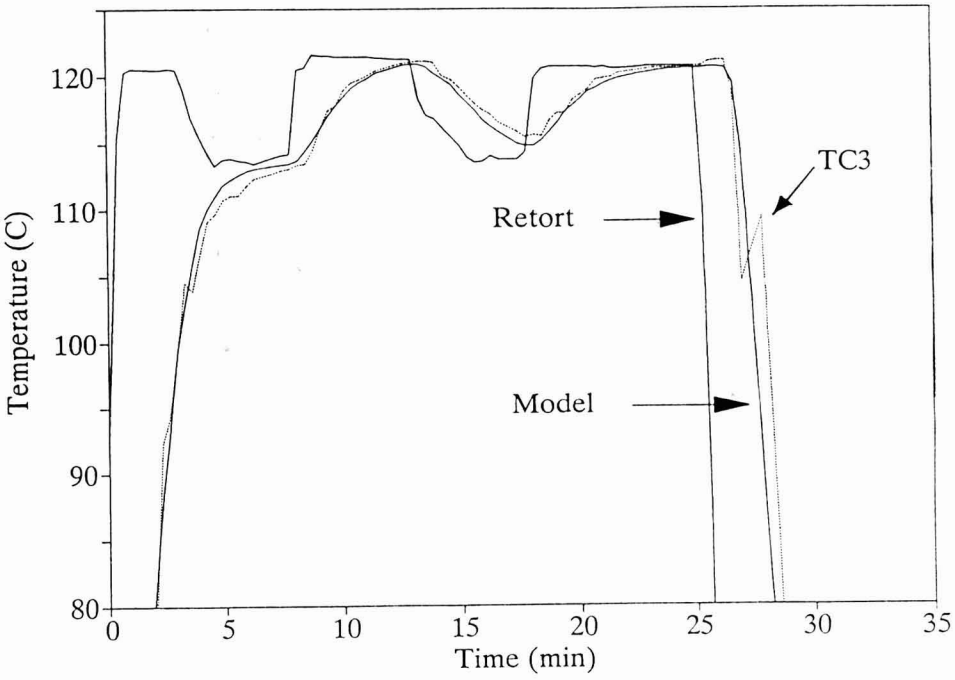

FIG. 9. ZOOM-UP OF FIG. 8b IN THE LETHAL TEMPERATURE RANGE TO MAGNIFY DIFFERENCES BETWEEN MODEL RESPONSE AND ACTUAL TEMPERATURES

for determination of process efficacy, it is important to understand how these small differences between model response and actual data would affect lethality calculations. It is in this regard (lethality) where there are important differences between the two types of deviations. In the first case, the model would predict higher temperatures than actual, and thus overpredict lethality, while in the second case the model would predict lower temperatures than actual and thus underpredict lethality. In order to minimize risk to public safety, the use of a model should be such that all known error should lead to an underprediction of lethality as a safety factor. Here, the thermal inactivation kinetics of bacterial spores works in favor of the model, since the rate of thermal inactivation increases exponentially with temperature in the lethal range (above 100C). Therefore, differences in calculated lethality will be significant only when internal product temperature is high in the lethal range when deviations cause the type 2 response error on the safe side. Type 1 response errors (on the unsafe side) occur when internal product temperature is relatively low in the lethal range where lethality accumulates very slowly and errors are likely to be insignificant.

CONCLUSION

A numerical conduction-heating model was modified so that it would accurately predict the internal product center temperature in response to any dynamic surface temperature history for products exhibiting a range of heat penetration characteristics from perfect mixing to pure conduction. Such a model may become a key component of a new generation of intelligent batch retort control systems capable of correcting unexpected process deviations on-line by automatically extending cook time to assure final delivered sterilization value. The modification of the model accounts for any degree of combined conduction and convection heat transfer in order to accurately predict the temperature profile of a specific point in canned foods exposed to either still or agitating retort systems. The computer model estimates the center temperature of the can, assuming a purely conductive substance described by the heating rate factor (f_h), but whose reaction to changes in the heating medium is advanced in time to compensate for a reduced lag factor (j), which is a measure of the amount of forced convection induced by mechanical agitation. Testing of model performance with a fully instrumented industrial pilot plant retort under constant temperature revealed that the model predicted center temperatures within one-half centigrade degree of actual measured temperatures apart from the erratic nature of an agitated cook (rotary retort at 5 RPM). The model also performed well in response to multiple retort temperature deviations as a deliberate challenge to unsteady boundary conditions.

ACKNOWLEDGMENT

The authors wish to acknowledge the FMC Corporation Food Processing Systems Division in Madera, CA; the Florida High Technology Industry Council in Tallahassee, FL; and the Florida Agricultural Experiment Station of the University of Florida's Institute of Food and Agricultural Sciences for support of this work.

REFERENCES

BALL, C.O. 1923. Thermal process time for canned foods. Bull. Natl. Resources Council 7, part 1.

BALL, C.O. 1928. Mathematical solution of problems on thermal processing of canned food. Univ. Calif. Press. Berkley Pub. Health *1*(2), 15–245.

BALL, C.O. and OLSON, F.C.W. 1957. *Sterilization in Food Technology*, McGraw-Hill, New York.

DATTA, A.K., TEIXEIRA, A.A. and MANSON, J.E. 1986. Computer-based retort control logic for on-line correction of process deviations. J. Food Sci. *51*(2), 480–483, 507.

MANSON, J.E. 1992. A New Approach to Determining Product Heating Factors from Heat Penetration Data, Tech. Knowledge, Bull. #201 Technical, Inc., Metaire, LA.

TEIXEIRA, A.A. 1989. Computer simulation of thermal processing for canned food sterilization, Part V. In *Food Properties and Computer-Aided Engineering of Food Processing Systems*, (R.P. Singh and A.G. Medina, eds.) pp. 543–552, NATO ASI Series E: Applied Science-V1, Kluwer Academic Publishers, London.

TEIXEIRA, A.A., DATTA, A.K., ADAMS, J.P. and PETERSON, W.R. 1984. Surface heat transfer considerations during immersion water cooling of retorted foods. Proc. 3rd Int. Cong. on Engineering and Food, Dublin, Ireland, Vol. I, Ch. 3. Elsevier Applied Science Publishers, Ltd., Barking, Essex, England.

TEIXEIRA, A.A., DIXON, J.R., ZAHRADNIK, J.W. and ZINSMEISTER, G.E. 1969. Computer optimization of nutrient retention in thermal processing of conduction-heated foods. Food Technol. *23*(6), 137–142.

TEIXEIRA, A.A., TUCKER, G.S., BALABAN, M.O. and BICHIER, J. 1992. Innovation in Retort Control System for Food Canning Operations. In *Advances in Food Engineering I*, (R.P. Singh and M.A. Wirakartakusumah, ed.) CRC Press, Boca Raton, FL.

TEIXEIRA, A.A., ZINSMEISTER, G.E. and ZAHRADNIK, J.W. 1975. Computer simulation of variable retort control and container geometry as possible means of improving thiamine retention in thermally-processed foods. J. Food Sci. *40*(3), 656–659.

DETERMINATION OF HEAT TRANSFER COEFFICIENTS DURING DRYING OF FOODSTUFFS

C. RATTI and G.H. CRAPISTE

PLAPIQUI (UNS-CONICET)
12 de octubre 1842
8000 - Bahía Blanca, Argentina

Accepted for Publication May 26, 1994

ABSTRACT

Heat transfer coefficients during drying of foods were evaluated from drying data and heat and mass balances. Experimental drying curves for slices and cylinders of potato, apple and carrot were obtained in a laboratory dryer under different drying conditions. The specific heat of the foodstuffs was measured as a function of water content and modelled through a linear relationship. Experimental heat transfer coefficients were correlated by the dimensionless expression $Nu_D = 0.249\ Re_D^{0.64}$ *and compared with predictions of different equations.*

INTRODUCTION

Modelling the drying of food particles is a complex problem involving simultaneous mass and energy transport in a hygroscopic system which shrinks during the process. Convective transfer coefficients are one of the most critical parameters required for the analysis and simulation of the process. Drying curves have generally two well-defined regions: the constant rate and falling rate periods. The constant rate period is characterized by an almost free water evaporation from the surface of the solid and may be predicted by the following heat and mass transfer equations:

$$n_w = k_g\ (p_{ws} - p_{wg}) \tag{1}$$

$$m_s(1+X)C_p\frac{dT}{dt} = h_g A_s(T_g - T) - n_w A_s \Delta H_s \tag{2}$$

Journal of Food Process Engineering **18** (1995) 41–53.

The water mass flux n_w can be expressed in terms of the water content on dry basis X as:

$$n_w = \frac{m_s}{A_s}\frac{dX}{dt} \tag{3}$$

The falling rate period is an extremely complex phenomenon, not perfectly understood, where the control for mass transfer generally takes place inside the particle. Solution of the partial differential equations that represent the heat and mass transfer during this period demands important and time-consuming calculations, particularly when the effect of shrinkage and the dependence of properties with water content and temperature are taken into account. However, in most practical situations the energy transport is not appreciably affected by the change in mass transfer control, the temperature profile can be assumed rather flat and Eq. (2) remains valid for the falling rate period.

Dependable values of heat transfer coefficients are needed to obtain accurate predictions of temperature of the solid during drying. Knowledge of temperature is very important, not only because of its strong coupling with the water content partial differential equation, but also as a control in dealing with heat sensitive materials. On the other hand, mass transfer coefficients can be evaluated from heat transfer coefficients with great confidence.

Heat transfer coefficients have been widely studied for different physical situations, particle geometry, types of fluid and regimes of fluid flow (Perry and Chilton 1973; Treybal 1980; Welty *et al.* 1984). Whitaker (1972) has reviewed the various correlations for heat transfer, including those for fluids flowing around submerged objects. Loncin and Merson (1979) presented several expressions and their application in food processing. Available correlations for heat transfer coefficients under forced convection are generally represented in terms of the Nusselt, Reynolds and Prandlt numbers as:

$$Nu = C\, Re^n\, Pr^b \tag{4}$$

Use of standard correlations is a common practice in drying of foodstuffs. This practice is justified by the fact that the coefficients theoretically depend on the geometry of the solid and the characteristics of the fluid regardless of the product being processed. Nevertheless, the validity of these equations as they apply to drying of foods has not been fully established. A comparative study between heat transfer coefficients determined from experimental drying data and those presented in the literature might be of primary interest.

The purpose of this work was to determine the heat transfer coefficients during dehydration of some foodstuffs, taking into account the effect of water evaporation, shrinkage and changes in properties. A suitable correlation of the experimental data in terms of dimensionless numbers is presented and a comparison with predictions from previous equations has been done.

MATERIALS AND METHODS

Drying Curves

Experimental drying curves during dehydration of individual particles of white potato, Red Delicious apple and carrot were carried out in a laboratory scale dryer. Samples were cut in two different geometrical shapes: slices (4 cm in diameter by 1 cm in height) and cylinders (1 cm in diameter by 5 cm in height).

The laboratory dryer consisted in a small drying chamber with a closed loop system in which air was recirculated by a controlled-velocity fan. The air flowed through a electrical heating system connected to a temperature controller. Relative humidity was fixed saturating the air as it bubbled through a saturated salt solution. All the variables were measured at the inlet of the drying chamber. The air temperature was varied from 40 to 65C, relative humidity from 11 to 50% and air velocity from 1 to 5 m/s. It is important to point out that in the experiments with slices, the air flowed parallel to the solid while in the case of cylinders the flow was perpendicular to the samples.

A discontinuous method was used to determine the weight loss of the particle. The dry weight was obtained by vacuum drying during 72 h, at 60C with phosphorous pentoxide as desiccant. Variations of temperature at the center and surface of the solid were measured with thin K-type thermocouples inserted in the sample. Temperatures were monitored and continuously recorded during the experiments. Because of shrinkage, some errors are introduced in measuring the surface temperature. Typical drying data are shown in Fig. 1.

Determination of Heat Transfer Coefficients

Introducing Eq. (3) into Eq. (2) and rearranging, the following expression for the heat transfer coefficient is obtained:

$$h_g = \frac{m_s}{A_s(T_g - T)}\left[C_p(1+X)\frac{dT}{dt} + \Delta H_s\frac{dX}{dt}\right] \qquad (5)$$

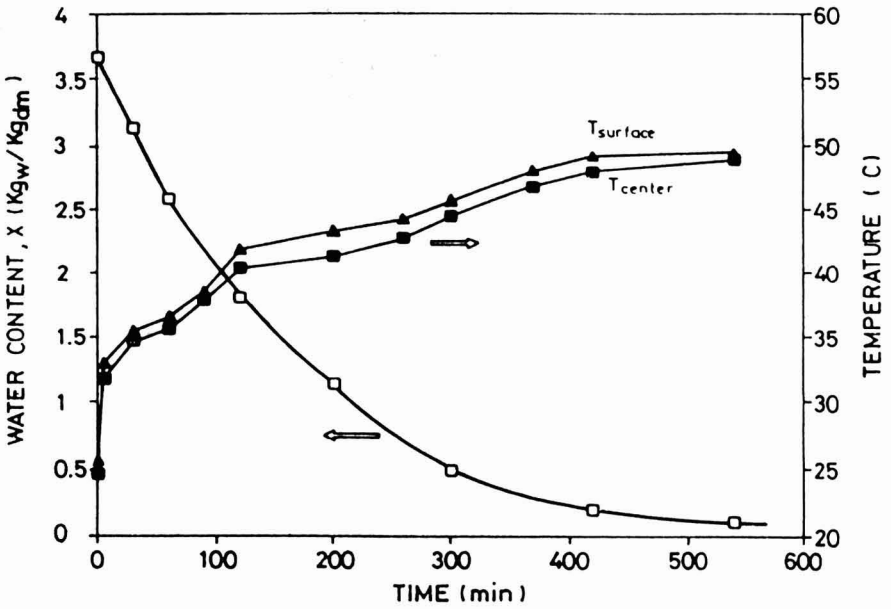

FIG. 1. TYPICAL EXPERIMENTAL RESULTS FOR DRYING OF POTATO

This result can be used to calculate h_g from drying data, provided Eq. (2) applies along the whole drying process. The method assumes that the temperature gradient within the product is negligible. For a particle being heated by convection, the Biot number (Bi_h) is defined as the ratio of internal to external heat transfer resistances:

$$Bi_h = \frac{h_g L_c}{k} \tag{6}$$

Here L_c is the characteristic dimension for heat conduction and k the particle thermal conductivity. It is usually assumed that when Bi_h is less than 0.1 the internal resistance for heat transfer can be neglected.

To evaluate h_g from Eq. (5), knowledge of variations in water content, X, and temperature of the solid, T, with time during drying is needed. By fitting the experimental X-t and T-t data with high order polynomials and differentiating the resulting expressions, the numerical derivatives dT/dt and dX/dt can be estimated with enough accuracy. Variations in the area of the particle, A_s, due to shrinkage during dehydration are also required. In addition, thermal properties such as the specific heat, C_p, and sorptional properties such as the heat of sorption, ΔH_s, must be known as a function of water content and temperature.

Thermophysical Properties

The specific heat of potato, apple and carrot was measured in a Differential Scanning Calorimeter Perkin-Elmer DSC-2. The temperature range was from 288 to 323 K. Air was used as reference. The difference between the base line and the curve for the product is proportional to its specific heat. The proportional constant was obtained with bidistilled water for which the specific heat is well-known (Perry and Chilton 1973). Samples of different moisture contents were obtained by partial dehydration in the dryer described above. After drying, the samples were wrapped in aluminum foil and kept for 24 h at constant conditions to ensure nearly uniform profiles before experiments.

Starting from thermodynamic definitions, the C_p can be expressed in terms of product composition as:

$$C_p = \sum_{j=i}^{N} w_j \, C_{pj} \tag{7}$$

where w_j and C_{pj} represent the mass fraction and the partial specific heat of the j component and N the number of components. If the sum in Eq. (7) is split into aqueous and solid components, the following expression for C_p can be obtained:

$$C_p = (1+X_o) \sum_{j=1}^{N-1} w_{jo} C_{pj} + [C_{p_w} - (1+X_o) \sum_{j=1}^{N-1} w_{jo} C_{pj}] \, w \tag{8}$$

This expression is based on the composition of the fresh product, w_{jo}, and water content on wet basis w.

The thermal conductivities of the foodstuffs were obtained from experimental data available in the literature (Mattea *et al.* 1986; Jankowski *et al.* 1981).

The values for the heat of sorption for apple, carrot and potato were calculated using the following equation:

$$\Delta H_s = [1+q_1 \exp(-q_2 X) X^{q3}] \, \Delta H_w \tag{9}$$

where the constants q_i were determined by nonlinear regression of the experimental sorption data resulting $q_1 = 0.0107$, $q_2 = 1.287$ and $q_3 = -1.513$ (Ratti *et al.* 1989). Changes in the dimensions of particles due to shrinkage as a function of drying conditions were studied in a previous work (Ratti 1994).

RESULTS AND DISCUSSION

Specific heat of potato, apple and carrot as a function of water content at 30C is presented in Fig. 2. At high water contents, the C_p tends towards the

value for pure water. A marked decrease from this value (up to 60%) is observed as the water content reduces to lower values. As can be seen from the figure, the experimental data compare well with those reported by other authors (Heldman 1975) for fresh apple and carrot, but is higher in the case of potato.

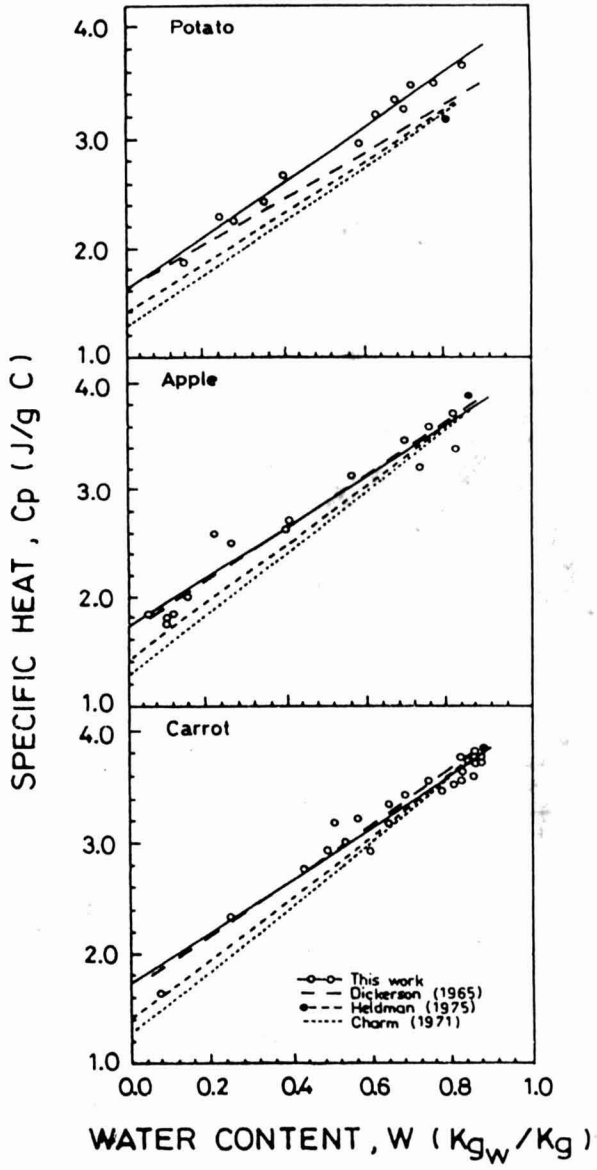

FIG. 2. SPECIFIC HEAT OF POTATO, APPLE AND CARROT AT 30C AS FUNCTION OF MOISTURE CONTENT

On the other hand, the variation of C_p with temperature was not pronounced and can be considered in the magnitude of the experimental error, at least in the range of temperatures analyzed. Therefore, the functionality of C_p with temperature can be assumed the same as for pure water.

Equation (8) indicates a linear relationship between C_p and water content on a wet basis, provided the partial specific heats remain constant. As can be seen in Fig. 2, experimental data show a behavior similar to that prediction. On this basis, a linear functionality of C_p with water content was assumed and the regression constants were obtained. The results are summarized in Table 1.

Several expressions based on Eq. (8) have been proposed to evaluate C_p of foodstuffs (Dickerson 1965; Charm 1971; Heldman 1975). Predictions of these equations are compared with experimental data in Fig. 2. The best predictions are given by the equation proposed by Dickerson (1965). The other two expressions underestimate the value of C_p, particularly in the case of potato, and seem to work better for fresh products.

In order to evaluate the heat transfer coefficients, assumptions in applying Eq. (5) should be satisfied. Preliminary results indicated that the Biot number ranged between 0.1 and 0.5. The characteristic length was taken as $L_c = 1/a_v$ where a_v is the area by volume ratio of the particle. Therefore, according to Eq. (6), the internal resistance for heat transfer cannot be neglected "a priori". However, this restriction has been derived for heat conduction and does not take into account the effect of evaporation in the product, which decreases the temperature profile.

A complete solution as a function of the Bi_h number, for the case of heat conduction in a solid with sorption of vapors at the surface, can be found in Crank (1975). Although the initial condition differs from the drying problem, an approximate idea of the behavior of the solution can be drawn from that case. Making some specific calculations in the range of Bi_h indicated above, it can be concluded that after approximately 15 min all the solutions approach that for $Bi_h \rightarrow 0$ (negligible internal resistance) with an error lower than 5%.

TABLE 1.
PARAMETERS FOR SPECIFIC HEAT CALCULATIONS

Foodstuff	A	B	r^2
Potato	1.665	2.966	0.985
Apple	1.729	2.385	0.940
Carrot	1.755	2.345	0.944

$C_p = A + B\,w$

On the other hand, our experimental data show that the difference between surface and center temperatures was less than 1.5C during the whole drying experiment. The effect of this difference on the h_g calculations becomes important at the final stage of the drying process when the product temperature tends to the air temperature.

Based on these observations, the following condition for the temperature range was stated:

$$0.2 < \frac{T-T_g}{T_o-T_g} < 0.8 \tag{10}$$

The instantaneous heat transfer coefficients were determined with Eq. (5) and the method described above. The average value for each run, along with the resulting Bi_h numbers evaluated at the initial conditions, are presented in Table 2. The results of the calculation of h_g, are shown in Fig. 3 in terms of dimensionless numbers. The Nu_D values for different products and geometries were plotted together and represented by a relationship like Eq. (4). In the case of air drying and within the range of temperatures analyzed in this work, the Pr number is almost constant and equal to 0.7. Therefore its effect can be neglected from Eq. (4) and its value can be included in constant C. The following expression was obtained from linear regression of data ($r^2 = 0.937$):

$$Nu_D = 0.249 Re_D^{0.64} \tag{11}$$

In a process such as drying of foodstuffs, the heat transfer coefficient changes during the process because the particles shrink. One approximate way to take into account this variation can be derived from Eq. (11) for both cylinders and slices:

$$h_g = h_{go}(a_v / a_{vo})^{0.36} \tag{12}$$

Several correlations presented in the literature were selected for evaluation. In the case of slices, the classical equation for the local heat transfer coefficient for flow parallel to a flat sheet obtained from the laminar boundary layer theory (Welty *et al.* 1984) can be integrated over the diameter giving:

$$Nu_D = 0.664 \left(\frac{8}{3\pi}\right) Pr^{1/3} Re_D^{0.5} \tag{13}$$

This equation is valid for $Re_D < 2\ 10^5$. Treybal (1975) reviewed existing correlations and for flow of gas parallel to the drying surface suggested:

$$Nu_D = 0.036 Re_D^{0.8} Pr^{1/3} \quad (14)$$

Although this equation is recommended for $Re_D > 15000$, it is widely used in drying applications.

TABLE 2.
AVERAGE HEAT TRANSFER COEFFICIENTS DURING DRYING OF DIFFERENT FOODSTUFFS

Product and geometry	Re_D	h_g (W/m^{2}K)	Bi_{ho}
Potato (S)	6370	38.8	0.231
Potato (S)	6370	42.0	0.250
Potato (S)	2123	25.8	0.153
Potato (S)	6370	35.7	0.212
Potato (S)	10618	45.8	0.272
Potato (S)	6370	55.8	0.332
Potato (S)	5850	53.0	0.315
Potato (C)	1587	71.8	0.291
Apple (S)	9000	63.7	0.524
Apple (S)	8020	61.5	0.506
Apple (S)	9000	63.7	0.524
Apple (S)	6354	41.7	0.343
Apple (S)	8494	58.5	0.481
Apple (C)	2107	88.3	0.495
Apple (C)	1596	68.0	0.381
Apple (C)	1580	83.2	0.466
Carrot (S)	5895	41.0	O.231
Carrot (S)	6108	45.7	0.258
Carrot (S)	8494	58.2	0.328
Carrot (C)	1477	81.2	0.312
Carrot (C)	1580	81.1	0.312
Carrot (C)	2150	93.2	0.358

S = slice, C = cylinder

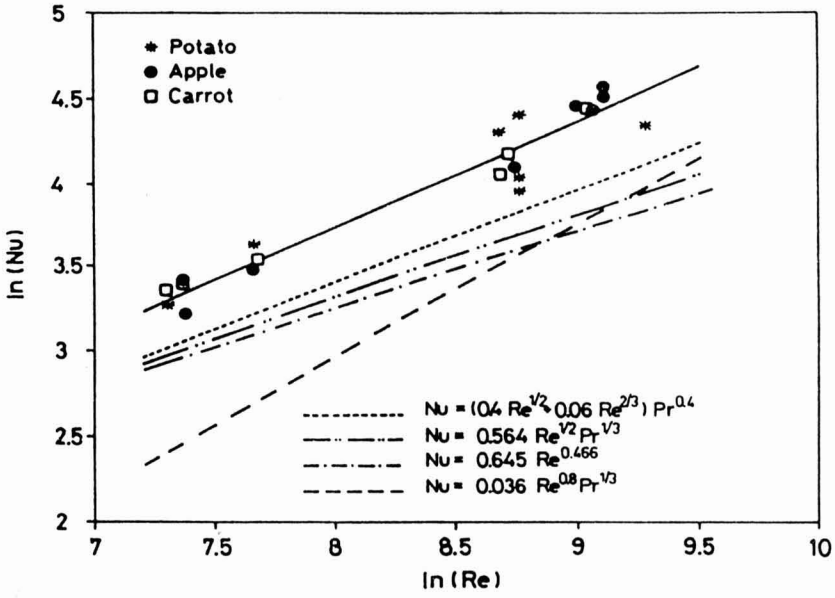

FIG. 3. DIMENSIONLESS CORRELATIONS OF CONVECTIVE HEAT TRANSFER COEFFICIENTS FOR DRYING OF FOODSTUFFS

In the case of cylinders in cross-flow, a suitable equation is presented by Welty *et al.* (1984):

$$Nu_D = 0.615Re_D^{0.466} \tag{15}$$

for $40 < Re_D < 4000$. On the other hand, for the same situation Whitaker (1972) proposed the correlation:

$$Nu_D = (0.4Re_D^{1/3} + 0.06Re_D^{2/3})\ Pr^{0.4} \tag{16}$$

Predictions of Eq. (13) to (16) are also presented in Fig. 3. In general, these correlations lead to analogous behavior but h_g values are up to 50% lower than those heat transfer coefficients determined from drying data. As expected, Eq. (14) yields the worst prediction, since its application has been extended to the laminar region. For both geometries, other existing correlations underpredict the values of Nu_D, being this difference less important at low Re_D numbers.

One factor that might contribute to increasing h_g values would be the influence of the moisture flux on the heat transfer to the surface. However, it can be proved that the Ackermann correction (Keey 1978):

$$\phi = \frac{n_w C_{pg} / h_g}{[\exp(n_w C_{pg} / h_g) - 1]} \tag{17}$$

which accounts for that effect, is negligible in our case. The higher experimental values may be due to roughness of the solid surface and deformation of the particle during drying, which would produce turbulence at the boundary layer, increasing the convective transport. Finally, some differences can be also explained in terms of the sample geometry, since while most correlations refers to one-dimensional systems, the experimental values include the effect of side surfaces.

CONCLUSIONS

Data on drying of food particles can be used to evaluate convective heat transfer coefficients for the process. A restriction in the range of temperature to be used has been obtained. Experimental h_g values ranged from 25 to 95 W/m^2K. No significant differences between potatoes, apples and carrots were observed. Calculated coefficients for slices and cylinders were adequately correlated by the dimensionless expression $Nu_D = 0.249\ Re_D^{0.64}$. Predictions of standard correlations yield lower values of heat transfer coefficients.

NOMENCLATURE

A_s Area of the particle, [m^2]
a_v Particle area-to-volume ratio, [m^2/m^3]
Bi_h Heat transfer Biot number, [-]
b Parameter in Eq. (4)
C Parameter in Eq. (4)
C_p Specific heat, [J/g C]
C_{pj} Partial specific heat of component j, [J/g C]
h_g Heat transfer coefficient, [W/m^2 K]
k Thermal conductivity, [W/m C]
k_g Mass transfer coefficient based on pressures, [kg/m^2 s kPa]
L_c Characteristic length, [m]
m_s Mass of dry solid, [kg]
N Number of components, [-]

Nu Nusselt number, [-]
n Parameter in Eq. (4)
n_w Water mass flux, [kg/m^2 s]
Pr Prandlt number, [-]
p_w Water vapor pressure, [kPa]
q_i (i = 1, 2 or 3) parameters in Eq. (9)
Re Reynolds number, [-]
T Temperature of the solid, [C]
T_g Temperature of the air, [C]
t Time [s]
w Water content (wet basis), [kg water/kg total mass]
w_j Mass fraction of component j, [kg of j/kg total mass]
X Water content (dry basis), [kg water/kg dry matter]

Greek Letters

ΔH_s Heat of sorption, [J/kg]
ΔH_w Heat of vaporization of pure water, [J/kg]

Subscripts

D Based on the diameter
s Solid
o Initial
w Water
g Bulk gas

REFERENCES

CHARM, S.E. 1971. *The Fundamentals of Food Engineering*, 2nd Ed., Van Nostrand Reinhold/AVI, New York.

CRANK, J. 1975. *The Mathematics of Diffusion*, 2nd Ed., Clarendon Press, Oxford .

DICKERSON, R.W. (Jr.). 1965. Thermal properties of foods. In *The Freezing Preservation of Foods*, 4th Ed., Vol. II, (D.K. Tressler, W.B. Van Arsdel and M.J. Copley, eds.), Van Nostrand Reinhold/AVI, New York.

HELDMAN, D.R. 1975. *Food Process Engineering*, Van Nostrand Reinhold/AVI, New York.

JANKOWSKI, T., JANKOWSKI, S. and KOZIOL, K. 1981. Some thermal properties of root vegetables. Acta Aliment. Polonica, *VII* (XXXI), 137.

KEEY, R.B. 1978. *Introduction to Industrial Drying Operations*, Pergamon Press, Oxford.

LONCIN, M. and MERSON, R.L. 1979. *Food Engineering: Principles and Selected Applications*, Academic Press, New York.

MATTEA, M., URBICAIN, M.J. and ROTSTEIN, E. 1986. Prediction of thermal conductivity of vegetable foods by the effective medium theory. J. Food. Sci. *51*, 113.

PERRY, R.H. and CHILTON, C.H. 1973. *Chemical Engineers' Handbook*, 5th Ed., McGraw Hill Kogakusha, Japan.

RATTI, C. 1994. Shrinkage during drying of foodstuffs. J. Food Eng. *23*, 91.

RATTI, C., CRAPISTE, G.H. and ROTSTEIN, E. 1989. A new water sorption equilibrium expression for solid foods based on thermodynamic considerations. J. Food Sci. *54*, 738.

TREYBAL, R.E. 1980. *Mass-Transfer Operations*, 3rd Ed., McGraw-Hill, New York.

WELTY, J.R., WICKS, C.E. and WILSON, R.E. 1984. *Fundamentals of Momentum, Heat, and Mass Transfer*. 3rd Ed., John Wiley & Sons, New York.

WHITAKER, S. 1972. Forced convection heat transfer correlations for flow in pipes, past flat plates, single cylinders, single spheres, and for flow in packed beds and tube bundles. AICHE J. *18*(2), 361–371.

COORDINATE SYSTEM INDEPENDENCE OF SHEAR RATE DURING ISOTHERMAL SINGLE-SCREW EXTRUSION OF A NEWTONIAN FLUID

MUKUND V. KARWE[1], RAMAN V. CHIRUVELLA[2,3] and YOGESH JALURIA[2]

[1]*Department of Food Science*
[2]*Department of Mechanical and Aerospace Engineering*
Rutgers - The State University of New Jersey
New Brunswick, NJ 08903

Accepted for Publication May 26, 1994

ABSTRACT

The analysis of fluid flow in a single screw extruder channel is presented by treating the screw as stationary and rotating the barrel in the opposite direction. It is shown that the calculated shear rates at the barrel and at the screw, during extrusion of a Newtonian fluid under isothermal conditions, do not depend on the choice of formulation, i.e., barrel moving or screw moving. It is also shown that they are independent of choice of coordinate system.

INTRODUCTION

In a single screw extruder, material is conveyed from hopper to die by rotating a screw inside a cylindrical barrel. The rotating screw surface drags the material with it while the stationary barrel exerts a drag on the material in the screw channel in the opposite direction. The screw flights and the helix angle of the screw impart net axial and down channel movement of the material. A similar equivalent situation can be obtained by keeping the screw stationary and rotating the barrel in the opposite direction. The two situations give similar results when the screw channel is wide and the channel depth is much smaller than the screw root diameter. Thus, under these conditions, the screw-moving and barrel-stationary situation can be analyzed by visualizing a stationary screw and barrel rotating in the opposite direction, i.e., as seen by the observer located on the screw. This has been used and employed by several investigators and

[1] Address all correspondence: Mukund V. Karwe, Department of Food Science, P.O. Box 231, Cook College, Rutgers - The State University of New Jersey, New Brunswick, NJ 08903.
[3] Current address: YSU - Technology Development Corp., 410 Wick Ave., Youngstown, OH 44555-3119.

Journal of Food Process Engineering **18** (1995) 55–69.

authors (Tadmor and Klein 1970; Fenner 1979; Tadmor and Gogos 1979; Rauwendaal 1986).

Recently, Tamura *et al.* (1993) claimed that for an isothermal flow of a Newtonian fluid in a single-screw extruder the shear rates at the screw root and at the barrel surface depend upon the coordinate frame of reference, i.e., barrel-moving and screw-stationary or vice versa. In this paper, it is shown that the calculated shear rates at the screw root and the barrel surface are independent of the frame of reference. The magnitude of the shear rate at the barrel is always twice the magnitude of the shear rate at the screw root, as against that concluded by Tamura *et al.* (1993).

ANALYSIS

The velocity and pressure distributions for a Newtonian fluid under isothermal conditions in a single screw extruder are obtained by choosing two different coordinate frames of reference and, in each case, both barrel moving and screw moving situations are considered. The coordinate frames of reference used are:

(1) Axial and Tangential coordinate system: Case-1 Barrel moving (Fig. 1); Case-2 Screw moving (Fig. 2).
(2) Down and Cross channel coordinate system: Case-3 Barrel moving (Fig.3); Case-4 Screw moving (Fig. 4).

AXIAL AND TANGENTIAL COORDINATE SYSTEM

Case-1: Barrel Moving Formulation

The coordinate system is shown in Fig.1. The details of formulation and assumptions can be found in many textbooks and papers. For a very shallow channel ($\frac{B}{H} \gg 1.0$, $\frac{D}{H} \gg 1.0$), employing the lubrication approximations, the governing equations of motion can be written as, Z-Momentum Equation:

$$\frac{\partial P}{\partial Z} = \mu \frac{\partial^2 W}{\partial Y^2} \qquad (1)$$

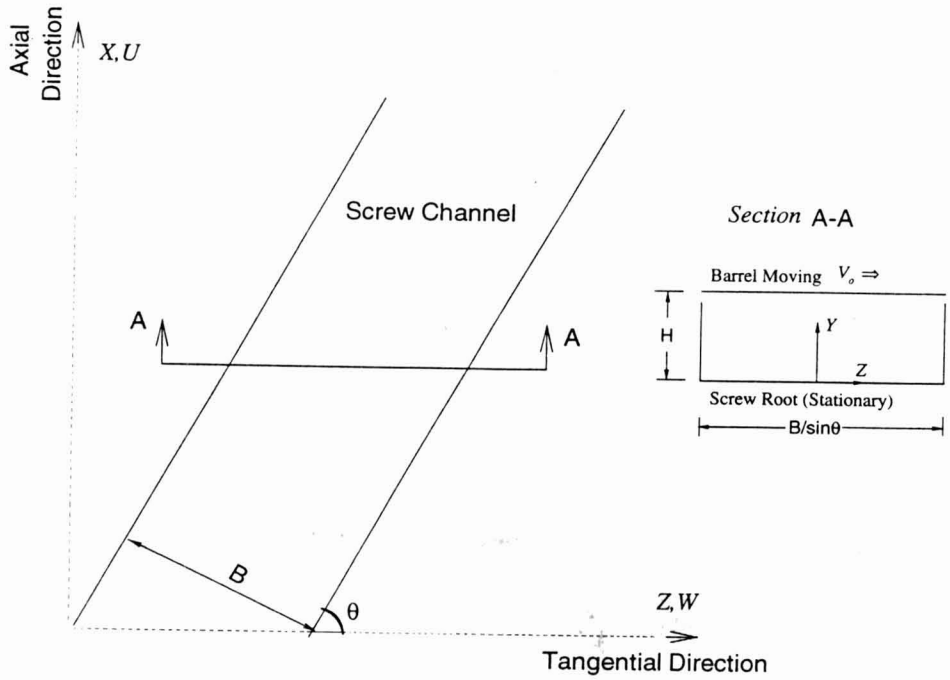

FIG. 1. COORDINATE SYSTEM FOR BARREL MOVING FORMULATION, CASE-1

Continuity Equation:

$$\int_o^H W dY = Q_t \tag{2}$$

Boundary Conditions:

$$\begin{aligned} &at\ Y = 0\ ;\ W = 0 \\ &at\ Y = H\ ;\ W = V_o \end{aligned} \tag{3}$$

In case of shallow channels P = P(Z,X). Therefore integrating Eq. (1) with respect to Y, and applying the boundary conditions specified in Eq. (3), results in

$$W = \frac{1}{2\mu}\left(\frac{\partial P}{\partial Z}\right)(Y^2 - YH) + V_o\left(\frac{Y}{H}\right) \tag{4}$$

Substituting for W in Eq. (2)

$$Q_t = -\frac{1}{2\mu}\left(\frac{\partial P}{\partial Z}\right)\left(\frac{H^3}{6}\right) + \frac{V_o H}{2}.$$

When the die is closed ($Q_t = 0$), which is similar to the situation reported by Tamura *et al.* (1993) in their helical screw rheometer (HSR), we get

$$\frac{1}{2\mu}\left(\frac{\partial P}{\partial Z}\right) = \frac{3V_o}{H^2}$$

Substituting for $\frac{\partial P}{\partial Z}$ in Eq. (4);

$$\frac{W}{V_o} = 3\left(\frac{Y}{H}\right)^2 - 2\left(\frac{Y}{H}\right) \tag{5}$$

Therefore, shear rate ($\dot{\gamma}$) can be written as,

$$\dot{\gamma} = \frac{\partial W}{\partial Y} = V_o\left(\frac{6Y}{H^2} - \frac{2}{H}\right).$$

The shear rate at the screw ($Y = 0$) is

$$\dot{\gamma}_s = -\frac{2V_o}{H} \tag{6}$$

and that at the barrel ($Y = H$) is

$$\dot{\gamma}_b = \frac{4V_o}{H} \tag{7}$$

The above expressions are similar to those reported by Tamura *et al.* (1993).

Case-2: Screw Moving Formulation

The coordinate system is shown in Fig. 2.

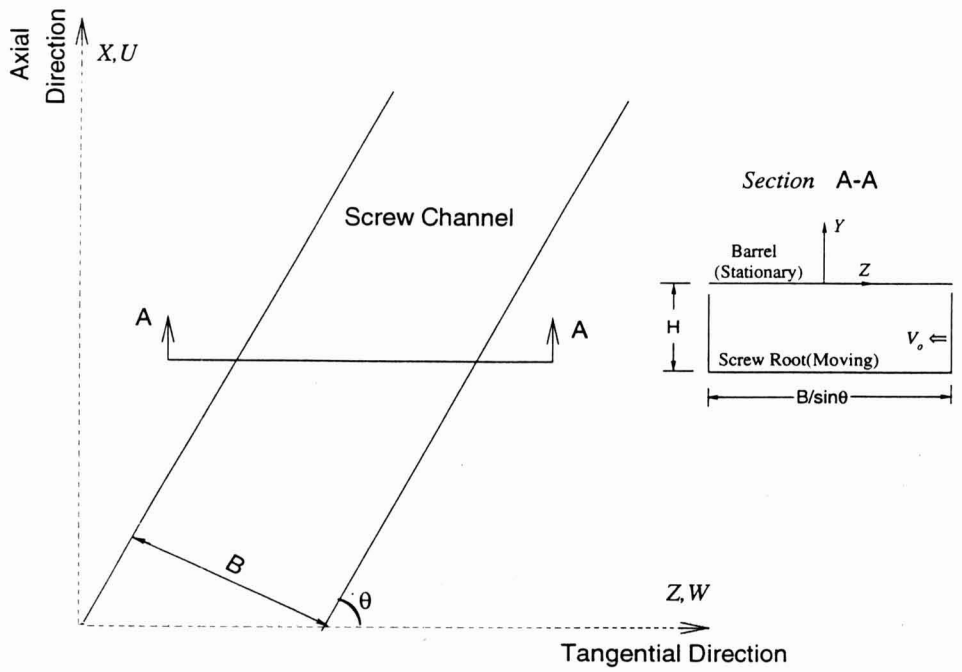

FIG. 2. COORDINATE SYSTEM FOR SCREW MOVING FORMULATION, CASE-2

Z-Momentum Equation:

$$\frac{\partial P}{\partial Z} = \mu \frac{\partial^2 W}{\partial Y^2} \tag{8}$$

Continuity Equation:

$$\int_{-H}^{0} W dY = -V_o H$$

Boundary Conditions:

$$\begin{aligned} &at\ Y = 0; W = 0 \\ &at\ Y = -H; W = -V_o \end{aligned} \tag{10}$$

Integrating Eq. (8) with respect Y and applying the boundary conditions specified in Eq. (10), we get

$$W = \frac{1}{2\mu}\left[\frac{\partial P}{\partial Z}\right](Y^2+YH) + V_o\left[\frac{Y}{H}\right] \tag{11}$$

Substituting Eq. (11) in Eq. (9) we obtain,

$$\frac{1}{2\mu}\left[\frac{\partial P}{\partial Z}\right] = \frac{3V_o}{H^2}$$

Substituting the above expression in Eq. (11),

$$\frac{W}{V_o} = 3\left[\frac{Y}{H}\right]^2 + 4\left[\frac{Y}{H}\right] \tag{12}$$

Therefore, the shear rate ($\dot{\gamma}$) can be calculated as,

$$\dot{\gamma} = \frac{\partial W}{\partial Y} = 6V_o\left[\frac{Y}{H^2}\right] + \frac{4V_o}{H}.$$

The shear rate at the screw (Y = -H) becomes

$$\dot{\gamma}_s = -\frac{2V_o}{H} \tag{13}$$

which is same as that obtained in Eq. (6). At the barrel (Y = 0) the shear rate is

$$\dot{\gamma}_b = \frac{4V_o}{H} \tag{14}$$

which is same as that obtained in Eq. (7).

Therefore, the shear rates obtained at the screw and at the barrel are same in barrel moving and screw moving formulations. Magnitude of shear rate at the barrel is twice of that at the screw.

DOWN AND CROSS CHANNEL COORDINATE SYSTEM

Case-3: Barrel Moving Formulation

The coordinate system is shown in Fig. 3.

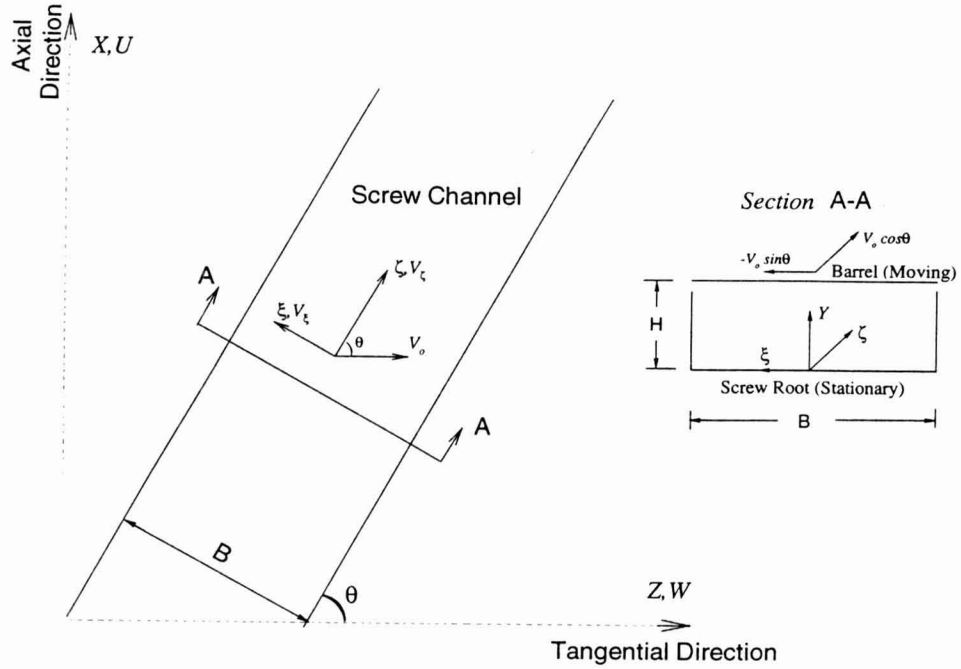

FIG. 3. COORDINATE SYSTEM FOR BARREL MOVING FORMULATION, CASE-3

ζ-Momentum Equation:

$$\frac{\partial P}{\partial \zeta} = \mu \frac{\partial^2 V_\zeta}{\partial Y^2} \tag{15}$$

ξ-Momentum Equation:

$$\frac{\partial P}{\partial \xi} = \mu \frac{\partial^2 V_\xi}{\partial Y^2} \tag{16}$$

Continuity Equation:

$$\int_0^H V_\zeta dY = Q \tag{17}$$

$$\int_0^H V_\xi dY = 0 \tag{18}$$

Boundary Conditions:

$$\begin{aligned} &at\ Y = 0; V_\zeta = 0 \\ &at\ Y = 0; V_\xi = 0 \\ &at\ Y = \mathrm{H}; V_\zeta = V_o\cos\theta \\ &at\ Y = \mathrm{H}; V_\xi = -V_o\sin\theta \end{aligned} \tag{19}$$

Integrating Eq. (15) with respect to Y, and applying the boundary conditions given in Eq. (19), we get

$$V_\zeta = \frac{1}{2\mu}\left[\frac{\partial \mathrm{P}}{\partial \zeta}\right](Y^2 - Y\mathrm{H}) + V_o\cos\theta\left[\frac{Y}{H}\right] \tag{20}$$

Substituting Eq. (20) in Eq. (17), an expression for pressure gradient can be obtained as

$$\frac{1}{2\mu}\left[\frac{\partial \mathrm{P}}{\partial \zeta}\right] = \frac{3V_o\cos\theta}{\mathrm{H}^2} - \frac{6Q}{\mathrm{H}^3}$$

Substituting the above expression in Eq. (20), it can be written as

$$V_\zeta = \left[3V_o\cos\theta - \frac{6Q}{\mathrm{H}}\right]\left[\left[\frac{Y}{\mathrm{H}}\right]^2 - \left[\frac{Y}{\mathrm{H}}\right]\right] + V_o\cos\theta\left[\frac{Y}{\mathrm{H}}\right] \tag{21}$$

Similarly solving Eq. (16) and (18) using the boundary conditions in (19), V_ξ can be expressed as

$$V_\xi = (-3V_o\sin\theta)\left[\left[\frac{Y}{\mathrm{H}}\right]^2 - \left[\frac{Y}{\mathrm{H}}\right]\right] - V_o\sin\theta\left[\frac{Y}{\mathrm{H}}\right]. \tag{22}$$

From Fig. 3, the expression for the tangential velocity can be written as

$$W = V_\zeta\cos\theta - V_\xi\sin\theta \tag{23}$$

Substituting Eq. (21) and (22) in the above Eq. (23) the expression for the tangential velocity can be obtained as

$$W = \left[\left(\frac{-6Q}{H}+3V_o\cos\theta\right)\left(\left(\frac{Y}{H}\right)^2-\left(\frac{Y}{H}\right)\right)+V_o\cos\theta\left(\frac{Y}{H}\right)\right]\cos\theta+ \left[(3V_o\sin\theta)\left(\left(\frac{Y}{H}\right)^2-\left(\frac{Y}{H}\right)\right)+V_o\sin\theta\left(\frac{Y}{H}\right)\right]\sin\theta \tag{24}$$

The shear rate ($\dot{\gamma}$) can be calculated as

$$\dot{\gamma} = \frac{\partial W}{\partial Y} = \left[\left(\frac{-6Q}{H}+3V_o\cos\theta\right)\left(2\left(\frac{Y}{H^2}\right)-\left(\frac{1}{H}\right)\right)+\left(\frac{V_o}{H}\right)\cos\theta\right]\cos\theta+ \left[(3V_o\sin\theta)\left(2\left(\frac{Y}{H^2}\right)-\left(\frac{1}{H}\right)\right)+\frac{V_o}{H}\sin\theta\right]\sin\theta \tag{25}$$

In the case of closed die ($Q = 0$), the shear rate at the screw ($Y = 0$) will be

$$\dot{\gamma}_s = \left[(3V_o\cos\theta)\left(-\frac{1}{H}\right)+\left(\frac{V_o}{H}\right)\cos\theta\right]\cos\theta+ \left[(3V_o\sin\theta)\left(-\frac{1}{H}\right)+\frac{V_o}{H}\sin\theta\right]\sin\theta \tag{26}$$

$$= -\frac{2V_o\cos^2\theta}{H}-\frac{2V_o\sin^2\theta}{H}$$

$$\dot{\gamma}_s = -\frac{2V_o}{H}$$

This is the same as that in Eq. (6) and (13).

The shear rate at the barrel (Y = H) in the case of closed die (Q = 0) is

$$\begin{aligned}\dot{\gamma}_b &= \left[(3V_o\cos\theta)\left[\frac{1}{\mathrm{H}}\right] + \left[\frac{V_o}{\mathrm{H}}\right]\cos\theta\right]\cos\theta + \\ &\quad \left[(3V_o\sin\theta)\left[\frac{1}{\mathrm{H}}\right] + \frac{V_o}{\mathrm{H}}\sin\theta\right]\sin\theta \\ &= \frac{4V_o\cos^2\theta}{\mathrm{H}} + \frac{4V_o\sin^2\theta}{\mathrm{H}} \\ \gamma_b &= \frac{4V_o}{\mathrm{H}}\end{aligned} \tag{27}$$

which is again the same as that in Eq. (7) and (14).

Case-4: Screw Moving Formulation

The coordinate system is shown in Fig. 4.

ζ-Momentum Equation:

$$\frac{\partial P}{\partial \zeta} = \mu\frac{\partial^2 V_\zeta'}{\partial Y'^2} \tag{28}$$

ξ-Momentum Equation:

$$\frac{\partial P}{\partial \xi} = \mu\frac{\partial^2 V_\xi'}{\partial Y'^2} \tag{29}$$

Boundary Conditions:

$$\begin{aligned} at\ Y' &= -\mathrm{H}\ ;\ V_\zeta' = -V_o\cos\theta \\ at\ Y' &= -\mathrm{H}\ ;\ V_\xi' = V_o\sin\theta \\ at\ Y' &= 0\ ;\ V_\zeta' = 0 \\ at\ Y' &= 0\ ;\ V_\xi' = 0 \end{aligned} \tag{30}$$

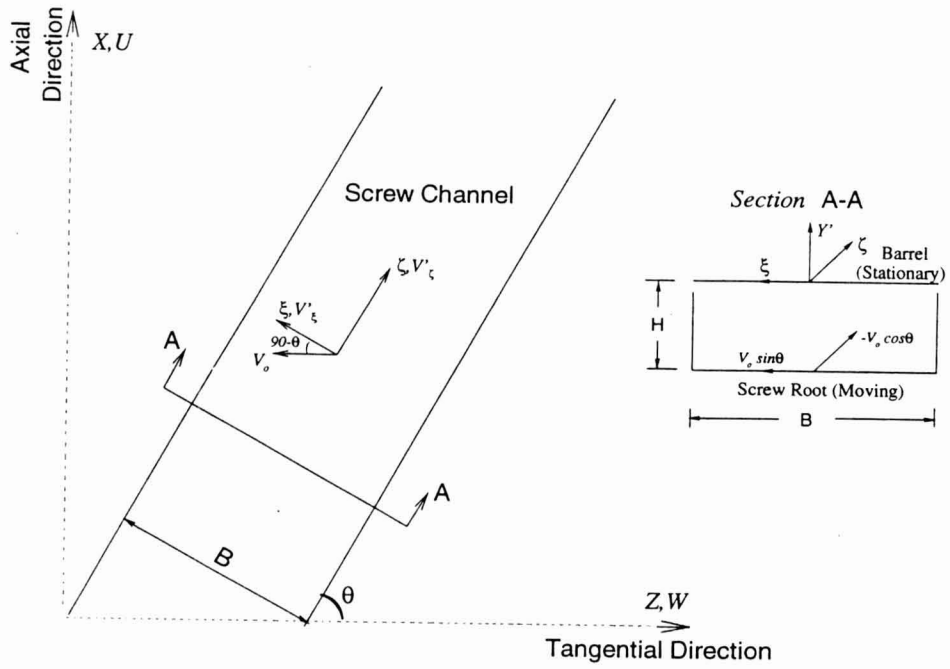

FIG. 4. COORDINATE SYSTEM FOR SCREW MOVING FORMULATION, CASE-4

In this formulation the screw is moving and the barrel is held stationary. The coordinate system is fixed on the barrel. The coordinate transformation between the screw moving and barrel moving formulations can be written as

$$\begin{aligned} Y' &= Y-\mathrm{H} \\ V'_\zeta &= V_\zeta - V_o\cos\theta \\ V'_\xi &= V_\xi + V_o\sin\theta \end{aligned} \tag{31}$$

From the vector diagram in Fig. 4,

$$\begin{aligned} U &= V'_\zeta\sin\theta + V'_\xi\cos\theta \\ W &= V'_\zeta\cos\theta - V'_\xi\sin\theta \end{aligned} \tag{32}$$

Equations (31) and (32) can be combined to obtain,

$$\begin{aligned} U &= V_\zeta\sin\theta + V_\xi\cos\theta \\ W &= V_\zeta\cos\theta - V_\xi\sin\theta - V_o \end{aligned} \tag{33}$$

Since the terms on the right hand side of the above Eq. (33) correspond to the barrel moving formulation, $Y = 0(Y' = -H)$ corresponds to the screw root and $Y = H(Y' = 0)$ corresponds to the barrel. Using Eq. (30) and (31) the boundary conditions for W can be obtained as,

$$at\ Y = 0(Y' = -H), V_\xi = 0, V_\zeta = 0 \Rightarrow W = -V_o$$
$$at\ Y = H(Y' = 0), V_\xi = -V_o\sin\theta, V_\zeta = +V_o\cos\theta \Rightarrow W = 0$$

which satisfies with the boundary conditions shown in Fig. 4. Substituting Eq. (21) and (22) in Eq. (33) for the tangential velocity, one can obtain

$$W = \left[\left(\frac{-6Q}{H} + 3V_o\cos\theta\right)\left(\left(\frac{Y}{H}\right)^2 - \left(\frac{Y}{H}\right)\right) + V_o\cos\theta\left(\frac{Y}{H}\right)\right]\cos\theta + \left[(3V_o\sin\theta)\left(\left(\frac{Y}{H}\right)^2 - \left(\frac{Y}{H}\right)\right) + V_o\sin\theta\left(\frac{Y}{H}\right)\right]\sin\theta - V_o \tag{34}$$

The shear rate ($\dot{\gamma}$) is obtained as given below

$$\dot{\gamma} = \frac{\partial W}{\partial Y}$$
$$= \left[\left(\frac{-6Q}{H} + 3V_o\cos\theta\right)\left(2\left(\frac{Y}{H^2}\right) - \left(\frac{1}{H}\right)\right) + \left(\frac{V_o}{H}\right)\cos\theta\right]\cos\theta + \left[(3V_o\sin\theta)\left(2\left(\frac{Y}{H^2}\right) - \left(\frac{1}{H}\right)\right) + \frac{V_o}{H}\sin\theta\right]\sin\theta \tag{35}$$

In the case of zero flow rate ($Q = 0$), the shear rate at the screw ($Y = 0$) will be

$$\dot{\gamma}_s = \left[(3V_o\cos\theta)\left[-\frac{1}{H}\right] + \left[\frac{V_o}{H}\right]\cos\theta\right]\cos\theta + \left[(3V_o\sin\theta)\left[-\frac{1}{H}\right] + \frac{V_o}{H}\sin\theta\right]\sin\theta$$
$$= \frac{-2V_o\cos^2\theta}{H} - \frac{2V_o\sin^2\theta}{H} \tag{36}$$
$$\dot{\gamma}_s = \frac{-2V_o}{H}$$

These are same as in Eq. (6), (13) and (26). The shear rate at the barrel (Y = H) is

$$\dot{\gamma}_b = \left[(3V_o\cos\theta)\left[\frac{1}{H}\right] + \left[\frac{V_o}{H}\right]\cos\theta\right]\cos\theta + \left[(3V_o\sin\theta)\left[\frac{1}{H}\right] + \frac{V_o}{H}\sin\theta\right]\sin\theta$$
$$= \frac{4V_o\cos^2\theta}{H} + \frac{4V_o\sin^2\theta}{H} \tag{37}$$
$$\dot{\gamma}_b = \frac{4V_o}{H}$$

which is again same as in Eq. (7), (14) and (27).

CONCLUSIONS

As shown in the preceding analysis, the shear rate obtained at the screw root does not depend upon the type of formulation or the frame of reference and is given as

$$\dot{\gamma}_s = -\frac{2V_o}{H}.$$

Similarly, the shear rate at the barrel also does not depend on the type of formulation or the frame of reference and is given as

$$\dot{\gamma}_b = \frac{4V_o}{\mathrm{H}}.$$

ACKNOWLEDGMENTS

This is publication No. D10544-3-94 of the New Jersey Agricultural Experiment Station, supported by State Funds and the Center for Advanced Food Technology (CAFT). The Center for Advanced Food Technology is a New Jersey Commission on Science and Technology. This work was also supported in part by the U.S. Army Research Office.

NOMENCLATURE

B Width of the screw channel
D Diameter of the barrel
H Screw channel height
N Screw speed in rpm
P Pressure
Q Volume flow rate per unit width
Q_t Volume flow rate per unit width in tangential direction
U Velocity in the X direction
V_o Barrel velocity $= \dfrac{\pi DN}{60}$
V_ξ Velocity in ξ direction
V_ζ Velocity in ζ direction
W Velocity in the Z direction
X Coordinate along the screw axis (axial direction)
Y Coordinate along the screw channel height, normal to screw root
Z Coordinate perpendicular to the screw axis (tangential direction)

Greek Letters

$\dot{\gamma}$ Shear rate
θ Helix angle

Subscripts

s At the screw
b At the barrel
ξ Cross channel direction normal to the screw flights
ζ Down channel direction along the screw helix

Superscripts

$'$ Screw moving situation in down and cross channel formulation

REFERENCES

FENNER, R.T. 1979. *Principles of Polymer Processing*, Chemical, New York.

RAUWENDAAL, C. 1986. *Polymer Extrusion*, Hanser Publishers, New York.

TADMOR, Z. and GOGOS, C.G. 1979. *Principles of Polymer Processing*, John Wiley & Sons, New York.

TADMOR, Z. and KLEIN, I. 1970. *Engineering Principles of Plasticating Extrusion*, Robert E. Krieger Publishing Co., Malbar, FL.

TAMURA, M.S., HENDERSON, J.M., POWELL, R.L. and SHOEMAKER, C.F. 1993. Analysis of the helical screw rheometer for fluid food. J. Food Process Engineering *16*, 93–126.

MODELING OF TRIGLYCERIDE DISTRIBUTION AND YIELD OF ANHYDROUS MILK FAT IN A CONTINUOUS SUPERCRITICAL CARBON DIOXIDE EXTRACTION SYSTEM

ZER-RAN YU, AJAY R. BHASKAR and SYED S.H. RIZVI

Institute of Food Science
Stocking Hall
Cornell University, Ithaca, NY 14853

Accepted for Publication March 13, 1994

ABSTRACT

A mathematical model was developed for continuous extraction of multicomponent mixture anhydrous milk fat (AMF) with supercritical carbon dioxide (SC-CO_2) as its solvent. At a constant temperature and pressure, the triglyceride mixture was separated into vapor and liquid fractions. The composition distribution (indicated by acyl carbon number), mass distribution and yield of AMF were calculated by the model based on thermodynamic equilibrium and material balance. The feed composition and distribution coefficient were required information in this model. The experimental values for the extract were in good agreement with the model used. The results for the raffinate were not as precisely modeled. The main factors which affected the model were temperature, pressure, solvent/feed ratio and extract fraction.

INTRODUCTION

Continuous extraction using supercritical fluid offers great potential in the industrial processing, as exemplified by the extraction of petroleum-derived oil mixtures using propane (Cotterman *et al.* 1984; Radosz *et al.* 1987), the extraction of fatty acids from edible oils with SC-CO_2 (Gutsche 1986), and the extraction of triglycerides in rapeseed oil (Klein and Schulz 1989) or in anhydrous milk fat (AMF) (Bhaskar *et al.* 1993) with SC-CO_2.

The equation of state has been used to predict the distribution of mixtures in continuous processes (Cotterman *et al.* 1984, 1985a,b; Gutsche 1986; Radosz *et al.* 1987; Ying *et al.* 1989). For convenience in calculating the equation of state, the continuous mixture distribution was replaced by a mathematical distribution function. Cotterman *et al.* (1985a,b) developed a method using Gaussian quadrature to predict composition distributions. Recently, Ying *et al.*

Journal of Food Process Engineering **18** (1995) 71–84.

(1989) introduced a new method based on a spline fit to improve the prediction. The composition distribution of AMF is an irregular function as indicated by acyl carbon number and, thus, is difficult to fit to the mathematical distribution function proposed by Cotterman *et al.* and Ying *et al.*

In the design of a continuous supercritical fluid extraction system, data are required on solubility, composition distribution and yield in the extract and raffinate. The solubility of AMF in SC-CO_2 can be obtained from experimental data (de Haan *et al.* 1990; Yu *et al.* 1992a,b) or can be predicted by using either the equation of state or a statistical method (Yu *et al.* 1994). The purpose of this study was to develop a mathematical model to predict AMF solubility, triglyceride composition distribution and yield of AMF in a continuous extraction system. This information can then be used to predict reasonable operation parameters for the processing of milk fat and similar multicomponent mixtures.

THEORY

The principles and the algorithms of a continuous extraction system are indicated in Fig. 1. The mixture of anhydrous milk fat (AMF) is indicated by the acyl carbon number of triglycerides from 24, 26, ..., to 54; and it is shown in the diagram as i component from 1, 2, ..., to 16. The multicomponent mixture (z(I)) of AMF (z(i)) with CO_2 (z(SC-CO_2)) is continuously fed into an extraction column at a constant temperature (T) and pressure (P). The mixture is extracted and separated into two fractions: vapor fraction (V) and liquid fraction (L). The vapor and liquid fractions contain I components in the extract (y(I)) and the raffinate (x(I)), respectively. The system's overall mass balance can be displayed as:

$$1 = V + L \tag{1}$$

and the composition balance is:

$$z(I) = V\, y(I) + L\, x(I) \tag{2}$$

If the system is assumed to reach thermodynamic equilibrium in the extract and the raffinate,

$$f^V(P,T,I) = f^L(P,T,I) \tag{3}$$

$$y(I)\, \phi^V(I)\, P = x(I)\, \phi^L(I)\, P \tag{4}$$

then the relation of composition in the vapor and liquid fractions can be written as:

$$\frac{y(I)}{x(I)} = \frac{\phi^{L}(I)}{\phi^{V}(I)} = K(I) \tag{5}$$

Using the thermodynamic equilibrium (Eq. 5) and the material balance (Eq. 1 and 2), y(I) and x(I) can be calculated from the following equations:

$$y(I) = \frac{z(I)\ K(I)}{1 + V\ (K(I)-1)} \tag{6}$$

and

$$x(I) = \frac{Z(I)}{1 + V(K(I)-1)} \tag{7}$$

The vapor fraction (V) in Eq. 6 and 7 is optimized by fitting the following equations:

$$\int I = SC\text{-}CO_2,\ i \text{ from } 1, 2, \ldots, \text{ to } 16^{\,x(I)\,=\,1}; \tag{8}$$

$$\int I = SC\text{-}CO_2,\ i \text{ from } 1, 2, \ldots, \text{ to } 16^{\,y(I)\,=\,1}; \tag{9}$$

or is correlated to the experimental data. The distribution coefficients (K(I)) in Eq. 5, 6 and 7 are obtained from the experimental data or estimated by the equation of state. In the former, the K(I) are obtained from the composition in both the extract and raffinate,

$$K(I) = \frac{y(I)}{x(I)} \tag{10}$$

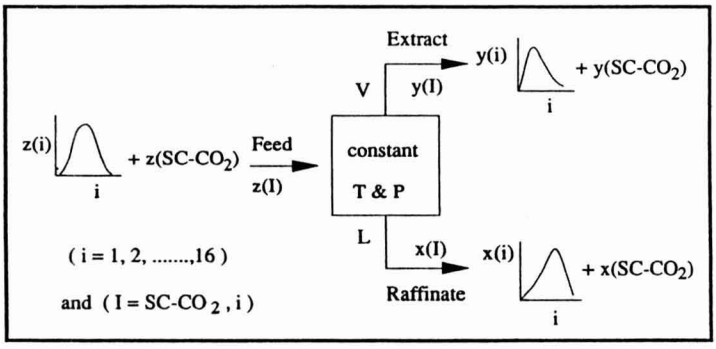

FIG. 1. SCHEMATIC DIAGRAM OF A CONTINUOUS EXTRACTION SYSTEM

The experimental y(I) and x(I) are obtained from fluid-liquid equilibrium data by either the static or dynamic method (King *et al.* 1983; Lahiere and Fair 1989). An alternative method to calculate K(I) is adopted from the equation of state. It is calculated by the fugacity in both phases ($\phi^V(I)$ and $\phi^L(I)$),

$$K(I) = \frac{\phi^L(I)}{\phi^V(I)} \tag{11}$$

The fugacity is derived from the thermodynamic relationship (Prausnitz *et al.* 1986)

$$RT \ln \phi_I = \int_v^\infty \left(\left(\frac{\partial P}{\partial n_I} \right)_{T,V,n_I} - \frac{RT}{V} \right) dV - RT \ln Z \tag{12}$$

and the Peng-Robinson equation with van der Waals mixing rule in this study (Peng and Robinson 1976).

$$P = \frac{RT}{v - B_M} - \frac{A_M}{v(v + B_M) + B_M(v - B_M)} \tag{13}$$

where

$$A_M = \sum_{I=1}^{N} \sum_{J=1}^{N} z(I)\ z(J)\ a(I,J) \tag{14}$$

$$a(I,J) = (1 - k(I,J))\ \sqrt{a(I)a(J)} \tag{15}$$

$$B_M = \sum_{I=1}^{N} z(I)\ b(I) \tag{16}$$

Equating

$$Z = \frac{Pv}{RT};\ A = \frac{A_M P}{R^2 T^2};\ B = \frac{B_M P}{RT} \tag{17}$$

then the fugacity coefficient of component in the mixture is given by:

$$\ln\Phi(I) = \frac{b(I)}{B_M}(Z-1) - \ln(Z-B) - \frac{A}{2\sqrt{2}B} * \left[\frac{2\sum_J z(J)a(J,I)}{A_M} - \frac{b(I)}{B_M}\right] * \ln\left[\frac{Z+2.414B}{Z-0.414B}\right] \quad (18)$$

EXPERIMENTAL METHODS

Phase Equilibria

Phase equilibria measurements of AMF triglycerides were done using a high pressure static method and have been reported (Yu *et al.* 1992a). Components of interest are circulated by a magnetic pump through a high pressure cell (capacity, 50 cm^3) to establish equilibrium between fluid and liquid phases. For a specified temperature and pressure, the fluid phase is defined as SC-CO_2 + extracted solutes and, conversely, the liquid phase is the insoluble material containing dissolved CO_2. After the system reaches equilibrium, the fluid and liquid samples are expanded into separate vessels, thus preventing cross contamination of phases.

Continuous Extraction

A continuous pilot-scale supercritical fluid system for extraction and fractionation of AMF was used as described (Bhaskar *et al.* 1993). Both AMF and SC-CO_2 were continuously fed countercurrently into a packed column at 24.1 MPa and 40C and separated into extract (material soluble in SC-CO_2) and raffinate (material insoluble in SC-CO_2). The column was packed with SS304 Goodloe knitted mesh packing.

RESULTS AND DISCUSSION

Correlation

AMF contains 97–98% triglycerides, 0.1–0.44% mono- and diglycerides, 0.3–0.7% free fatty acids and 0.2–0.4% cholesterol (Arul *et al.* 1988). The solvent/feed ratio, mass distribution, composition distribution, and yield are defined as:

$$\text{solvent/feed ratio} = \frac{z(SC-CO_2)}{\sum z(i)} \quad (19)$$

mass distribution for each phase

$$= \frac{z(i)}{\sum z(I)} ; \frac{y(i)}{\sum y(I)} * V ; \frac{x(i)}{\sum x(I)} * (1-V) \quad (20)$$

composition distribution for each phase

$$= \frac{z(i)}{\sum z(i)} ; \frac{y(i)}{\sum y(i)} ; \frac{x(i)}{\sum x(i)} \quad (21)$$

$$\text{yield}(\%) = \frac{\sum y(i)}{\sum z(i)} * V * 100\% \quad (22)$$

The mass and composition distributions are estimated from Eq. 6–7 and 20–21 when the feed composition (z(I)) and vapor fraction (V) are given and distribution coefficients (K(I)) are obtained from the experimental data (Yu *et al.* 1992a,b). The value of vapor fraction for this model can be correlated to the experimental data or it can be optimized from fitting Eq. 8 and 9. To determine an optimum value of V, the mass and composition distribution of triglycerides (indicated by acyl carbon number) and yield of AMF are correlated and compared to the experimental data at 24.1 MPa/313.15 K using a solvent/feed ratio of 62 (Bhaskar *et al.* 1993). In Fig. 2, the predicted mass distribution correlated well to the experimental data with a value of 0.99 for vapor fraction (V). However, as shown in Fig. 3, the predicted composition distribution is a poor fit to the raffinate data. Based on these results the value of V as 0.99 was chosen for further calculations.

Extract Loading and Solvent/Feed Ratio

The extract loading is used as an index to monitor the extract capacity for the solutes at different solvent/feed ratios and is defined as:

$$\text{extract loading} = \frac{\sum y(i)}{y(SC\text{-}CO_2)} \quad (23)$$

The extract loading predicted from the model at different solvent/feed ratios for 24.1 MPa and 313.15 K is shown in Fig. 4. The predicted value is higher than the experimental data at the low solvent/feed ratio, but exhibits good agreement at the high solvent/feed ratios. Since the extraction column does not attain the equilibrium state at the low solvent/feed ratio, an optimum solvent/feed ratio above 50 is chosen because the experimental data are close to the equilibrium extract loading value. This is also confirmed by the work of Bhaskar *et al.* (1993) in which they use a high solvent/feed ratio of 62 in their experiments on AMF fractionation with SC-CO_2.

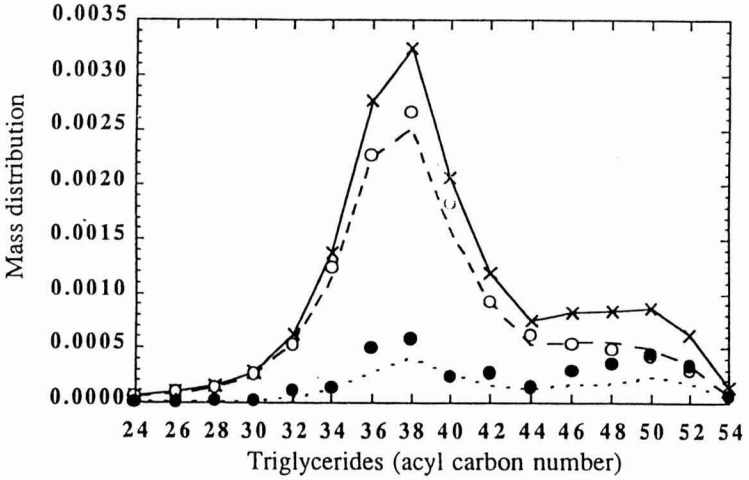

FIG. 2. MEASURED (BHASKAR *ET AL.* 1992) AND CALCULATED MASS DISTRIBUTION OF TRIGLYCERIDES IN THE SC-CO_2 + AMF SYSTEM AT 24.1 MPa AND 313.15 K

×: feed; ○: extract; ●: raffinate; —: feed; – –: predicted extract; ····: predicted raffinate

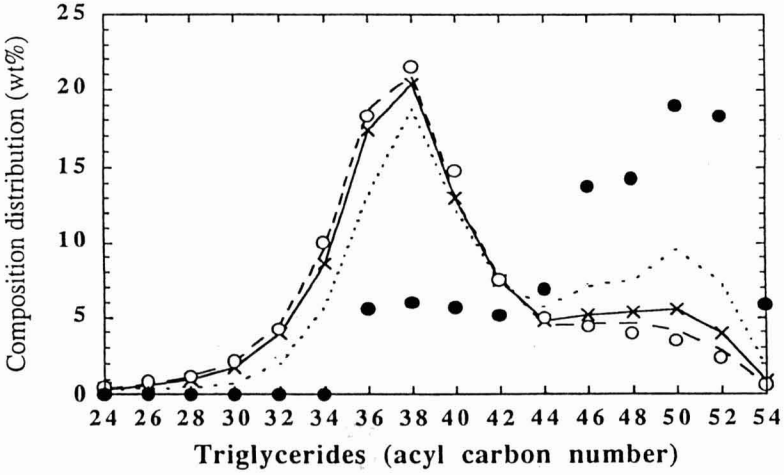

FIG. 3. MEASURED (BHASKAR *ET AL.* 1992) AND CALCULATED COMPOSITION DISTRIBUTION OF TRIGLYCERIDES IN THE SC-CO_2 + AMF SYSTEM AT 24.1 MPa AND 313.15 K

×: feed; ○: extract; ●: raffinate; —: feed; – –: predicted extract; ····: predicted raffinate

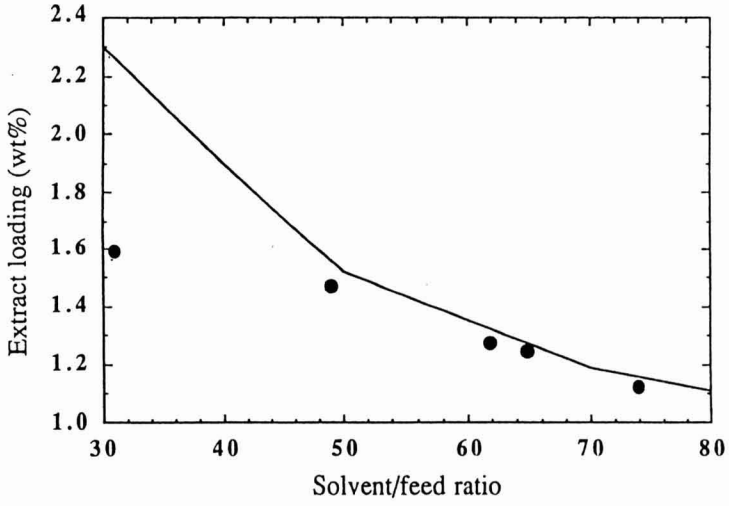

FIG. 4. MEASURED (BHASKAR *ET AL.* 1992) AND CALCULATED EXTRACT LOADING AGAINST DIFFERENT SOLVENT/FEED RATIOS AT 24.1 MPa AND 313.15 K
●: measured value; —: predicted value

Distribution Coefficients

Another method to calculate the composition distribution is to apply the distribution coefficients (K(I)) from an equation of state to the mathematical model. In this study, the K(I) in the model are calculated by the Peng-Robinson equation with the van der Waals mixing rule. When the interaction parameters (k(I,J)) are used in the Peng-Robinson equation, a value of zero is used between two components I and J, and it is estimated between each component in AMF (indicated by acyl carbon number (ACN)) with SC-CO_2 by the following equation:

$$k(ACN,SC\text{-}CO_2) = 0.49 - (ACN - 24)*0.005 \qquad (24)$$

which was obtained from the data of Yu *et al.* (1994). Using this information, the calculated distribution coefficient of each component in AMF is compared to the experimental data (Yu *et al.* 1992b) in Fig. 5. The experimental distribution coefficients correlate well to the model values for ACN C_{30} through C_{38}. The poor fit for other ACN may be due to either that the interaction parameters between solutes are not zero or that the equation of state is not suitable for high molecular weight compounds (Cotterman *et al.* 1985b). Since

this information is difficult to apply in predicting the triglycerides distribution and yield of AMF in a continuous extraction system, the predictions obtained from the equation of state are not suitable for AMF. It is suggested to use the distribution coefficients from the experimental data as shown in the work of Yu *et al.* (1992a,b).

Temperature and Pressure

The distribution coefficients (K(I)) are dependent on temperature and pressure (Eq. 3–5) and hence the composition distribution and yield of AMF will vary by fitting different K(I) into the model. The model is tested for continuous AMF extraction with SC-CO_2 at a solvent/feed ratio of 60 for pressures of 10, 20 and 30 MPa, and temperatures of 313.15 and 333.15 K. The distribution coefficients used at these conditions are taken from Yu *et al.* (1992b). The triglycerides are divided into three groups, namely low-melting triglycerides (C_{24} - C_{34}), medium-melting triglycerides (C_{36} - C_{40}) and high-melting triglycerides (C_{42} - C_{54}). Figure 6 shows the grouped triglyceride distribution and yield of AMF at different temperatures and pressures as predicted by the model. At 30 MPa and both 313.15 and 333.15 K, a high yield of AMF and a low low-melting triglycerides composition are obtained in the extract. Since the experimental data for continuous extraction was available only at 24.1 MPa and 313.15 K, these results were compared to another study by Yu *et al.* (1992b). At 30 MPa

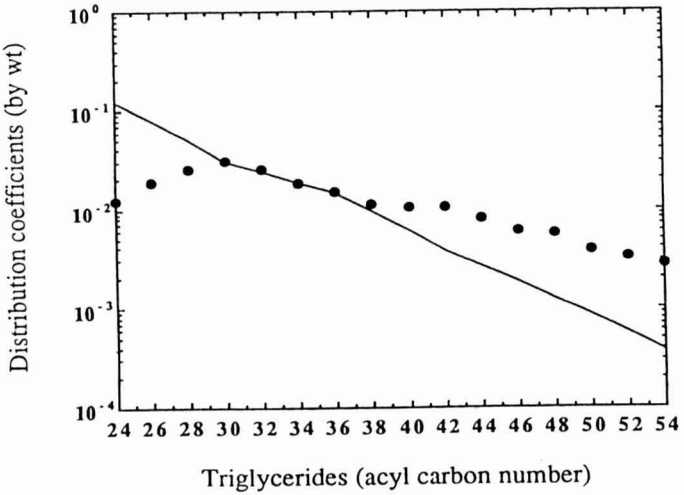

FIG. 5. MEASURED (YU *ET AL.* 1992b) AND CALCULATED DISTRIBUTION COEFFICIENTS OF TRIGLYCERIDES IN THE SC-CO_2 + AMF SYSTEM AT 20.84 MPa AND 313.15 K
●: measured value; —: predicted value

and both 313.15 and 333.15 K, their results show high distribution coefficients and low relative composition of low-melting triglycerides in the fluid phase as seen by the model (Tables 1 and 2 and Fig. 7).

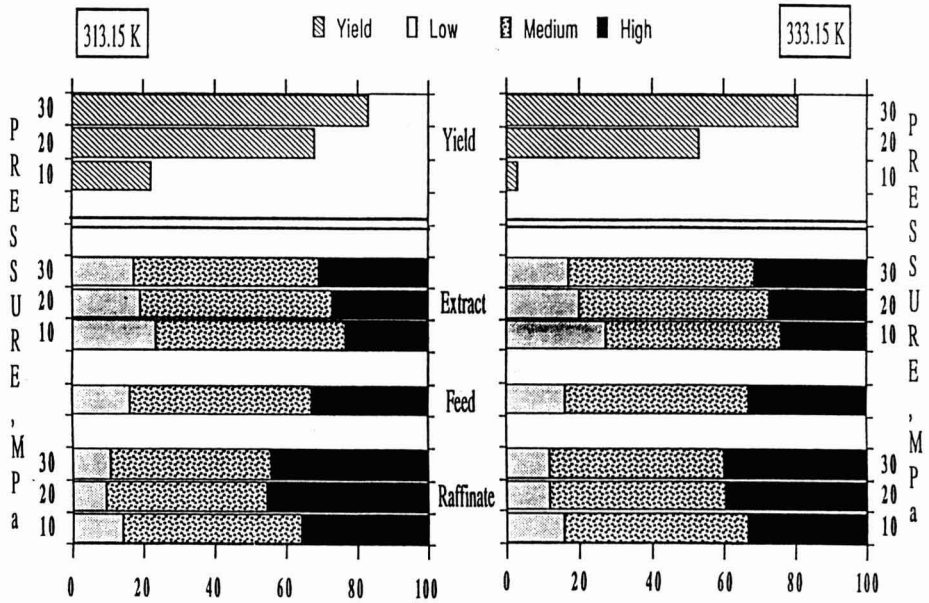

FIG. 6. PREDICTED YIELD OF AMF AND COMPOSITION DISTRIBUTION OF TRIGLYCERIDES IN THE SC-CO_2 + AMF SYSTEM AT 10, 20 AND 30 MPa, AND 313.15 AND 333.15 K

TABLE 1.
COMPOSITION DISTRIBUTION OF AMF TRIGLYCERIDES AT 313.15 K

Pressure (MPa)	Extract-Model				Fluid Phase-Yu *et al.* (1992b)		
	Low	Medium	High	Yield	Low	Medium	High
10	23.54	53.43	23.03	22	28.24	39.97	31.79
20	19.36	53.57	27.07	68	31.59	40.79	27.62
30	17.37	52.00	30.63	83	25.39	40.66	33.95

TABLE 2.
COMPOSITION DISTRIBUTION OF AMF TRIGLYCERIDES AT 333.15 K

Pressure (MPa)	Extract-Model				Fluid Phase-Yu *et al.* (1992b)		
	Low	Medium	High	Yield	Low	Medium	High
10	15.92	50.86	33.22	3	29.40	36.06	34.54
20	11.84	48.44	39.73	53	27.72	39.50	32.78
30	12.10	47.94	39.96	81	21.23	38.72	39.05

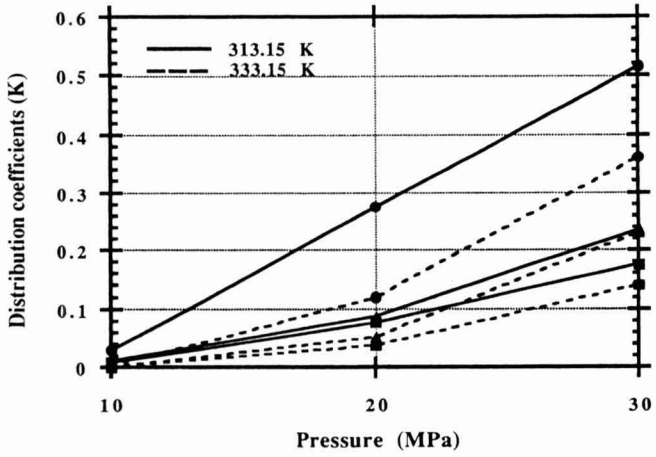

FIG. 7. DISTRIBUTION COEFFICIENTS OF AMF TRIGLYCERIDES AT 313.15 AND 331.15 K FOR DIFFERENT PRESSURES (YU *ET AL.* 1992b)
●- low; ▲-medium; ■-high

CONCLUSIONS

Using SC-CO_2 as the solvent, an extract and raffinate are continuously obtained from feeding AMF into an extraction column. An optimum value of the vapor fraction is correlated and obtained from the experimental data. The temperature, pressure, solvent/feed ratio and vapor fraction are the main parameters in the model that can be used to predict the solubility, mass distribution, composition distribution and yield in a continuous extraction system. In this model it is better to use the distribution coefficient from the experimental data than the distribution coefficient from an equation of state.

NOMENCLATURE

a	Attraction parameter
A_M	Constant defined by Eq. 14
A	Constant defined by Eq. 17
b	van der Waals covolume
B_M	Constant defined by Eq. 16
B	Constant defined by Eq. 17
f	Fugacity
i	Free-solvent continuous mixtures defined in Fig. 1
I and J	Continuous mixtures defined in Fig. 1
k	Interaction parameter
K	Distribution coefficient
L	Liquid fraction
N	Number of components
P	Pressure
R	Gas constant
T	Temperature
v	Volume
V	Vapor fraction
x	Mass or mole fraction of component in the raffinate
y	Mass or mole fraction of component in the extract
z	Mass or mole fraction of component in the feed
Z	Compressibility factor

Greek Letters

ϕ	Fugacity coefficient

Superscripts

V	Supercritical fluid phase
L	Liquid phase

REFERENCES

ARUL, J., BOUDREAU, A., MAKHLOUF, J., TARDIF, R. and BELLAVIA, T. 1988. Fractionation of anhydrous milk fat by short-path distillation. JAOCS, *65*, 1642–1645.

BHASKAR, A.R., RIZVI, S.S.H. and HARRIOTT, P. 1993. Performance of a packed column for continuous supercritical carbon dioxide processing of anhydrous milk fat. Biotechnol. Prog. *9*, 70–74.

COTTERMAN, R.L., BENDER, R. and PRAUSNITZ, J.M. 1985a. Phase equilibria for mixtures containing very many components. Development and application of continuous thermodynamics for chemical process design. Ind. Eng. Chem. Process Des. Dev. *24*, 194–203.

COTTERMAN, R.L., DIMITRIOS, D. and PRAUSNITZ, J.M. 1984. Supercritical-fluid extraction calculations for high-boiling petroleum fractions using propane. Application of continuous thermodynamics. Ber. Bunsenges. Phys. Chem. *88*, 796–801.

COTTERMAN, R.L. and PRAUSNITZ, J.M. 1985b. Flash calculations for continuous or semicontinuous mixtures using an equation of state. Ind. Eng. Chem. Process Des. Dev. *24*, 434–443.

GUTSCHE, B. 1986. Phase equilibria in oleochemical industry. Application of continuous thermodynamics. Fluid Phase Equilibria *30*, 65–73.

de HAAN, A.B., de GRAAUW, J., SCHAAP, J.E. and BADING, H.T. 1990. Extraction of flavor from milk fat with supercritical carbon dioxide. J. Supercritical Fluids *3*, 15–19.

KING, M.B. *et al.* 1983. Some vapour/liquid and vapour/solid equilibrium measurements of relevance for supercritical extraction operations, and their correlation. In *Chemical Engineering at Supercritical Conditions*, (M.E. Paulaitis, J.L. Penninger, R.D. Gray, and P. Davidson, eds.) pp. 31–80, Ann Arbor, MI.

KLEIN, T. and SCHULZ, S. 1989. Phase equilibria in mixtures of glycerides and carbon dioxide and application of continuous thermodynamics to mixtures of rapeseed oil and carbon dioxide. Fluid Phase Equilibria *50*, 79–100.

LAHIERE, R.J. and FAIR, J.R. 1989. Novel technique to measure equilibria of supercritical solvents and liquid mixture. J. Chem. Eng. Data *34*, 275–278.

PENG, D.Y. and ROBINSON, D.B. 1976. New two-constant equation of state. Ind. Eng. Chem. Fundam. *15*, 59–64.

PRAUSNITZ, J.M., LICHTENTHALER, R.N. and de AZEVEDO, E.G. 1986. *Molecular Thermodynamics of Fluid-Phase Equilibria*, 2nd Ed., Prentice-Hall, Englewood Cliffs, NJ.

RADOSZ, M., COTTERMAN, R.L. and PRAUSNITZ, J.M. 1987. Phase equilibria in supercritical propane systems for separation of continuous oil mixtures. Ind. Eng. Chem. Res. *26*, 731–737.

YING, X., YE, R. and HU, Y. 1989. Phase equilibria for complex mixtures. Continuous-thermodynamics method based on spline fit. Fluid Phase Equilibria *53*, 407–414.

YU, Z.R., RIZVI, S.S.H. and ZOLLWEG, J.A. 1992a. Phase equilibria of oleic acid, methyl oleate, and anhydrous milk fat in supercritical carbon dioxide. J. Supercritical Fluids *5*, 112–122.

YU, Z.R., RIZVI, S.S.H. and ZOLLWEG, J.A. 1992b. Fluid-liquid equilibria of anhydrous milk fat with supercritical carbon dioxide. J. Supercritical Fluids *5*, 123-126.

YU, Z.R., SINGH, B., RIZVI, S.S.H. and ZOLLWEG, J.A. 1994. Solubilities of fatty acids, fatty acid esters, triglycerides, fat and oils in supercritical carbon dioxide. J. Supercritical Fluids *7*(1), 51–59.

A COMPARISON OF ALTERNATIVE FORMULATIONS FOR THE PREDICTION OF ELECTRICAL HEATING RATES OF SOLID-LIQUID FOOD MATERIALS

LI ZHANG and P.J. FRYER[1]

Department of Chemical Engineering
Pembroke St., Cambridge, CB2 3RA, UK

Accepted for Publication March 13, 1994

ABSTRACT

The modelling of the electrical heating of solid-liquid food mixtures is an active area of research, reflecting its new importance as a commercial process. Two published models for electrical heating have been compared, and the accuracy of the use of circuit analogies for the prediction of heating rate was examined. It is shown that circuit analogies may not predict the heating rate correctly, especially at low solids fraction. The applicability of circuit analogies for the calculation of the heating effects of isolated particles of significantly different conductivity to the medium is discussed.

INTRODUCTION

The recent development of a commercial food sterilization process in which solid-liquid food mixtures of high solids fractions are sterilized by the application of electric current (Biss *et al.* 1989) has led to a number of attempts to model the process. de Alwis and Fryer (1988) and de Alwis *et al.* (1989) showed the range of effects which could result during electrical processing; depending on the solid and liquid electrical conductivities and the orientation of particles to the electric field, particles can heat both faster and slower than the liquid. It was noted that particles of basically uniform cross-section, such as spheres and cubes, displayed little variation in heating rate with orientation, while particles with a larger aspect ratio could experience significant variation in heating rate. This phenomenon was modelled by de Alwis and Fryer (1990), who demonstrated that the process could be modelled by solving Laplace's equation

$$\nabla.(\kappa\nabla V)=0 \qquad (1)$$

[1] Correspondent: Prof. P.J. Fryer, School of Chemical Engineering, University of Birmingham, Edgbaston, Birmingham B15 2TT, UK.

Journal of Food Process Engineering **18** (1995) 85-97.

where V is voltage, throughout the system. If this equation is solved, the electric field intensity, $E = \text{grad } V$, and the heat generation $Q = \kappa|E|^2$ can then be calculated at each point, and incorporated into models for thermal conduction and convection. A finite element model of the heater was developed and compared to experimental results.

de Alwis (1990) and de Alwis and Fryer (1992) developed this model to consider the range of conductivities which could be used to generate satisfactory heating rates in a realistic system, and described two sorts of problems in materials selection:

(1) selection of the correct overall electrical conductivity of the mixture to ensure that the mixture heats at a commercially satisfactory rate,
(2) ensuring that the local electrical conductivity of the medium is not such that local cold or hot spots arise.

Possible effects of particles of very high and very low electrical conductivity were modelled by de Alwis (1990); such particles will heat at a very slow rate, and will affect the temperature distribution within the surrounding fluid (Fryer *et al.* 1993). Such particles thus represent a possible threat to the sterility of the system, and it is important to be able to estimate the effect that they have on system temperatures and thus on system sterility.

The model of de Alwis and Fryer (1990) was only two-dimensional; significant extra computing power is required to model three-dimensional systems. The use of a 3D system was reported by de Alwis *et al.* (1991, 1992), who used the commercial program, ANSYS (Swanson Analysis Systems, Houston, PA), to solve Eq. (1) for three-dimensional systems. Zhang *et al.* (1992) presented a model for the heating of a 3D model based on the identification of repeating 'unit cells' in the system, as discussed below.

More recently, an alternative approach to modelling electrical heating has been suggested by Sastry and Palaniappan (1992a,b), who used a circuit analogy to approximate the behavior of a food material. Sastry (1992) presented a model for a commercial heater based on this approach. The aim of this note is to compare the two approaches and determine the range of situations for which a circuit analogy may be appropriate.

MODELS FOR ELECTRICAL HEATING

As noted in the paper, the circuit analogy used by Sastry (1992) is considerably less expensive in computer time than the solution of Laplace's equation advocated by de Alwis and Fryer. The method approximates the behavior of a solid-liquid mixture of solids fraction ϕ, in a section of thickness Δx, in terms

of three resistances, corresponding to liquid and solid in parallel and liquid in series, as shown in Fig. 1. The size of the three resistances depends on the electrical conductivity of the two materials and on the solids fraction.

The method effectively assumes that the electric current is everywhere parallel to the direction of flow. In practice, however, current flow lines will be curved, as demonstrated by de Alwis and Fryer (1989), who solved Laplace's equation for the current flow around an isolated spherical particle. The more complex effects which occur in systems of higher solids fraction and complex geometries are shown in Zhang and Fryer (1993a). The current flow in any system will in practice not be that predicted by the simple circuit analogy. This may lead to errors in the calculation of the heating rates.

Zhang *et al.* (1992) suggest a model which, like Sastry, assumes that sections of the fluid can be modelled as representative of the whole. If it is assumed that the distribution of particles in the liquid is uniform, the tube can be divided into

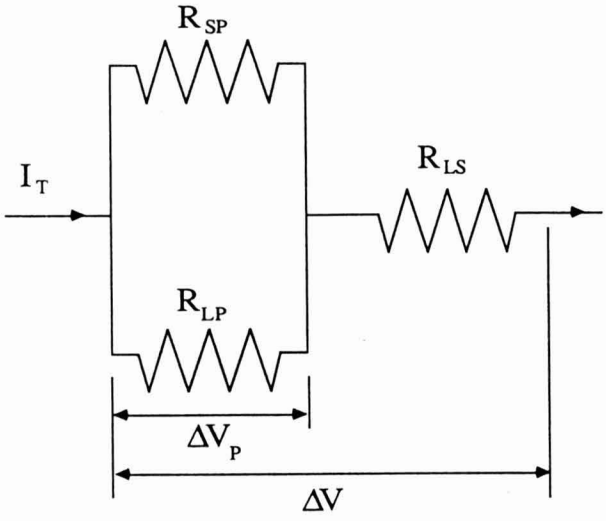

FIG. 1. THE CIRCUIT ANALYSIS OF A SECTION OF SOLID-LIQUID MIXTURE USED BY SASTRY (1992)

a number of 'unit cells' each containing a number of particles; this approach is common in systems which show symmetry (McKie and McKie 1986). Each unit cell is identical, so it is only necessary to model one to predict the behavior of the whole. Figure 2 shows a possible cell pattern in which particles are distributed on a cubic lattice; cell size can be adjusted to solve for any solids fraction. The boundary conditions are (1) no current flow across the boundary (A-A) (so the wall of the heater can be placed there), and (2) constant voltage across (B-B), i.e., current flow perpendicular to the surface. Due to internal symmetry, only one eighth of the cell needs to be simulated. ANSYS has been used to solve Eq. (1) for such cells to predict the voltage distribution of the solid and liquid phases.

The 'unit cell' model forms the basis of the model for electrical heating given by Zhang and Fryer (1993b) in which data from the unit cell model is incorporated into enthalpy balance models for the two flowing phases, solid and liquid. If the heat generation rates in the solid and liquid are uniform it is possible to approximate the response of the system; Fryer *et al.* (1993) show that uniform heating in the liquid is possible and Zhang and Fryer (1993b) show that a rotating particle can heat uniformly.

The two models use similar assumptions about the flows and enthalpy balances. To compare them, it is thus necessary only to compare the different formulations for the heating term. In the model of Zhang *et al.* (1992) ANSYS was used to predict Q as a function of solids fraction and the ratio of solid to liquid electrical conductivity, $R_\kappa = \kappa_S/\kappa_L$. It was found convenient to define ratios of the local heat generation rate at a point relative to the heat generation rate (per unit volume of material) that would result if only the liquid were present, Q_1;

$$Q_1 = \kappa_L |E|^2 \tag{2}$$

so that

$$R_Q = \frac{Q}{Q_1} \tag{3}$$

This produces a generalized dimensionless ratio. Zhang and Fryer (1993) gave plots of the heat generation ratios R_Q in the two phases using the unit cell model (for unit cells containing a single sphere) and gave a sample calculation for the solution of the heating of a system of constant physical properties.

Using the circuit assumptions of Sastry's model, it is thus possible to calculate R_Q algebraically. Values for the three resistances in the pipe section of Fig. 1 are given by Sastry (1992), as (modified to our nomenclature, shown in Fig. 1):

$$R_{LS}=\frac{\Delta x_s}{A_{LS}\kappa_L} \qquad R_{LP}=\frac{\Delta x_p}{A_{LP}\kappa_L} \qquad R_{SP}=\frac{\Delta x_p}{A_{SP}\kappa_s} \tag{4}$$

where the relationship between the various areas and distances is given by

$$\Delta x=\Delta x_s+\Delta x_p \qquad \Delta x_p=\Delta x\phi^{1/3} \qquad \Delta x_s=\Delta x(1-\phi^{1/3}) \tag{5}$$

$$A_{sp}=A\phi^{2/3} \qquad A_{LP}=A(1-\phi^{2/3}) \qquad A_{LS}=A \tag{6}$$

where A is the area of the section. The above equations assume that the solids are cubic, and make no assumption of the size of the pipe. Similar assumptions are used by Zhang *et al.* (1992) in the derivation of the size of the unit cell for spheres (Fig. 2).

Two liquid heating rates and one solid heating rate can be calculated using the above equations. It is unclear from the paper of Sastry (1992) how a mean liquid temperature is produced from the model; we have thus only examined the heating of solids using the two techniques. The ratio

$$R_{QS}=\frac{Qs}{Q1} \tag{7}$$

has been calculated using ANSYS to solve Laplace's equation for a unit cell containing a single cube centered in the cell, and of sides parallel to the cell sides, for various $R\kappa$ and ϕ. The corresponding ratio for the circuit theory has been calculated as follows. For the section of Fig. 1:

$$Q_s=(\frac{\Delta V_p}{\Delta x_p})^2\kappa_s \qquad Q_1=(\frac{\Delta V}{\Delta x})^2\kappa_L \tag{8}$$

so that

$$R_{QS}=\frac{Q_s}{Q_1}=R_\kappa(\frac{\Delta V_p}{\Delta V}\frac{\Delta x}{\Delta x_p})^2 \tag{9}$$

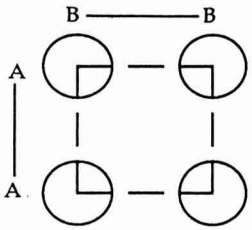

(a) regular lattice of circles in 2D

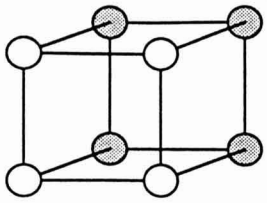

(b) regular lattice of spheres in 3D

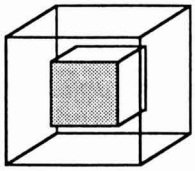

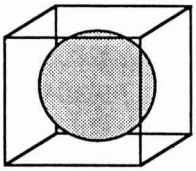

(c) Unit cells used here; cube and sphere centered in cell.

FIG. 2. THE 'UNIT CELL' APPROACH OF ZHANG *ET AL.* (1992) AND ZHANG AND FRYER (1993b).

In the system of Fig. 1, the resistance of the parallel section can be written

$$\frac{1}{R_P}=\frac{1}{R_{LP}}+\frac{1}{R_{SP}} \tag{10}$$

so that the voltage drop across the parallel section can be written as

$$\Delta V_P=R_P I_T \tag{11}$$

where I_T is the total current flowing, and the voltage drop across the whole section can be written as

$$\Delta V=(R_p+R_{LS})I_T \tag{12}$$

giving

$$\frac{\Delta V_P}{\Delta V} = \frac{R_P}{(R_P + R_{LS})} \tag{13}$$

Substitution of Eq. (13) into Eq. (9), followed by substitution of Eq. (5) and (6) and manipulation, gives an equation which relates the heat generation ratio to the solids fraction and the ratio of the phase conductivities:

$$R_{QS} = \frac{R_\kappa}{[(\phi^{2/3} - \phi)(R_\kappa - 1) + 1]^2} \tag{14}$$

Figure 3 plots the heat generation for a cube centered in a unit cell, using ANSYS, giving R_{QS} as a function of R_κ and solids fraction ϕ. A series of smooth curves are produced which all pass through the point (1,1), i.e., when the solid conductivity is equal to the liquid, heat is generated at the same rate within both phases.

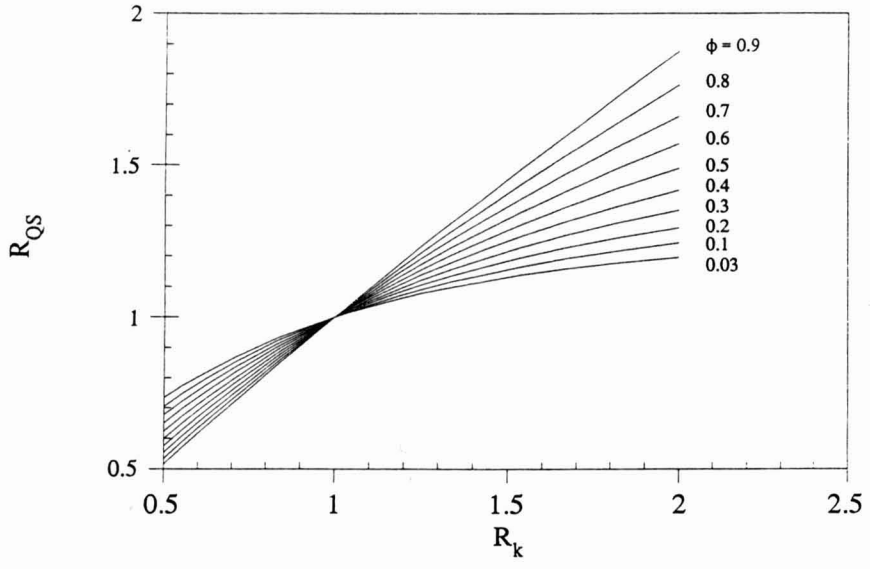

FIG. 3. HEAT GENERATION DATA PRODUCED BY SOLVING LAPLACE'S EQUATION FOR A UNIT CELL CONTAINING A SINGLE CUBE CENTERED IN THE CELL

R_{QS} can also be calculated as a function of R_κ and ϕ from Eq. (14). This data is plotted in Fig. 4. As with the Laplace's equation solution, the curves all pass through (1,1). However, while the curves in Fig. 3 change smoothly with ϕ, those of Fig. 4 do not; for $R_\kappa > 1$, R_{QS} first decreases with increasing ϕ and then increases. Figure 4 includes a curve for the small solids fraction of 0.1%, which the circuit theory predicts as having a higher R_{QS} than a solids fraction of 0.9. The minimum R_{QS} for a given R_κ for the circuit model can be found by differentiating Eq. (14); at $R_\kappa = 2$, the minimum occurs at $\phi = 0.296$.

The two models do not give the same results, therefore. Figure 5 plots the relative error between the two, calculated as:

$$\frac{\text{Value from equation (14)} - \text{Laplace solution}}{\text{Laplace solution}} \times 100\% \qquad (15)$$

While at high solids fractions the differences between the two methods are small, significant errors of up to 30% in the range $0.5 \leq R\kappa \leq 2$, are found at lower concentrations. Even small errors can give rise to temperature differences which may give significant errors in sterility and quality values. Outside the calculated range of R_κ, the error will be larger.

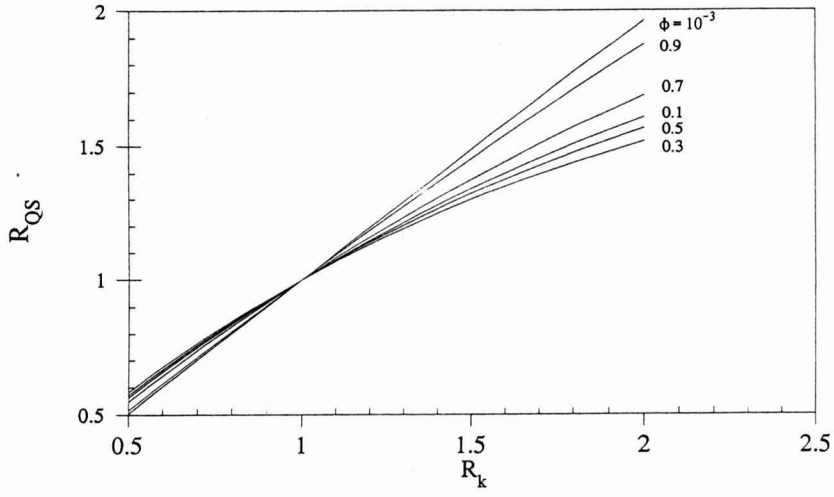

FIG. 4. HEAT GENERATION DATA PRODUCED BY SOLVING EQ. (14) FOR THE CIRCUIT ANALYSIS

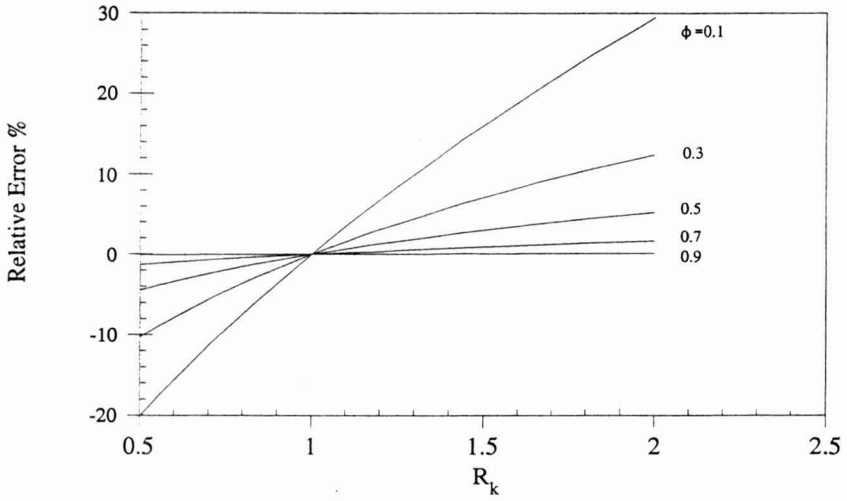

FIG. 5. RELATIVE ERROR BETWEEN THE SOLUTION OF LAPLACE AND THE CIRCUIT ANALYSIS

The calculations indicate that the circuit analogy model gives a result significantly different from Laplace's equation for this geometry and for low solids fractions. The unit cell model may not be an accurate representation of the conditions in the electrical heater, since it assumes a uniform dispersion of particles which may not be the case in practice. However, it here provides an accurate test of the applicability of the circuit approximation. The circuit model should probably not be used for solids fractions below about 30%. Since the commercial unit operates at high solids fractions, where the two models give very similar results, this does not limit the use of the model in some areas. However, one important problem in electrical heating is the calculation of the effect that isolated particles of significantly different conductivity will have on the process, i.e., the effect of passing particles of different material through the heater. In conduction heating of solid-liquid mixtures, the thermal response of different particles can be approximated by first calculating a mean liquid temperature profile and exposing the particle to it, as in the model of Sastry (1986). Since in electrical heating any particle will significantly affect the temperature field around it by distorting the electrical field (as shown by Fryer *et al.* 1993) it is not possible to assume that the particle will not affect the local conditions, and thus its thermal response. To study and confirm the safety of electrical heating it is important to be able to determine the local temperature field caused by particles of different conductivity. The circuit analogy does not

appear appropriate in this case, since the inclusion particle will effectively have a low solids fraction; in this case, it will probably be necessary to solve Laplace's equation in the chosen geometry.

Equations (4)–(6) assume that the particles in the unit cell are cubes. As noted by Sastry (1992), these equations will not be valid for the case of particles of nonuniform aspect ratio, such as the particles studied by de Alwis *et al.* (1989) and de Alwis and Fryer (1990). However, even for spherical particles, which have a uniform aspect ratio, differences can arise between the Laplace solution and the circuit analogy. Figure 6 shows the relative error between the circuit analogy (Eq. 14) and the solution of Laplace's equation for a cell containing a single sphere centered in the cell. Here the upper limit of the unit cell model is a solids fraction of 0.68, corresponding to the close packing limit. As before, errors of up to 20% are found, but the dependence of the error on the solids fraction is different. Unit cells can be constructed to represent any given situation, and Laplace's equation solved to give estimates of heating rate; the accuracy of the circuit analogy to a general situation is questionable.

It should be emphasized that this is a purely theoretical analysis. Both the Laplace model and the circuit analogy have been shown to represent experimental data in certain cases (de Alwis *et al.* 1990; de Alwis and Fryer, 1990; Sastry and Palaniappan 1992b). As noted by Sastry (1992), in the absence of experimental verification on an operating heater, it is necessary to make approximations to model the system. Given the temperature sensitivity of the

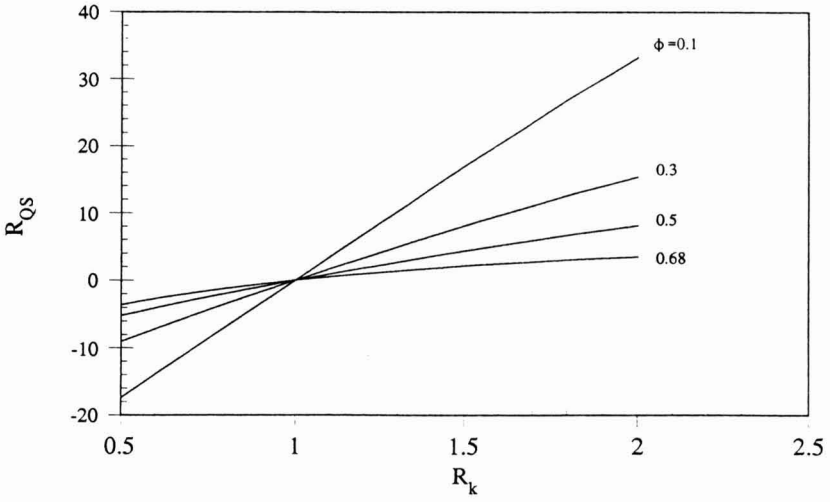

FIG. 6. RELATIVE ERROR BETWEEN SOLUTION OF LAPLACE'S EQUATION FOR A UNIT CELL CONTAINING A SINGLE SPHERE CENTERED IN THE CELL, AND THE CIRCUIT ANALYSIS

equations for sterility and quality loss, however, it is important that such approximations should solve the basic equations as accurately as possible. The circuit theory model is a computationally cheap way of modelling the system. However, the direct solution of Laplace's equation in this case, although more computationally expensive, is a more general approach to this difficult problem. It should be noted that the unit cell model assumes that particles are uniformly distributed on a lattice, which is unlikely to be the case in practice; it is possible that grouping of particles will lead to current channeling in ways not predicted by the unit cell approach. Equally, however, the circuit analogy would have problems in this case. Any model should thus be used with care.

CONCLUSIONS

Two published methods (Zhang *et al.* 1992; Sastry 1992) for the calculation of particle heating rates in electrical ('ohmic') heating have been compared. The calculation using Laplace's equation is more complex in time and computing power than the use of a circuit analogy. However, it has been shown that the circuit analogy may not be appropriate in some cases, and can give significant errors at low solids fractions. It is thus difficult to apply it to the case of an single particle of significantly different conductivity, a case which may be important in determining the safety of the process.

ACKNOWLEDGMENTS

Original financial support for work on electrical heating at Cambridge was provided by APV Baker. This work was supported by an AFRC grant to LZ. We are grateful for the provision of the ANSYS program at an academic rate by Strucom Ltd., Croydon, Surrey.

NOMENCLATURE

A	Cross sectional area of section (m^2)
A_{LP}	Area of liquid in parallel section (m^2)
A_{LS}	Area of liquid in series section (m^2)
A_{SP}	Area of solid in parallel section (m^2)
E	Voltage gradient (V/m)
I_T	Total current flowing (A)
Q	Heat generation rate (W/m^3)
Q_l	Heat generation rate for liquid alone (W/m^3)
Q_s	Heat generation rate in solid (W/m^3)

R_κ Conductivity ratio $\frac{\kappa_s}{\kappa_L}$
R_{LP} Resistance of liquid in parallel section (Ω)
R_{SP} Resistance of solid in parallel section (Ω)
R_{LS} Resistance of liquid in series section (Ω)
R_Q Ratio $\frac{Q}{Q_1}$
R_{QS} Ratio $\frac{Q_s}{Q_1}$
V Voltage
ΔV Voltage drop across any section (V)
ΔV_p Voltage drop across parallel section (V)
Δx Length of section (m)
Δx_p Length of parallel section (m)
Δx_S Length of series section (m)
κ Electrical conductivity (S m^{-1})
κ_L Liquid electrical conductivity (S m^{-1})
κ_s Solid electrical conductivity (S m^{-1})
ϕ Solids fraction

REFERENCES

BISS, C.H., COOMBES, S.A. and SKUDDER, P.J. 1989. The development and application of ohmic heating for the continuous heating of particulate foodstuffs. In *Engineering Innovation for the Food Industry*, (J.A. Howell and R. Field, eds.) Elsevier, London.

DE ALWIS, A.A.P. 1990. Ohmic heating of foods, Ph.D. thesis, Cambridge University.

DE ALWIS, A.A.P. and FRYER, P.J. 1988. Preliminary experiments on heat transfer during the ohmic heating of foods. In *Proceedings of the 2nd UK Nat. Heat. Transf. Conf.*, Vol. I, IMechE.

DE ALWIS, A.A.P. and FRYER, P.J. 1990. A finite element analysis of heat generation and transfer during ohmic heating of food. Chem. Eng. Sci. *45*, 1547–1560.

DE ALWIS, A.A.P. and FRYER, P.J. 1992. Operability of the ohmic heating process: electrical conductivity effects. J. Food Eng. *15*, 21–48.

DE ALWIS, A.A.P, HALDEN, K. and FRYER, P.J. 1989. Shape and conductivity effects in the ohmic heating of foods. Chem. Eng. Res. Des. *67*, 159–168.

DE ALWIS, A.A.P, ZHANG, L. and FRYER, P.J. 1992. Modelling sterilisation and quality in the ohmic heating process. In *Advances in Aseptic Processing Technologies*, (R.K. Singh and P.E. Nelson, eds.) pp. 103–142, Elsevier, New York.

FRYER, P.J., DE ALWIS, A.A.P, KOURY, E., STAPLEY, A.G.F. and ZHANG, L. 1993. Ohmic heating of solid-liquid foods; heat generation and convection effects. J. Food Eng. *18*, 101–125.

McKIE, D.M. and McKIE, C.H. 1986. Fundamentals of Crystallography, John Wiley & Sons, London.

SASTRY, S.K. 1986. Mathematical evaluation of process schedules for aseptic processing of low-acid foods containing discrete particles. J. Food Sci. *51*, 1323–1332.

SASTRY, S.K. 1992. A model for heating of liquid-particle mixtures in a continuous flow ohmic heater. J. Food Proc. Eng. *15*, 263–278.

SASTRY, S.K. and PALANIAPPAN, S. 1992a. Influence of particle orientation on the effective electrical resistance and ohmic heating rate of a liquid-particle mixture. J. Food Proc. Eng. *15*, 213–227.

SASTRY, S.K. and PALANIAPPAN, S. 1992b. Mathematical modeling and experimental studies on ohmic heating of liquid-particle mixtures in a static heater. J. Food Proc. Eng. *15*, 241–261.

ZHANG, L. and FRYER, P.J. 1993a. Electrical resistance heating of foods. Trend in Food Sci. Technol. *4*, 364–369.

ZHANG, L. and FRYER, P.J. 1993b. Models for the electrical heating of solid-liquid food mixtures. Chem. Eng. Sci. *48*, 633–643.

ZHANG, L., LIU, S., PAIN, J.-P. and FRYER, P.J. 1992. Heat transfer and flow of particle-liquid food mixtures. IChemE Symp. Ser. *126*, 79–88.

EVALUATION OF CONTINUOUS THERMAL PROCESSES USING THERMOCOUPLE DATA AND CALIBRATING REACTIONS

J.J. MILES, Ph.D.[1] and K.R. SWARTZEL, Ph.D.

Department of Food Science
North Carolina State University
Raleigh, NC 27695-7624

Accepted for Publication March 13, 1994

ABSTRACT

Twelve continuous thermal processes were evaluated with the equivalent point method based on time-temperature histories and the destruction of Blue #2 at four different pH's to provide different kinetic parameters as calibrating reactions. The Arrhenius kinetic parameters for the four reactions were estimated under continuous flow conditions. Three were used as calibrating reactions to determine the equivalent times and temperatures for each process. The loss of blue #2 for the fourth was estimated for each process, using its kinetic parameters and equivalent points based on thermocouple and calibrating reactions. Log concentration reductions, using equivalent points based on calibrating reactions, more closely matched (slope = 0.962, r^2 = 0.999) actual results than did equivalent points based on thermocouple data (slope = 1.030, r^2 = 0.976). Thermal process estimates based on calibrating reactions were more useful to estimate kinetic parameters or product quality because they more closely represented the process actually experienced by the product.

INTRODUCTION

Evaluation of the microbial destruction of continuous thermal (UHT) processes is normally limited to the holding section of the process to produce a conservative estimate of product safety, and because adequate temperature data is lacking for heating and cooling operations during run times. Since thermal effects during heating and cooling may significantly alter product characteristics, an accurate evaluation must include the entire thermal process. This evaluation may be based on the time temperature history experienced by the product or on concentration changes of product constituents.

[1] Correspondence should be addressed to Dr. J.J. Miles, President, MicroThermics, Inc., 5024-F Departure Dr., Raleigh, NC 27604.

Journal of Food Process Engineering **18** (1995) 99–113.

The system-wide impact of continuous thermal processes has been investigated by a number of researchers. Burton (1958a,b) and Burton *et al.* (1959, 1977) evaluated the efficiency of a laboratory-scale steam infusion process. Their studies attempted to resolve the difference between observed bacterial reductions and those estimated from simulations using process temperature history data and batch-generated kinetic data. The agreement between the observed and simulated results was improved by integrating the residence time distribution into the simulation. It was further improved when kinetic data obtained from the continuous process was used in the simulation; however, considerable differences remained.

Swartzel (1982) described a method (later called the Equivalent Point Method or EPM), to evaluate indirect continuous thermal processes, that expressed the nonisothermal process as if it were isothermal. The value of this method lay in its independence from activation energy. Additionally, it permitted the determination of the equivalent point for a process from concentration changes in three or more calibrating reactants.

Swartzel and Jones (1985) used the EPM to calibrate a continuous thermal processing system for kinetic studies. The EPM was further investigated by Sadeghi (1987) who found that Blue #2 and sucrose at controlled pH's could be used as calibration materials to determine the equivalent time and temperature (E(t,T)cm) for a process. Sadeghi determined equivalent points based upon temperature measured by thermocouples (E(t,T)tc) and calibration materials for the same process. Discrepancies between the two equivalent points were attributed to two factors. Batch kinetic data were used to generate the E(t,T)cm for a continuous process, and errors may result from the exponential integrals used to calculate the E(t,T)tc. The authors recommended that kinetic data generated under continuous flow conditions be used to evaluate continuous processes. More detailed research into this system was restricted by relatively large batch requirements and sampling limitations.

A laboratory scale continuous thermal processing system (LSTPS) for generating kinetic data under ultra high temperature (UHT) processing conditions was described by Miles and Swartzel (1993) (Fig. 1). The system was designed with multiple heat exchangers, and temperature and sample ports to support kinetic data generation under both isothermal and nonisothermal conditions. Ungrounded thermocouples and sample tubes were positioned adjacent to each other at the flow axis to measure and sample material at the "cold point" in the process. By applying the equivalent point method of analysis, 12 equivalent points that were cumulative for the process to each sample port were determined. Each equivalent point represented a different time-temperature history, i.e., a different thermal process. Thus, the system provided the capability to determine Ea and Ao for a test material under 12 different processes covering a wide range of time-temperature conditions in one

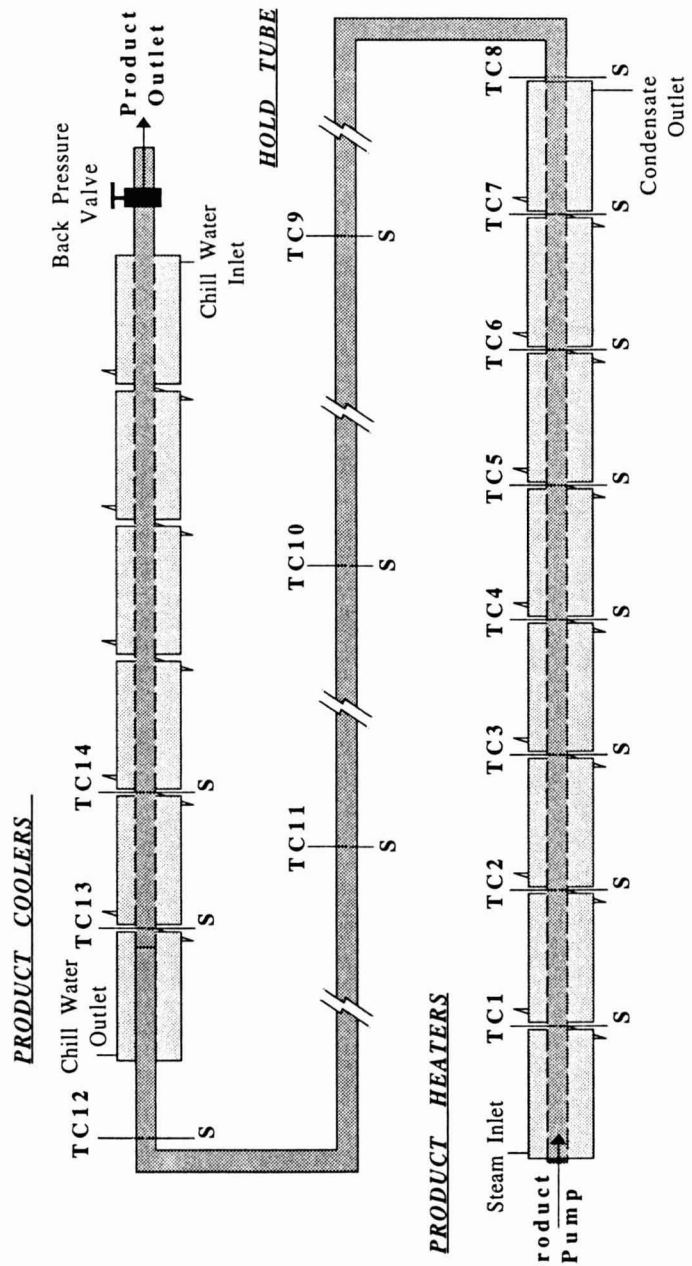

FIG. 1. SCHEMATIC REPRESENTATION OF THE LSTPS SHOWING HEATERS, HOLD TUBE, AND COOLERS WITH SAMPLE (S) AND TEMPERATURE (TC) PORTS

operation. Miles (1993) used the system to evaluate the acid hydrolysis of sucrose under UHT processing conditions. Data and kinetic parameters from their study supported first order reaction kinetics, and agreed well with literature values. The LSTPS was then used to further detail the alkaline destruction of Blue #2 under isothermal continuous-flow conditions (Miles 1993). Four pH, buffer and dye reaction mixtures were identified that yielded different Ea and Ao values for this reaction, and were useful as calibration reactions to evaluate continuous thermal processes.

The use of calibration reactions may provide a more complete description of the thermal process experienced by product materials than temperature history because of the limitation of cold-point positioning of temperature sensors, and lack of comprehensive residence time distribution data. The objective of this study was to compare the use of thermocouple measurements and calibration reactions for evaluating continuous thermal processes. These two methods would then be compared based on their ability to predict the actual impact of the process on an unknown.

MATERIALS AND METHODS

Thermal Processing System

The LSTPS (Fig. 1) described by Miles (1993) was equipped with an extended hold tube and additional sample ports (Table 1) so that a total of 14 cumulative time-temperature processes and corresponding samples could be obtained in one operation.

The extended hold tube was constructed using 6.35 mm × 1.24 mm wall (1/4 in. * 0.049 in.) stainless steel tubing to provide high velocities at relatively low flow rates for more precise sampling. Four 6.1 m (20 ft.) sections were wound into 20.3 cm (8 in.) diameter coils, insulated, and joined with cross connections to provide five locations for sample and temperature probes. This hold tube provided residence times applicable to both HTST and UHT processes and fluid velocity sufficient for turbulent flow with most low viscosity fluids (Reynolds No. >20,000.)

In both the LSTPS and extended hold tube, type T grounded thermocouples were positioned so that the tip of the thermocouple sheath was located along the flow axis. The system was operated at 930 ml/min flow rate, with temperatures at the exit of the heat exchangers ranging from 75 to 140C. At these conditions, flow in the first heat exchanger would not be fully-developed turbulent flow, and static mixers were installed inside each heat exchanger to enhance turbulence and sampling.

TABLE 1.
THERMOCOUPLE AND SAMPLE PORT LOCATIONS

Sample Port	System Location
1	heater #1 exit
2	heater #2 exit
3	heater #3 exit
4	heater #4 exit
5	heater #5 exit
6	heater #6 exit
7	heater #7 exit
8	heater #8 exit
9	hold section #1 exit
10	hold section #2 exit
11	hold section #3 exit
12	hold section #4 exit
13	cooler #1 exit
14	cooler #2 exit

An IBM PC (IBM, Armonk, NY 10504) equipped with EXP-16 and Dash-8 boards (MetraByte Corporation, Taunton, MA 02780) and Labtech™ Notebook (Laboratory Technologies Corp., Wilmington MA 01887) were used to record process temperatures. The entire data acquisition system was calibrated, as it was to be used, against a standard reference mercury thermometer, using an oil bath at eight points from 60 to 145C. The slope and intercept of each thermocouple channel were determined over the entire range and used to transform recorded data to the standard before further analysis.

Calibrating Mixtures and Processing

Calibrating reaction mixtures, consisting of Blue #2 at four different pH's in 0.1M carbonate-bicarbonate buffer (Table 2), were prepared in 32-L batches with distilled water. The blue dye was added to the buffer solutions immediately before processing. Rheological properties of the reaction mixtures were considered to be identical because of only slight differences in dye concentration and pH. Each was processed under steady state conditions using the LSTPS. Triplicate samples, of 15 ml each, were taken from the raw product and at each sample port, and cooled immediately for each mixture processed. Samples were taken using a 1.58mm (1/16 in.) sample tube with the tip positioned at

TABLE 2.
REACTION MIXTURES OF BLUE #2 IN 0.1 M
CARBONATE-BICARBONATE BUFFER

Reaction Mixture	pH	M	[Dye] ppm
A	10.12	0.1	124
B	10.21	0.1	124
C	9.93	0.1	130
D	9.74	0.1	104

the center of the product flow path which was connected to a tubular heat exchanger, of the same diameter, which cooled the product very rapidly (Miles 1993). Cooling time estimates based on the sample temperature, flow rate, and heat exchanger size indicated that each sample was cooled in less than 0.1 s.

Samples were acidified to stabilize the reaction until analysis by mixing 5:1 (v/v) with 0.4M citric acid. Final sample pH was 5.6. The start and end times for each sampling period were recorded and used to retrieve temperature history data. Absorbance of each sample was measured at 602 nm using a Shimatzu recording spectrophotometer (Shimatsu Corporation, Columbia MD 27405), and used for subsequent calculations to indicate dye concentration.

Temperature History Determination and Evaluation

Sample temperatures during processing were determined by averaging the temperature measurements logged during the sampling period at each sample port. Flow rate and system dimensions, and static mixer displacement were then used to determine transit time between each port and construct the temperature history. The equivalent point method (Nunes and Swartzel 1990) was used to determine cumulative equivalent times and temperatures (E(t,T)tc) from the start of the process to each sample port.

Data Analysis

In this study, the kinetic parameters (Ea and Ao) for all four calibrating mixtures were estimated under continuous flow nonisothermal conditions from approximately 70 to 145C. This provided estimates generated under the same conditions as those to which they were to be applied. Parameters estimated by Miles (1993) used data from a more narrow temperature range (130–150C) under nearly isothermal conditions from 130 to 150C. This study required a

wider temperature range to allow evaluation of the lower temperatures of the early heating stages of the process.

Equation (1) was used with experimentally determined concentrations, and equivalent times to calculate G′ for each reaction mixture. Linear regression was then used to regress ln(G′) on 1/Te as given by Eq. (2) to estimate Ea/R and ln(Ao) as the slope and intercept for each reaction mixture.

$$G' = \frac{\ln(Co/C)}{t_e} \tag{1}$$

$$\ln(G') = \ln(A_o) - \frac{E_a}{R}\frac{1}{T_e} \tag{2}$$

The kinetic parameters for reaction mixtures B, C, and D were then used to determine E(t,T)cm at each sample port in the process using Eq. (3). The G value was calculated using the newly determined Ao, and this was regressed against Ea/R to produce the equivalent time and temperature based on calibration materials, E(t,T)cm, for each sample port.

$$\ln(G) = \ln(t_e) - \frac{E_a}{R}\frac{1}{T_e} \qquad \text{where } G = \frac{\ln(Co/C)}{A_o} \tag{3}$$

Reaction mixture A was omitted from the determination of equivalent times and temperatures so that it would have no impact on the calibration material based equivalent points. Thus, it provided a basis for comparing the accuracy of thermocouple and calibration material based equivalent points. To compare the accuracy of these two equivalent points, predicted log reductions (as ln(Co/C)) for mixture A were determined using the experimentally determined kinetic parameters, Eq. (4), and both E(t,T)tc and E(t,T)cm.

$$\ln(Co/C) = t_e A_o e\left(\frac{-E_a}{RT_e}\right) \tag{4}$$

RESULTS AND DISCUSSION

Time-temperature histories from all four processes were virtually identical and are superimposed in Fig. 2. Standard deviations of the temperature

measurements across all four process runs ranged from 0.09 at 141.5C to 0.92 at 76C. Consequently, the temperature of each sample port, averaged across all four process runs was used for subsequent calculations. The thermocouple-based equivalent point (E(t,T)tc) for the process up to each sample port are shown in Table 3. These represent the cumulative effect of the thermal process leading to each sample port, expressed as a unique isothermal treatment, and are 12 different thermal processes.

Preliminary evaluation of the concentration data showed that the samples from the first sample port exhibited only very small concentration changes. The associated error was large relative to the unprocessed samples (Co) and produced variability that interfered with subsequent calculations. Only concentration data from sample ports 2–14 were used in subsequent analysis. Estimates for the slope (Ea/R) and intercept (ln(Ao) were obtained using Eq. (1) and (2), E(t,T)tc, and concentration data, and are shown in Fig. 3 and Table 4.

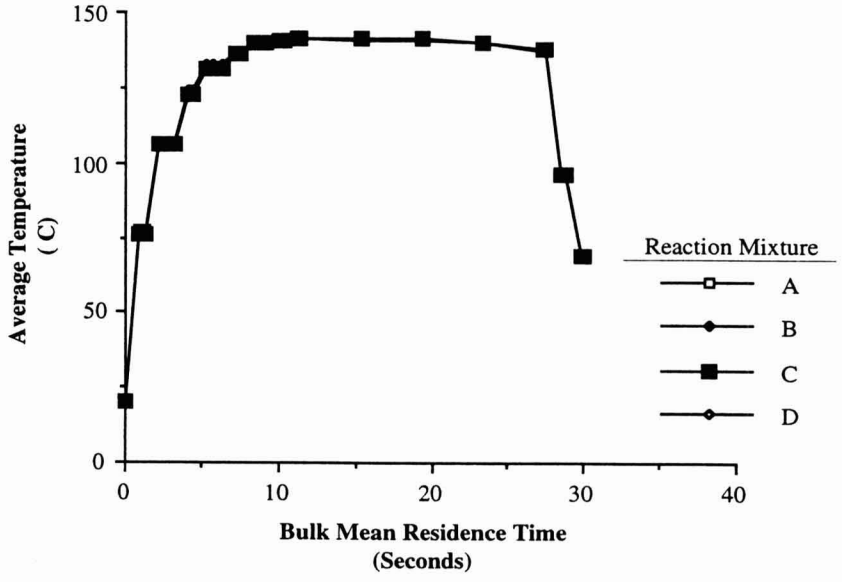

FIG. 2. OVERLAYED TIME-TEMPERATURE HISTORIES FROM PROCESSING FOUR REACTION MIXTURES

TABLE 3.
EQUIVALENT POINTS DETERMINED USING THERMOCOUPLE AND CALIBRATING REACTIONS B, C, AND D

Sample Port	Thermocouple Equivalent Points		Calibration Equivalent Points	Reaction
	te_{tc}	Te_{tc}	te_{cm}	Te_{cm}
1	0.78	76.65	n a	n a
2	1.29	103.43	0.66	81.48
3	1.61	119.87	1.35	102.35
4	2.18	128.55	2.00	114.33
5	3.03	132.97	2.88	117.18
6	3.76	136.26	3.36	127.36
7	4.77	138.16	4.10	131.72
8	5.81	139.05	4.94	133.47
9	9.50	140.26	7.36	140.15
10	13.43	140.48	9.83	143.74
11	17.38	140.49	12.49	145.62
12	21.10	140.27	14.80	147.56
13	21.51	140.18	15.21	147.38
14	21.51	140.18	15.15	147.32

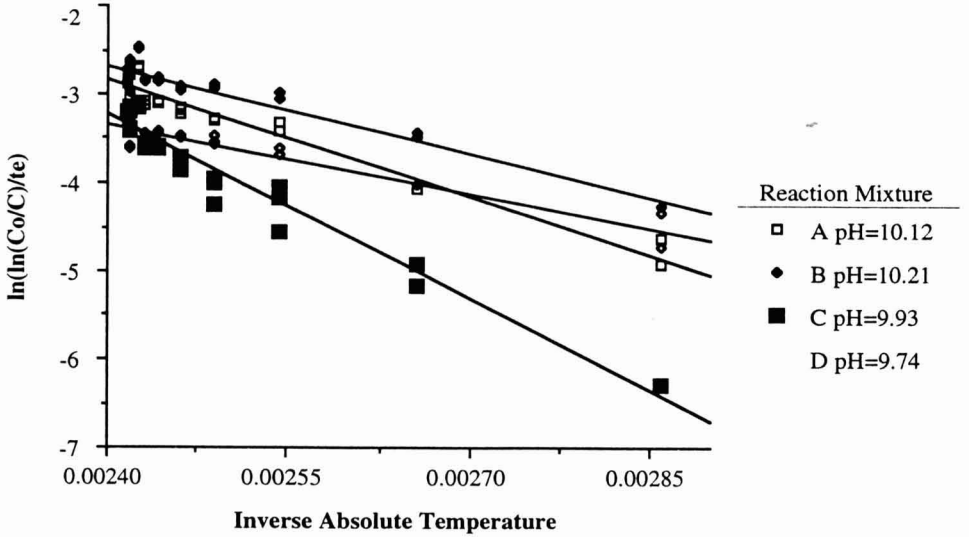

FIG. 3. KINETIC PARAMETER ESTIMATION FOR THE FOUR REACTION MIXTURES

TABLE 4.
KINETIC PARAMETER ESTIMATES DETERMINED EXPERIMENTALLY FOR EACH REACTION MIXTURE

Reaction Mixture	Ea/R	Std. Error	ln(Ao)	Std. Error	R^2
A	4422.5	183.1	7.779	0.455	0.942
B	3300.4	176.7	5.241	0.441	0.904
C	6972.8	248.2	13.525	0.617	0.956
D	2695.4	160.6	3.141	0.401	0.887

Equivalent points based on calibration materials were determined using the kinetic parameters from mixtures B, C, and D. This was done using Eq. (3) for each sample port, and is shown in Fig. 4. Each sample port is represented by a line with slope equaling the natural log of the equivalent time, and the intercept equaling inverse temperature in degrees Kelvin. There were three replicates at each point along each line. These equivalent points, E(t,T)cm's, are also summarized in Table 3.

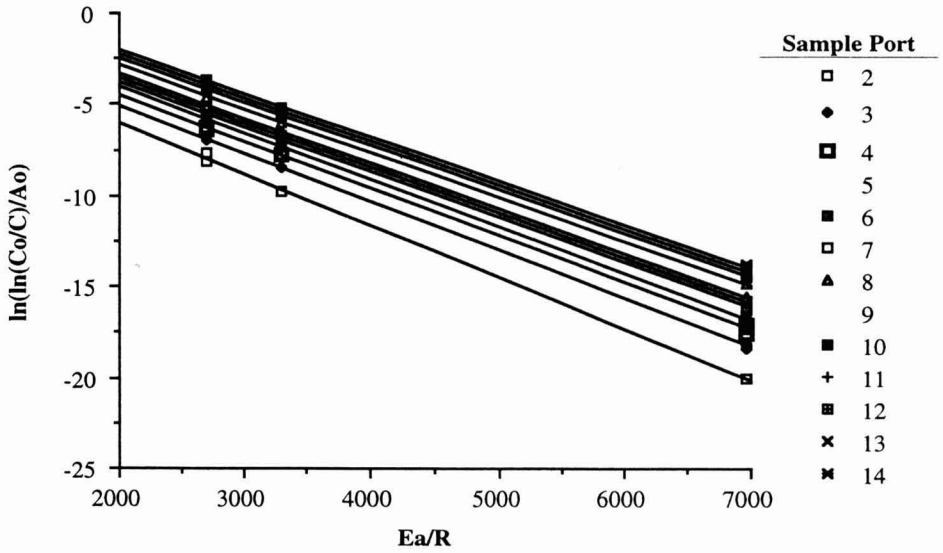

FIG. 4. EQUIVALENT POINT ESTIMATION PLOTS FOR 12 PROCESSES USING THE 3 CALIBRATING REACTIONS

The log reductions for the unknown, predicted using E(t,T)tc and E(t,T)cm, and actual log reductions are shown in Fig. 5. Results from regression analysis of these relationships are summarized in Table 5. The slopes and intercepts of both curves are significantly different from each other (alpha = 0.01). E(t,T)cm had a lower standard error than E(t,T)tc and was a more reliable predictor of dye reduction. Evaluation of residual errors of the relationship between predictions based on each method and actual data also indicated that E(t,T)cm was more useful to predict the unknown's performance. The accuracy of predictions based on the calibrating reactions indicated that they expressed the thermal process, actually experienced by a product in bulk, more accurately than time-temperature measurements.

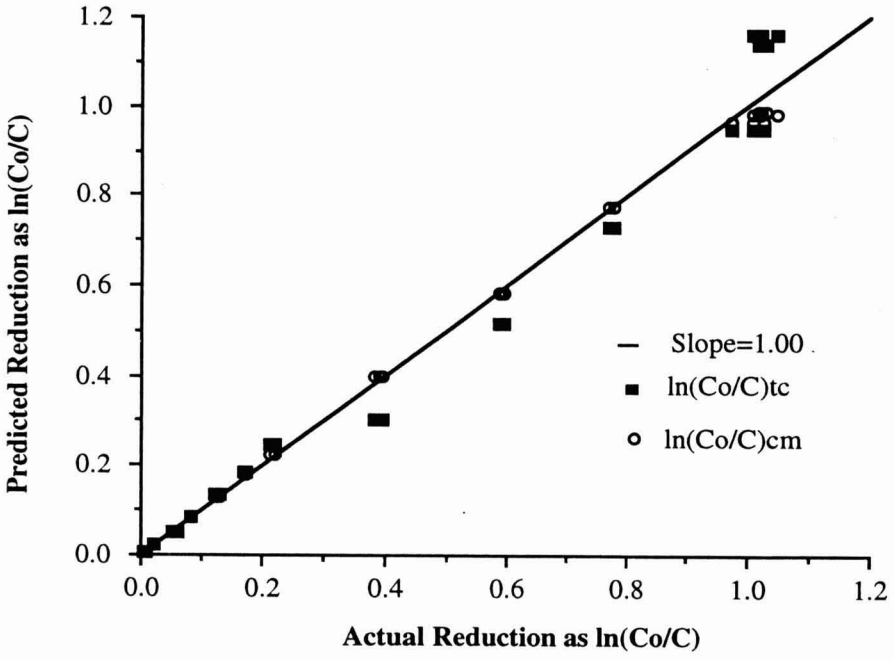

FIG. 5. DYE DESTRUCTION PREDICTED USING E(t,T)tc AND E(t,T) cm EQUIVALENT POINTS VERSUS ACTUAL DESTRUCTION

TABLE 5.
REGRESSION STATISTICS FOR PREDICTED VERSUS ACTUAL LOG REDUCTION

Evaluation Method	Slope	Standard Error	Intercept	Standard Error	R^2
E(t,T)tc	1.030	0.027	-0.013	0.015	0.976
E(t,T)cm	0.962	0.005	0.008	0.003	0.999

The thermal processes that were evaluated here, represented cumulative portions of a larger process (Fig. 2). In Fig. 6, these are plotted as equivalent time-temperature histories, using both the thermocouple and calibration material results. The difference in shape between the two curves reflects the different information incorporated into each. The E(t,T)tc line represents only the time and temperature information provided by process flow data and thermocouples.

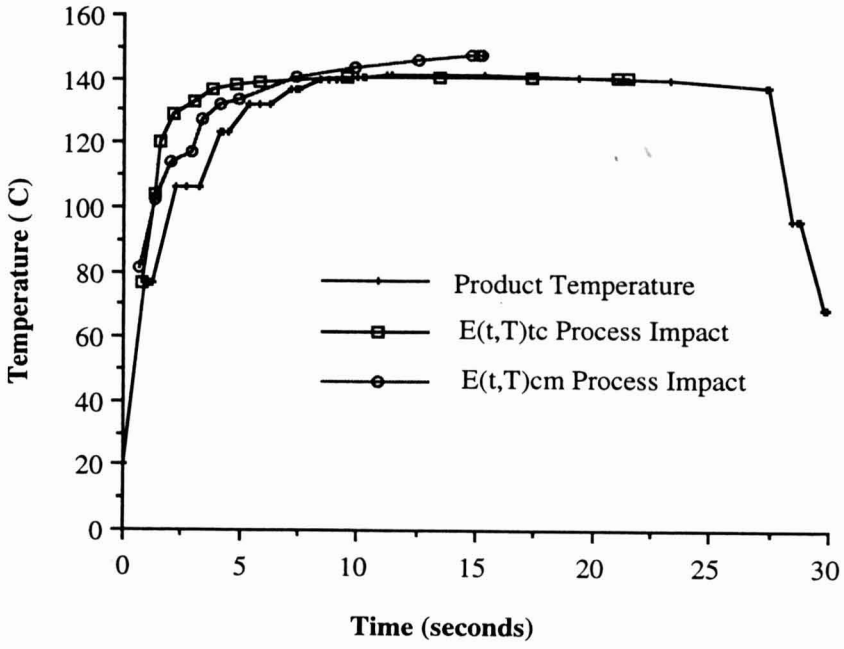

FIG. 6. EQUIVALENT TIME-TEMPERATURE HISTORIES USING CALIBRATION REACTION AND THERMOCOUPLE DATA

Each thermocouple was positioned at the center, presumably the cold point of the product stream, during assembly. Temperatures measured at these locations represented only the temperature of the fluid element passing the thermocouple's tip. The E(t,T)cm curve contained the additional information conveyed by the calibration materials as they experienced the process. This included their thermal exposure at all points throughout the heat exchangers and hold tube, residence time distribution, as well as sampling and analytical error.

The relative positions of the two curves is useful to explain differences observed between product quality predictions based on thermocouple and flow data, and product quality that may be actually observed. As the process proceeds into the hold tube, the lines diverge, with the calibration material line continuing to higher temperatures. Thus, the bulk process is actually much more severe than is indicated by thermocouple data.

SUMMARY

Research into the evaluation of continuous thermal processes indicates that the evaluation is improved when as much data as possible from the material being processed is included in the calculations. In this study, a continuous thermal process was evaluated using its impact on calibration materials that were processed as product, as well as thermocouple data. The effectiveness of both methods was based on their ability to estimate the impact of the process on an unknown. Predictions using both were highly correlated with the actual results. Those based on calibrating reactions more effectively predicted the actual results relative to product quality.

ACKNOWLEDGEMENTS

The authors gratefully acknowledge the support of the North Carolina Agricultural Research Service and the Center for Aseptic Processing and Packaging Studies.

Paper number FSR93-25 of the journal of the series of the Department of Food Science. The use of trade names does not imply endorsement by the North Carolina Agricultural Service of the products named, nor criticism of similar ones not mentioned.

NOMENCLATURE

Parameter	Definition	Units
Ao	Arrhenius preexponential constant	seconds^{-1}
Co	Concentration at time zero	
C	Concentration at time t	
Ea	Activation energy determined from the slope of the Arrhenius plot.	J/g mole
E(t,T)tc	Equivalent point based on thermocouple measurements	seconds at °C
E(t,T)cm	Equivalent point based on calibrating reactions	seconds at °C
G	Thermal reduction coefficient	seconds
G′	Reaction rate based on Te and te	seconds $^{-1}$
R	Universal gas constant	8.314 J/mole
t_{etc}	Equivalent time based on thermocouple measurements	seconds
T_{etc}	Equivalent temperature based on thermocouple measurements	°C or °K
t_{ecm}	Equivalent time based on calibrating reactions	seconds
T_{ecm}	Equivalent temperature based on calibrating reactions	°C or °K
t_e	Equivalent time	seconds
T_e	Equivalent temperature	°C or °K

REFERENCES

BURTON, H. 1958a. An analysis of the performance of an ultra-high temperature milk sterilizing plant. I. Introduction and physical measurements. J. Dairy Res. *25*, 75.

BURTON, H. 1958b. An analysis of the performance of an ultra-high temperature milk sterilizing plant. II. Calculation of the bactericidal effectiveness. J. Dairy Res. *25*, 324.

BURTON, H. *et al.* 1959. An analysis of the performance of an ultra-high-temperature milk sterilizing plant. IV. Comparison of experimental and calculated sporicidal effects for a strain of *Bacillus stearothermophilus*. J. Dairy Res. *26*, 221.

BURTON, H., PERKIN, A.G., DAVIES, F.L. and UNDERWOOD, H.M. 1977. Thermal death kinetics of *Bacillus stearothermophilus* spores at ultrahigh temperatures. III. Relationship between data from capillary tube experiments and from UHT sterilizers. J. Food Technol. *12*, 149.

MILES, J.J. 1993. Kinetic data generation under ultra-high temperature continuous processing conditions. Ph.D. dissertation. North Carolina State University, Raleigh.

NUNES, R.V. and SWARTZEL, K.R., 1990. Modeling thermal processes using the equivalent point method: parameter estimation. J. Food Eng. *11*, 103.

SADEGHI, F. 1987. Kinetic studies of calibrations materials for thermal process evaluation of food systems. Ph.D. Dissertation, North Carolina State University, Dept. Food Science.

SWARTZEL, K.R. 1982. Arrhenius kinetics as applied to product constituent losses in ultra high temperature processing. J. Food Sci. *47*, 1886.

SWARTZEL, K.R. and JONES, V.A. 1985. System design and calibration of a continuous flow apparatus for kinetic studies. J. Food Sci. *50*, 1203.

KINETIC ENERGY CORRECTION FACTOR OF A HERSCHEL-BULKLEY FLUID

J.L. BRIGGS and J.F. STEFFE[1]

Department of Agricultural Engineering
Department of Food Science and Human Nutrition
Michigan State University
East Lansing, MI 48824-1323

Accepted for Publication July 8, 1994

ABSTRACT

Two simple equations were developed to estimate the kinetic energy correction factor (α) of a Herschel-Bulkley fluid in laminar flow. These approximations result in errors of less than 3% when compared to the exact values of α.

INTRODUCTION

The behavior of incompressible fluids in a pipe may be described using the mechanical energy balance equation:

$$gZ_1 + \frac{P_1}{\rho} + (KE)_1 + W = gZ_2 + \frac{P_2}{\rho} + (KE)_2 + E_f \qquad (1)$$

where subscripts 1 and 2 refer to different locations in the system, and the kinetic energy term is defined as

$$KE = \frac{\bar{u}^2}{\alpha} \qquad (2)$$

The numerical value of α, the kinetic energy correction factor, is dependent on fluid type and flow regime. Table 1 shows α values for various fluids in laminar and turbulent flow. Note that the value of c, the ratio of yield stress to the shear stress at the wall, may range from $0 \leq c < 1$; however, when $\sigma_o = 0$, $c = 0$ causing the Herschel-Bulkley equation to collapse into the power law model. Values of $c \geq 1.0$ are physically meaningless because no fluid movement would occur, making the kinetic energy equal to zero.

[1]Direct correspondence to J.F. Steffe, Dept. of Agricultural Engineering.

Journal of Food Process Engineering **18** (1995). 115–118.

TABLE 1.
KINETIC ENERGY CORRECTION FACTORS FOR LAMINAR AND TURBULENT FLOW

Fluid [Mathematical Model]	α Laminar Flow*	α Turbulent Flow
Newtonian $[\sigma = \mu\dot{\gamma}]$	1.0	2.0
Power Law $[\sigma = K(\dot{\gamma})^n]$	$\alpha = \frac{2(2n+1)(5n+3)}{3(3n+1)^2}$	2.0
Bingham Plastic $[\sigma = \mu_{pl}\dot{\gamma} + \sigma_o]$	$\alpha = \frac{2}{2-c}$	2.0
Herschel-Bulkley $[\sigma = K(\dot{\gamma})^n + \sigma_o]$	See text	2.0

From Steffe (1992).
*Laminar flow solution for the Bingham plastic material is an approximation from Metzner (1956) which is within 2.5% of the true solution.

Osorio and Steffe (1984) developed an analytical solution for α for a Herschel-Bulkley fluid in laminar flow:

$$\alpha = [2(1 + 3n + 2n^2 + 2n^2c + 2nc + 2n^2c^2)^3 (2 + 3n)(3 + 5n)(3 + 4n)]/ [[(1 + 2n)^2 (1+3n)^2] [18 + n (105 + 66c) + n^2 (243 + 306c + 85c^2) + n^3(279 + 522c + 350c^2) + n^4 (159 + 390c + 477c^2) + n^5(36 + 108c + 216c^2)]] \quad (3)$$

This expression, though exact, is long and cumbersome. The objective of this work was to develop a simple approximation for Eq. (3).

MATERIALS AND METHODS

Many attempts, based on trial and error efforts of the authors, were made to fit actual kinetic energy correction factors to different mathematical equations using standard regression techniques. One equation could not be found to fit the entire range of both n and c. The following two equations were developed to keep errors within acceptable levels:

for $0.06 \leq n \leq 0.38$ use

$$\ln(\alpha) = 0.168(c) - 1.062(nc) - 0.954(n)^{0.5} - 0.115(c)^{0.5} + 0.831 \quad (4)$$

and for $0.38 < n \leq 1.60$ use

$$\ln(\alpha) = 0.849(c) + 0.296(nc) - 0.600(n)^{0.5} - 0.602(c)^{0.5} + 0.733 \quad (5)$$

Errors of less than 3.0% are generated (Fig. 1) when using Eq. (4) or (5) to approximate Eq. (3) for $0.1 \leq c < 1.0$. If Eq. (4) and (5) are used for $0.0 < c < 0.1$, error levels up to 14.2% may be encountered. Using the approximation equations in this range of c is not recommended. Prediction equations for the kinetic energy correction factor involving flow behavior indexes in the range of $0.06 \leq n \leq 1.6$ for c values from $0.1 \leq c < 1.0$ will be applicable to most practical problems involving fluid foods which obey the Herschel-Bulkley model.

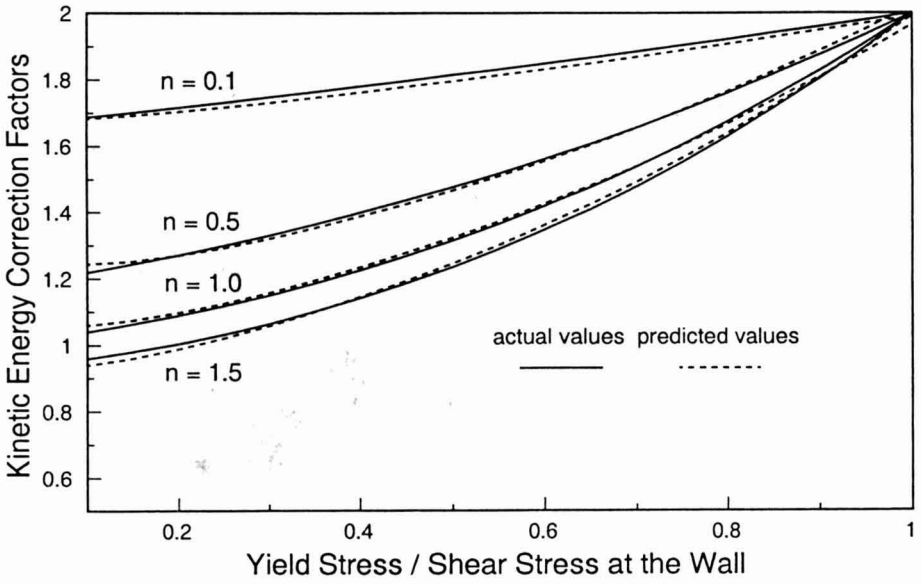

FIG. 1. PREDICTED [EQ. (4) AND (5)] AND ACTUAL [EQ. (3)] KINETIC ENERGY CORRECTION FACTORS FOR HERSCHEL-BULKLEY FLUIDS

NOMENCLATURE

c	Yield stress/shear stress at the wall, dimensionless
E_f	Energy losses due to friction, J/kg
g	Gravitational acceleration, 9.81 m/s^2

K	Consistency coefficient, Pa s^n
KE	Average kinetic energy per unit mass of fluid, J/kg
n	Flow behavior index, dimensionless
P	Pressure, Pa
$\bar{u}$	Volumetric average velocity, m/s
W	Work term in the mechanical energy balance, J/kg
Z	Height term in the mechanical energy balance, m
α	Kinetic energy correction factor, dimensionless
$\dot{\gamma}$	Shear rate, 1/s
μ_{pl}	Plastic viscosity, Pa s
ρ	Density, kg/m^3
σ	Shear stress, Pa
σ_O	Yield stress, Pa

REFERENCES

METZNER, A.B. 1956. Non-Newtonian technology: fluid mechanics, mixing, heat transfer. In *Advances in Chemical Engineering, Vol. 1*, (T.B. Drew and J.W. Hoopes eds.) pp. 77–153, Academic Press, New York.

OSORIO, F.A. and STEFFE, J.F. 1984. Kinetic energy calculations for non-Newtonian fluids in circular tubes. J. Food Sci. *49*, 1295–1296, 1315.

STEFFE, J.F. 1992. *Rheological Methods in Food Process Engineering*, Freeman Press, E. Lansing, MI.

FNP PUBLICATIONS IN FOOD SCIENCE AND NUTRITION

Journals

JOURNAL OF FOOD LIPIDS, F. Shahidi
JOURNAL OF RAPID METHODS AND AUTOMATION IN MICROBIOLOGY, D.Y.C. Fung and M.C. Goldschmidt
JOURNAL OF MUSCLE FOODS, N.G. Marriott, G.J. Flick, Jr. and J.R. Claus
JOURNAL OF SENSORY STUDIES, M.C. Gacula, Jr.
JOURNAL OF FOODSERVICE SYSTEMS, C.A. Sawyer
JOURNAL OF FOOD BIOCHEMISTRY, J.R. Whitaker, N.F. Haard and H. Swaisgood
JOURNAL OF FOOD PROCESS ENGINEERING, D.R. Heldman and R.P. Singh
JOURNAL OF FOOD PROCESSING AND PRESERVATION, D.B. Lund
JOURNAL OF FOOD QUALITY, J.J. Powers
JOURNAL OF FOOD SAFETY, T.J. Montville
JOURNAL OF TEXTURE STUDIES, M.C. Bourne and M.A. Rao

Books

OF MICROBES AND MOLECULES: FOOD TECHNOLOGY AT M.I.T., S.A. Goldblith
MEAT PRESERVATION: PREVENTING LOSSES AND ASSURING SAFETY, R.G. Cassens
S.C. PRESCOTT, M.I.T. DEAN AND PIONEER FOOD TECHNOLOGIST, S.A. Goldblith
FOOD CONCEPTS AND PRODUCTS: JUST-IN-TIME DEVELOPMENT, H.R. Moskowitz
MICROWAVE FOODS: NEW PRODUCT DEVELOPMENT, R.V. Decareau
DESIGN AND ANALYSIS OF SENSORY OPTIMIZATION, M.C. Gacula, Jr.
NUTRIENT ADDITIONS TO FOOD, J.C. Bauernfeind and P.A. Lachance
NITRITE-CURED MEAT, R.G. Cassens
POTENTIAL FOR NUTRITIONAL MODULATION OF AGING, D.K. Ingram *et al.*
CONTROLLED/MODIFIED ATMOSPHERE/VACUUM PACKAGING OF FOODS, A.L. Brody
NUTRITIONAL STATUS ASSESSMENT OF THE INDIVIDUAL, G.E. Livingston
QUALITY ASSURANCE OF FOODS, J.E. Stauffer
THE SCIENCE OF MEAT AND MEAT PRODUCTS, 3RD ED., J.F. Price and B.S. Schweigert
HANDBOOK OF FOOD COLORANT PATENTS, F.J. Francis
ROLE OF CHEMISTRY IN PROCESSED FOODS, O.R. Fennema, *et al.*
NEW DIRECTIONS FOR PRODUCT TESTING OF FOODS, H.R. Moskowitz
PRODUCT TESTING AND SENSORY EVALUATION OF FOODS, H.R. Moskowitz
ENVIRONMENTAL ASPECTS OF CANCER: ROLE OF FOODS, E.L. Wynder *et al.*
FOOD PRODUCT DEVELOPMENT AND DIETARY GUIDELINES, G.E. Livingston, R.J. Moshy, and C.M. Chang
SHELF-LIFE DATING OF FOODS, T.P. Labuza
ANTINUTRIENTS AND NATURAL TOXICANTS IN FOOD, R.L. Ory
UTILIZATION OF PROTEIN RESOURCES, D.W. Stanley *et al.*
VITAMIN B_6: METABOLISM AND ROLE IN GROWTH, G.P. Tryfiates
POSTHARVEST BIOLOGY AND BIOTECHNOLOGY, H.O. Hultin and M. Milner

Newsletters

MICROWAVES AND FOOD, R.V. Decareau
FOOD INDUSTRY REPORT, G.C. Melson
FOOD, NUTRITION AND HEALTH, P.A. Lachance and M.C. Fisher
FOOD PACKAGING AND LABELING, S. Sacharow

GUIDE FOR AUTHORS

Typewritten manuscripts in triplicate should be submitted to the editorial office. The typing should be double-spaced throughout with one-inch margins on all sides.

Page one should contain: the title, which should be concise and informative; the complete name(s) of the author(s); affiliation of the author(s); a running title of 40 characters or less; and the name and mail address to whom correspondence should be sent.

Page two should contain an abstract of not more than 150 words. This abstract should be intelligible by itself.

The main text should begin on page three and will ordinarily have the following arrangement:

Introduction: This should be brief and state the reason for the work in relation to the field. It should indicate what new contribution is made by the work described.

Materials and Methods: Enough information should be provided to allow other investigators to repeat the work. Avoid repeating the details of procedures that have already been published elsewhere.

Results: The results should be presented as concisely as possible. Do not use tables *and* figures for presentation of the same data.

Discussion: The discussion section should be used for the interpretation of results. The results should not be repeated.

In some cases it might be desirable to combine results and discussion sections.

References: References should be given in the text by the surname of the authors and the year. *Et al.* should be used in the text when there are more than two authors. All authors should be given in the Reference section. In the Reference section the references should be listed alphabetically. See below for style to be used.

RIZVI, S.S.H. 1986. Thermodynamic properties of foods in dehydration. In *Engineering Properties of Foods*, (M.A. Rao and S.S.H. Rizvi, eds.) pp. 133–214, Marcel Dekker, New York.

MICHAELS, S.L. 1989. Crossflow microfilters ins and outs. Chem. Eng. *96*, 84–91.

LABUZA, T.P. 1982. *Shelf-Life Dating of Foods,* pp. 66–120, Food & Nutrition Press, Trumbull, CT.

Journal abbreviations should follow those used in *Chemical Abstracts*. Responsibility for the accuracy of citations rests entirely with the author(s). References to papers in press should indicate the name of the journal and should only be used for papers that have been accepted for publication. Submitted papers should be referred to by such terms as "unpublished observations" or "private communication." However, these last should be used only when absolutely necessary.

Tables should be numbered consecutively with Arabic numerals. The title of the table should appear as below:

TABLE 1.
ACTIVITY OF POTATO ACYL-HYDROLASES ON NEUTRAL LIPIDS, GALACTOLIPIDS AND PHOSPHOLIPIDS

Description of experimental work or explanation of symbols should go below the table proper. Type tables neatly and correctly as tables are considered art and are not typeset. Single-space tables.

Figures should be listed in order in the text using Arabic numbers. Figure legends should be typed on a separate page. Figures and tables should be intelligible without reference to the text. Authors should indicate where the tables and figures should be placed in the text. Photographs must be supplied as glossy black and white prints. Line diagrams should be drawn with black waterproof ink on white paper or board. The lettering should be of such a size that it is easily legible after reduction. Each diagram and photograph should be clearly labeled on the reverse side with the name(s) of author(s), and title of paper. When not obvious, each photograph and diagram should be labeled on the back to show the top of the photograph or diagram.

Acknowledgments: Acknowledgments should be listed on a separate page.

Short notes will be published where the information is deemed sufficiently important to warrant rapid publication. The format for short papers may be similar to that for regular papers but more concisely written. Short notes may be of a less general nature and written principally for specialists in the particular area with which the manuscript is dealing. Manuscripts that do not meet the requirement of importance and necessity for rapid publication will, after notification of the author(s), be treated as regular papers. Regular papers my be very short.

Standard nomenclature as used in the engineering literature should be followed. Avoid laboratory jargon. If abbreviations or trade names are used, define the material or compound the first time that it is mentioned.

EDITORIAL OFFICE: DR. D.R. HELDMAN, COEDITOR, *Journal of Food Process Engineering*, Food Science/Engineering Unit, University of Missouri-Columbia, 235 Agricultural/Engineering Bldg., Columbia, MO 65211 USA; or DR. R.P. SINGH, COEDITOR, *Journal of Food Process Engineering*, University of California, Davis, Department of Agricultural Engineering, Davis, CA 95616 USA.

JOURNAL OF FOOD PROCESS ENGINEERING VOLUME 18, NUMBER 1

CONTENTS